Luminescence and tenebrescence in aluminate sodalites and related materials

Author:

Madara Tomele

06.06.2024

Turku

Master's thesis

Subject: Chemistry
Author(s): Madara Tomele
Title: Luminescence and tenebrescence in aluminate sodalites and related materials
Supervisor(s): Prof. Mika Lastusaari, Adj. Prof. Anssi Peuronen
Number of pages: 77
Date: 06.06.2024

Research into inorganic luminescent and tenebrescent (colour-changing) materials with tunable properties has gained increasing attention in recent years. Hackmanite $Na_8Al_6Si_6O_{24}(Cl,S)_2$ is a member of the sodalite group that possesses both luminescent and tenebrescent properties.

Various studies exchanging framework and extra-framework ions have been performed in order tune optical properties of hackmanites. It has been observed that by expanding the cage-like structure of the framework F-centers, point defects also known as colour centers which are responsible for the colour change in inorganic solids, absorb longer wavelengths of light. It is also known that exchanging extra-framework cations and anions can affect the luminescent and tenebrescent properties of these materials. Based on these observations it can be concluded that by synthesizing a sodalite with a larger framework by, for example, exchanging Si atoms for Al and using aluminate sodalites as the base material as well as using various dopants, new compounds with different luminescence and tenebrescence properties could be produced.

Samples containing $Ca_8Al_{12}O_{24}S_2$ modified using various dopants were synthesized and their luminescence and tenebrescence properties were analyzed. First S^{2-} ions were exchanged with Cl^- ions, which are necessary for the tenebrescence mechanism, in various proportions. Next the Ca^{2+} ions were exchanged with Li^+, Na^+, K^+ and Rb^+ ions. The aim of this project was to analyze the effects of different ions on the optical properties of these materials.

Sample with the S/Cl ratio of $S_{1.4}Cl_{1.2}$ had some of the highest photo- and thermoluminescence intensity of all calcium aluminate sodalite containing samples. All alkali metal dopants increased the photoluminescence emission intensity of the base material, with $M_{1.2}Ca_{7.4}$ (M – alkali metal) being the ratio with the highest intensity in all doped samples. Tenebrescence after irradiation with 254 nm UV was not observed in any of the samples, however, a sample containing only $LiAlO_2$ phase showed a clear colour change after irradiation with X-rays from the X-ray fluorescence measurement.

Key words: sodalites, luminescence, tenebrescence, photochromism

Table of contents

Abbreviations

LED	–	light emitting diode
OSL	–	optically stimulated luminescence
PeL	–	persistent luminescence
pp	–	percentage points
RE	–	rare earth
TL	–	thermoluminescence
XRD	–	X-ray powder diffraction
XRF	–	X-ray fluorescence spectroscopy

1. INTRODUCTION

Luminescent and tenebrescent materials have gained increasing interest in the fields of photonics [1], dosimetry [2], optical data storage [3] and anti-counterfeiting [4]. While organic photochromic and luminescent materials have the advantage of being more tunable and easier to modify in comparison to inorganic materials, one of the major drawbacks of using organic compounds is their relatively low thermal, mechanical and chemical stability. [5] For this reason, research into inorganic luminescent and tenebrescent materials with tunable properties has gained increasing attention in the recent years. Some of these inorganic materials include transition metal oxides [3,6], ferroelectric ceramics [3] and sodalites [7].

Luminescence is the process of excited electrons from a higher energy orbital moving to a lower energy orbital resulting in emission of light. There are many types of luminescence depending on the excitation source: chemiluminescence (excitation via chemical reaction), cathodoluminescence (excitation via electron beam), thermoluminescence (release of energy after heating the material due to defect recombination), photoluminescence (excitation via photons) and many others. [8] In this work only photoluminescence and thermoluminescence will be examined.

1.1.   Principles and applications of photo- and thermoluminescent materials

The first step in the photoluminescence mechanism is always the formation of free electrons and electron holes by absorbing photons from a primary radiation source. The electrons are excited to a higher energy orbital, while the holes (empty orbitals, where an electron was once located) remain at ground state. These free electrons then diffuse through the material until they recombine with the electron holes or get trapped at different defects. Recombination can be radiative or non-radiative and the difference is whether it results in the emission of photons or other processes not involving light. [9]

There are three types of phosphors categorized by the roles of the matrix (bulk material) and the dopants: host luminophores in which luminescence centers are formed from intrinsic defects and no doping is needed; host and activator, in which the intrinsic defects do not luminescence and dopants are used to form luminescence centers; host, activator and sensitizer in which additional ions known as sensitizers are used to transfer absorbed energy to the activator enhancing the materials optical properties. [10]

If the electrons are trapped before recombination can occur, additional energy must be supplied to free the electrons, after which recombination can take place. Trap depth (minimum energy

necessary to excite and free the trapped electron), determines at what temperatures the traps are stable. Traps that are unstable at room temperature can decay at different rates, which then also dictates how long after irradiation photon emission may occur (as seen in persistent luminescence (PeL) phosphors). [9] For traps that are stable at room temperature, thermoluminescence (TL) and optically stimulated luminescence (OSL) are two methods that can be used to free trapped electrons and stimulate luminescence using either heat or photons respectively. [11]

Photoluminescent materials are used in light emitting diodes (LEDs), plasma and vacuum fluorescent displays. They are usually doped with rare earth (RE) elements due to their wide range of energy levels that can be used to obtain emissions in a wide variety of colors. White LEDs are considered as a good alternative to halogen, xenon and incandescent lamps due to high luminescence efficiency, long life time, good light stability and environmental friendliness. [10]

Photoluminescent materials are also used for sensing applications, for example, in non-contact temperature sensors in which the change of fluorescence intensity, which is affected by the temperature, is used to measure temperature [12]. PeL phosphors can also be used in the medical field for biosensing and bioimaging. For these applications materials with stable luminescence, long afterglow, appropriate size, target-triggered signal change for biosensing and passive or active targeting ability for bioimaging are necessary. [13]

Photoluminescent materials can switch between two states, on and off, under optical stimuli, representing 1 and 0 in binary code, allowing them to be used in optical information storage technology. During irradiation with UV the charge is stored in deep traps, which function as optical storage units, and recombines when stimulated by infrared light, whenever a signal is necessary. Optical information storage has the advantage of having a larger capacity and faster response than magnetic or semiconductor storage and is considered to be the most promising out of the three. [14]

Thermoluminescent materials are most notably used in dosimetry, to assess the dose of absorbed alpha, beta or gamma radiation, for example, in radiation therapy, radiation diagnostics and nuclear medicine. For these types of applications, it is necessary that the energy used to stimulate luminescence would be high enough to not cause recombination during use. TL glow peaks around 180-300°C correspond to relatively deep traps with high excitation energy and any promising materials must show TL in this range. [15]

1.2. Principles and applications of tenebrescent materials

Tenebrescence, also known as reversible photochromism, is the change of colour induced by electromagnetic radiation that can be reversed by exposure to heat or visible light. It can also be defined as a reversible transformation of a compound between two states, one of which is stable and

the other, which is obtained after irradiation, is metastable. [16] Different tenebrescent materials can respond to a broad spectrum of electromagnetic radiation (commonly in the range of UV to visible light) or respond selectively to a narrow bandwidth. This property can be found in both organic and inorganic compounds. Some of the mechanisms for light initiated colour change in organic compounds are pericyclic reactions, cis-trans isomerization, dissociation, intramolecular hydrogen transfers or group transfers and electron charge transfers. [5]

In inorganic materials photochromic behaviour is mainly caused by photo-induced charge carriers. The tenebrescence process typically includes the formation of the colored state, photon absorption and decoloration or return to the ground state. The excitation of electrons with an appropriate wavelength of light to the metastable colored state is the first step, after which certain wavelengths of light may be absorbed. If these wavelengths are in the visible light range, colour change can be observed. However, if the absorbed light has enough energy to cause the electrons to return to the ground state the reverse process known as bleaching will take place. [16]

One of the known mechanisms include redox reactions, as is the case in glasses containing silver halide, which is reduced to silver particles upon exposure to UV. The metallic silver aggregates are formed on the surface of the material and absorb the incoming light resulting in colour change. In the dark, the reverse reaction occurs. Temporary F-center formation is another well-known tenebrescence mechanism. F-centers are point defects also known as colour centers, which can be described as anionic vacancies occupied by one or more unpaired electrons. [6]

Transition metal oxides like WO_3, TiO_2, V_2O_5, more robust oxides like $(K,Na)NbO_3$, $Y_3Al_2Ga_3O_{12}$ and $Na_8Al_6Si_6O_{24}Cl_2$ as well as RE doped compounds, one of which is CaF_2 commonly doped with Ce, Gd and Eu, and metal halides are some of the groups of inorganic materials with tenebrescent properties. [16]

Smart glasses, both lenses and windows or building facades, are the most prominent applications of tenebrescent materials. The first tenebrescent lenses were created in the 1970s using a borosilicate glass doped with copper and silver salts, that utilized the previously mentioned redox mechanism to create a layer of metallic silver on the glass surface. Recently, smart glazing for building facades and car windows, that allows better control of solar illumination, has been developed. Other applications of these types of materials include anti-counterfeiting, where tenebrescent inks are used to authenticate documents, light-based sensors and optical data storage due to the stability of the defects created during irradiation with electromagnetic radiation. [6]

1.3. Luminescence and tenebrescence in sodalites

Sodalites are a group of inorganic compounds with the general formula $A_8[M'M''O_4]_6X_2$. They are sometimes known as robust oxides as they are characterized by a symmetrical cage-like framework consisting of alternating $M'O_4$ and $M''O_4$ tetrahedra. In this formula M' and M'' represent Si and Al or other transition metals, while A and X are extra-framework cations and anions that are located in the cavities of these structures. Hackmanite $Na_8Al_6Si_6O_{24}(Cl,S)_2$ is the most well-known member of this group and possesses both luminescent and tenebrescent properties. [17]

Aluminosilicate sodalites (further referred to as hackmanites for convenience) are the most common type to be found naturally. They form in low silica alkaline rocks and thus mostly contain sodium, chloride, sulfide and/or sulfate as extra framework ions. Hackmanites acquired from various countries exhibit different tenebrescence properties. For example, Greenland hackmanite changes colour from pink to green, colourless or grey, while sodalites found in Norway, Afghanistan and Canada show colour change from pink to blue. Exhibiting tenebrescence does not necessarily guarantee strong luminescence as some of them show no luminescence at all. [18] These differences in minerals from various countries can be explained by different dopants characteristic to those specific environments and by analysing naturally occurring materials new insights into creating synthetic materials with tailored optical properties can be discovered.

When analysing natural hackmanites from Greenland, Koksha valley (Afghanistan), Mont Saint Hilaire (Canada) and Pakistan under, various luminescence bands, in addition to the orange emission from S_2^- ions that is characteristic to hackmanite, were observed. Under 295 nm UV excitation blue-green emission around 500 nm appeared in most of these and was assigned to Ti^{3+} ions interacting with oxygen vacancies. Red emission was also observed in Mont Saint Hilaire sample and is thought to originate from Fe^{3+} ions at the Al^{3+} site. [19] Mn^{2+} in Na^+ sites have been reported to produce luminescence centers with emission peak around 550 nm, Ce^{3+} is attributed to emissions peaking at around 365 nm and blue luminescence is attributed to O_2^-, which are defects in the aluminosilicate framework and require no external activators. [20]

The tenebrescence mechanism in hackmanite is possible due to the small concentration of sulfur, specifically S_2^{2-} ions, that substitute the Cl^- ion in some of the aluminosilicate cages, creating an anionic vacancy in the cage next to it in order to achieve charge neutrality. The colour change occurs when, during irradiation with UV, one of the electrons from the disulfide ion is transferred to the anionic vacancy and forms an F-center. It has also been noted that the Na_4 tetrahedron, which surrounds the anions, contracts around the F-center to stabilize it as the trapped electron attracts the cations and expands as the electron is transferred back to the sulfur ion during bleaching. The size of the sodalite cage affects the Na_4 tetrahedron's ability to expand thus also affecting the tenebrescence.

By exchanging the sodium ions with different alkaline ions the activation energy could also be controlled. [21]

Studies exchanging framework and extra-framework ions have been performed in order tune optical properties of hackmanites. It has been observed that by exchanging Al ions with Ga and Si ions with Ge the unit cell expands. Similar effect was obtained using larger extra-framework anions, such as Br and I instead of Cl, while partially replacing Na ions with Li resulted in the decrease of the unit cell. Both the size of the framework and the size of extra-framework ions affect the size of the anionic vacancy. The larger the vacancy the smaller the energy difference between the ground and the excited state, which allows even photons with a longer wavelength to promote excitation and the formation of F-centers. Therefore, by adjusting the size of the vacancy using different framework and extra-framework ions, it is possible to tune the colour of tenebrescence in sodalites. [22]

Based on these observations it can be concluded that by synthesizing a sodalite with a larger framework as well as using various dopants, new compounds with different luminescence and tenebrescence properties could be produced. Aluminate sodalite is a promising starting material, as it has been proven to be stable enough to exist [23], yet its optical properties have not been analysed.

1.4.   Synthesis of aluminate sodalites

Aluminate sodalites are quite unusual as they do not follow the Löwenstein's rule. This rule states that Al-O-Al bonds cannot exist in ordinary zeolites, meaning the AlO_4 tetrahedra must not share any oxygen atoms and thus the maximum allowed Si/Al ratio in any zeolite is Si/Al=1. There is a small number of other materials in which this rule is disobeyed, such as zeolite stilbite, bicchulite and aluminosilicate glasses. It has been observed that Löwenstein-disobeying materials with high Al content are often synthesized at very high temperatures. [24]

A variation of aluminate sodalite containing calcium and sulfate ions ($Ca_8Al_{12}O_{24}(SO_4)_2$, known as ye'elimite) is also the main component of sulfoaluminate cement. Solid state synthesis is the most common way to synthesize this material using $CaCO_3$, Al_2O_3 and $CaSO_4$ as precursors. While at 1100°C the precursors, CaO and $CaAl_2O_4$ are the main phases found in the mixture, ye'elimite also starts to form in small quantities. However, exceeding 1300°C the sodalite phase starts to decompose into $Ca_{12}Al_{14}O_{33}$, $CaAl_2O_4$ and $Ca_3Al_2O_6$. The sodalite content in samples at temperatures from 1100°C to 1300°C depends greatly on the sintering duration as the formation of the sodalite phase was accelerated at expense of the other aluminate phases. However, even at the optimal conditions the maximum sodalite content in the sample typically does not exceed around 85%. [25]

While solid-state synthesis is the commonly used method for ye'elimite synthesis due to its simplicity and suitability for large scale synthesis, other methods, like organic steric entrapment method, the Pechini method and self-propagating combustion method have also been used to synthesize various aluminate phases including sodalite. All three methods use an organic matrix to dissolve the precursors achieving a more homogenous mixture than in the case of solid-state synthesis. [26] Using these methods a slightly higher sodalite content up to 98% could be achieved, although $CaAl_2O_4$ and $CaAl_4O_7$ could still be detected in all samples. [27]

1.5. Luminescence and tenebrescence in aluminates

Various aluminate phases are known to be intermediates leading to the formation of the sodalite phase and also the result of the sodalite cage collapsing. Aluminates are important phosphor hosts and are frequently used in solid-state lighting, PeL phosphors, solid-state lasers, upconverting materials and scintillators. Yttrium aluminum garnet or YAG is one of the most versatile of aluminate phosphor hosts as it is used commercially in most of the previously mentioned applications. Even though dopants have a significant role in dictating the luminescence properties, the host itself can affect the absorption spectra of the material. For example, in $BaMgAl_{10}O_{17}:Eu^{2+}$ phosphor, the host absorbs radiation in the vacuum ultraviolet region (120-240 nm) and so through energy transfer from the host to the dopant, luminescence at these wavelengths is possible. [28] Eu and Nd doped $CaAl_2O_4$ is a PeL phosphor that emits blue light and even though lanthanides will not be used in this work, this information might give more insight into the luminescence properties of calcium aluminates. [29]

Dopant-free calcium aluminate glasses have been reported to be photochromic. The colour change that occurs during irradiation with UV is stable at temperatures up to 150°C and the bleaching takes place at temperatures above 250°C. Two colour centers in these materials have been determined to be ozonide (O_3^-) and an aluminum-oxygen hole center, a defect in which one of the oxygens on the aluminate ion is missing an electron. Both F-centers are paramagnetic and were discovered using electron paramagnetic resonance spectroscopy. [30]

2. EXPERIMENTAL

2.1. Aims of the project

The aim of this work is to analyze the effects of different extra-framework ions on the optical properties of aluminate sodalites:

1. $Ca_8Al_{12}O_{24}S_2$ will be synthesized first and then modified using various dopants.

2. S^{2-} ions will be exchanged with Cl^- ions, which are necessary for the tenebrescence mechanism, in various proportions.

3. Ca^{2+} ions will be exchanged with Li^+, Na^+, K^+ and Rb^+ ions.

2.2. Sample preparation

$Ca_8Al_{12}O_{24}Cl_4$, $Ca_8Al_{12}O_{24}S_2$ and $Ca_8Al_{12}O_{24}(S,Cl)_2$ with different S:Cl ratios were synthesized following the protocol reported by Brenchley and Weller. [23] Stoichiometric amounts of $CaCl_2$, $CaSO_4$, $CaCO_3$ and Al_2O_3 were ground up and mixed in an agate mortar. Mass amounts of used precursors can be seen in Table 2.1.

Table 2.1. Mass amounts of precursors depending on the sample S:Cl ratio.

S/Cl ratio	$m_{CaCl_2 \cdot 6H_2O}$, g	m_{CaSO_4}, g	m_{CaCO_3}, g	$m_{Al_2O_3}$, g
Cl_4	0.3744	-	0.5132	0.5228
$S_{0.2}Cl_{3.6}$	0.3392	0.0234	0.5166	0.5263
$S_{0.4}Cl_{3.2}$	0.3036	0.0472	0.5201	0.5298
$S_{0.6}Cl_{2.8}$	0.2674	0.0712	0.5236	0.5334
$S_{0.8}Cl_{2.4}$	0.2308	0.0956	0.5272	0.5370
S_1Cl_2	0.1936	0.1203	0.5308	0.5407
$S_{1.2}Cl_{1.6}$	0.1560	0.1454	0.5345	0.5445
$S_{1.4}Cl_{1.2}$	0.1178	0.1708	0.5382	0.5483
$S_{1.6}Cl_{0.8}$	0.0791	0.1966	0.5420	0.5521
$S_{1.8}Cl_{0.4}$	0.0398	0.2227	0.5458	0.5560
S_2	-	0.2492	0.5497	0.5600

Resulting mixture was transfered to an alumina crucible and heated at 1200°C for 20 hours in air atmosphere with a heating rate of 10°C/min. After heating $Ca_8Al_{12}O_{24}Cl_4$ and intermediates $Ca_8Al_{12}O_{24}(SO_4)_2$ and $Ca_8Al_{12}O_{24}(SO_4,Cl)_2$ were obtained.

First, two samples of $Ca_8Al_{12}O_{24}(SO_4)_2$ were reduced under 1) 50% H_2 and 50% N_2; 2) 12% H_2 and 88% N_2 atmosphere at 900°C for 8h using a heating rate of 10°C/min. X-ray powder

diffraction (XRD) patterns of each of the reduced samples were then recorded and quantitative phase analysis was carried out using the reference intensity ratio method. Results of quantitative phase analysis showed that both samples had approximately 80% $Ca_8Al_{12}O_{24}S_2$ content, thus the rest of $Ca_8Al_{12}O_{24}(SO_4,Cl)_2$ samples were reduced under 12% H_2 and 88% N_2 atmosphere.

$S_{1.4}Cl_{1.2}$ sample showed high photoluminescence intensity and duration and good TL intensity and thus was chosen as the optimal S/Cl ratio for the alkali metal doped samples. Samples doped with Li, Na, K and Rb ions were synthesized by exchanging $CaCl_2$, $CaSO_4$ and $CaCO_3$ with corresponding alkali metal salts. Mass amounts of used precursors for the doped samples can be seen in Table 2.2.

Table 2.2. Mass amounts of precursors depending on sample Ca/alkali metal ratio.

Li/Ca ratio	m_{CaSO_4}, g	m_{CaCO_3}, g	$m_{Al_2O_3}$, g	m_{LiCl}, g	$m_{Li_2SO_4·H_2O}$, g	$m_{Li_2CO_3}$, g
$Li_{1.2}Ca_{7.4}$	0.1733	0.5459	0.5561	0.0462	-	-
Li_4Ca_6	-	0.6222	0.6338	0.0478	0.1685	-
Li_8Ca_4	-	0.3960	0.6051	0.0503	0.1772	0.1462
$Li_{12}Ca_2$	-	0.2088	0.6382	0.0531	0.1869	0.3083
Li_{16}	-	-	0.6751	0.0561	0.1977	0.4892
Na/Ca ratio	m_{CaSO_4}, g	m_{CaCO_3}, g	$m_{Al_2O_3}$, g	m_{NaCl}, g	$m_{Na_2SO_4}$, g	$m_{Na_2CO_3}$, g
$Na_{1.2}Ca_{7.4}$	0.1703	0.5365	0.5465	0.0626	-	-
Na_4Ca_6	-	0.5326	0.5425	0.0622	0.1763	-
Na_8Ca_4	-	0.3513	0.5369	0.0615	0.1745	0.1860
$Na_{12}Ca_2$	-	0.1739	0.5313	0.0609	0.1727	0.3683
Na_{16}	-	-	0.5259	0.0603	0.1710	0.5468
K/Ca ratio	m_{CaSO_4}, g	m_{CaCO_3}, g	$m_{Al_2O_3}$, g	m_{KCl}, g	$m_{K_2SO_4}$, g	$m_{K_2CO_3}$, g
$K_{1.2}Ca_{7.4}$	0.1674	0.5274	0.5372	0.0786	-	-
K_4Ca_6	-	0.5038	0.5132	0.0751	0.2047	-
K_8Ca_4	-	0.3157	0.4823	0.0705	0.1924	0.2179
$K_{12}Ca_2$	-	0.1489	0.4550	0.0665	0.1814	0.4111
K_{16}	-	-	0.4306	0.0630	0.1717	0.5836
Rb/Ca ratio	m_{CaSO_4}, g	m_{CaCO_3}, g	$m_{Al_2O_3}$, g	m_{RbCl}, g	$m_{Rb_2SO_4}$, g	$m_{Rb_2CO_3}$, g
$Rb_{1.2}Ca_{7.4}$	0.1596	0.5028	0.5122	0.1215	-	-

2.3. Sample characterization

After the synthesis, elemental and phase composition of the final products were analyzed using XRD and X-ray fluorescence spectroscopy (XRF).

After the two-step synthesis, the powdered sample was removed from the alumina crucible and ground up to ensure homogeneity. It was placed in a stainless-steel sample holder with a silica cavity to minimize the background and a 7-minute XRD measurement was performed.

XRD patterns were obtained using PANalytical Aeris powder X-ray diffractometer operating at 40.0 kV and 7.5 mA with PIXcel1D-Medipix3 detector and Cu-K$_{\alpha 1, \alpha 2}$ radiation (λ = 1.5406 Å, 1.5444 Å). The following optical and data collection settings were used: nickel beta-filter, 0.04 rad soller slits, 1/4° divergence slit, 13 mm fixed mask, high beam knife, 9 mm anti-scatter slit, 1 rps spinner speed, scan rate of 0.201 °/s and step size of 0.0217°. XRD patterns were analysed using HighScore software [31] that employs the ICDD PDF-4+ database [32]. Background was determined with a bending factor of 2 and granularity 20 using smoothed input data. Peaks with a minimum significance of 3.00, minimum tip width: 0.01, maximum tip width: 1.00, peak base width: 2.00 were searched using the minimum 2nd derivative method and compared to a pattern list found in the ICDD PDF-4+ database. Phase composition was analysed via quantitative phase analysis using available background as the method in global variables.

After XRD, the elemental composition of the samples was analysed using PANalytical Epsilon 1 X-ray fluorescence spectrometer with internal Omnian calibration, a 50 kV Ag-anode X-ray tube with K$_\alpha$ emission at $\approx$ 22 keV and SDD5 detector. The powder sample was placed in a sample holder covered by a translucent film at the bottom and placed in the sample compartment of the instrument for an hour-long measurement. Elements heavier than sodium and lighter than uranium could be detected using this instrument.

2.4. Luminescence spectroscopy

Luminescence emission spectra of the samples were taken during irradiation with 254, 302 and 365 nm UV radiation. The emission peaks seen in these spectra were then used to obtain the excitation spectra.

Varian Cary Eclipse fluorescence spectrometer was used in phosphorescence mode during excitation and emission measurements and the parameters were total decay time of 0.0051 s, delay time: 0.1 ms, gate time: 5.0 ms, number of flashes: 1, excitation slit: 10 nm, emission slit: 2.5 nm, data interval: 0.2000 nm, delay time: 0.0050 s, medium and high PMT detector voltage. No filters were used during these measurements.

PeL emission spectra were also measured using the Varian Cary Eclipse spectrometer after irradiating the samples for 5 minutes with 254 nm UV radiation. There was 1 minute waiting time between irradiation and the measurement that was performed in the bio-/chemiluminescence mode.

Measurement parameters used to obtain the PeL emission spectra were emission slit: 20 nm, data interval: 1.0 nm and high PMT detector voltage.

Additionally, emission spectra of samples under irradiation with 254, 302 and 365 nm UV radiation were also obtained using Edinburgh Instruments FLS-1000 spectrometer in order to confirm the presence of excitation harmonics in the emission spectra obtained using Varian Cary Eclipse spectrometer. This spectrometer can be equipped with a long-pass filter allowing to filter out the said excitation harmonics.

Measurement parameters of Edinburgh Instruments FLS-1000 spectrometer were Xenon lamp as the radiation source, reference correction and scan correction by file, excitation bandwidth: 2.00 nm, emission bandwidth: 1.00 nm, dwell time: 0.20 s, step: 0.50 nm and Visible PMT-900 detector. 331 nm long-pass emission filter was also used for the 254 and 302 nm emission spectra.

2.5.   Thermoluminescence

Approximately 10 mg of the sample was placed in an aluminum sample holder and heated up to 400°C in the TL apparatus to empty all the traps. Then the sample was irradiated with 254, 302, 365 nm UV radiation and standard solar spectrum for 5 minutes. The sample was placed in the TL apparatus and glow curves were measured 1 minute after irradiation.

Glow curves were obtained using MikroLab Thermoluminescent Materials Laboratory Reader RA'04 apparatus (software Mikrolab, TLD Reader/Analyser v0.9.401, 2001). The heating parameters were test: 1750, heat rate: 10.0 C/s, max temp: 400.0 C, temp 1: 40.0 C, temp 2: 265.0 C, temp 3: 400.0 C, time 1: 1.00 s, time 2: 1.00 s, time 3: 1.00 s, time test: 10.00 s, time BKGN: 60.00 s, ACOMP-M: 4, ACOMP-T: 8.

LOT QD LS0500 solar simulator, UVP model UVLS-24 EL 4W 254/365 nm hand-held lamp and Analytik Jena model UVM-57 6 W 302 nm hand-held lamp were used as irradiation sources.

2.6.   Luminance fading

Immediately after irradiating samples with 254, 302, 365 nm UV radiation and standard solar spectrum for 5 minutes PeL fading was quantified using a Hagner ERP-105 luminance photometer with Hagner SD-27 detector coupled to a Fluke 189 multimeter, the control software being FlukeView Forms v3.8.0003, 2014.

2.7. Reflectance

Reflectance spectra of the samples before and after irradiation with 254 UV radiation was obtained using an Avaspec HS-TEC CCD detector. AvaLight-DHc deuterium-halogen lamp with the wavelength range of 200 to 2500 nm was used as the light source during measurement.

First, light and dark references were taken using a MgO powder as a standard due to its high reflectivity. A fresh sample was placed on a plastic, non-luminescent sample holder and reflectance of the sample before irradiation was taken. The position of the lamp and sample holder did not change, and no other light sources were used during measurements. Samples were irradiated with 254 nm UV in complete darkness for 5 minutes, after which the lamp was switched on and reflectance was immediately measured. Due to most of the samples exhibiting PeL, another measurement was taken 10 minutes after irradiation. The samples were kept in complete darkness during the waiting period as to not promote further optical bleaching. In some samples, reflectance was also measured for a fresh sample and sample after XRF measurements due to a noticeable change in colour.

3. RESULTS AND DISCUSSION

3.1. Composition, luminescence, and reflectance of samples with different S/Cl ratios

Calcium aluminate sodalite samples with different S/Cl ratios were synthesized. The result was a mixture of different phases: sodalites and various species of aluminates. The content of these samples and their optical properties will be discussed in the following chapters.

3.1.1. X-ray powder diffraction and X-ray fluorescence spectroscopy

First $Ca_8Al_{12}O_{24}S_2$ containing no chloride ions was synthesized in order to analyse the luminescence and tenebrescence properties of the base material.

XRD patterns of $Ca_8Al_{12}O_{24}(SO_4)_2$ intermediates before the reduction, seen in Fig. 1., show the main sodalite phase as well as a non-stoichiometric aluminate $Ca_{12}Al_{14}O_{32.55}$. It has been reported that when synthesizing $Ca_8Al_{12}O_{24}(SO_4)_2$, aluminate phases $CaAl_2O_4$, $CaAl_4O_7$ and $Ca_{12}Al_{14}O_{32.55}$ begin to form at around 1100°C-1200°C. By sintering the reaction mixture at temperatures 1200°C-1300°C formation of $Ca_8Al_{12}O_{24}(SO_4)_2$ is accelerated at the expense of these aluminate phases, specifically $CaAl_2O_4$ and $CaAl_4O_7$. $Ca_{12}Al_{14}O_{32.55}$ in this case could be the unreacted intermediate, however, it could also be a decomposition product as $Ca_8Al_{12}O_{24}(SO_4)_2$ is known to decompose at temperatures higher than 1300°C or when heated at 1200°C for more than four hours. [25]

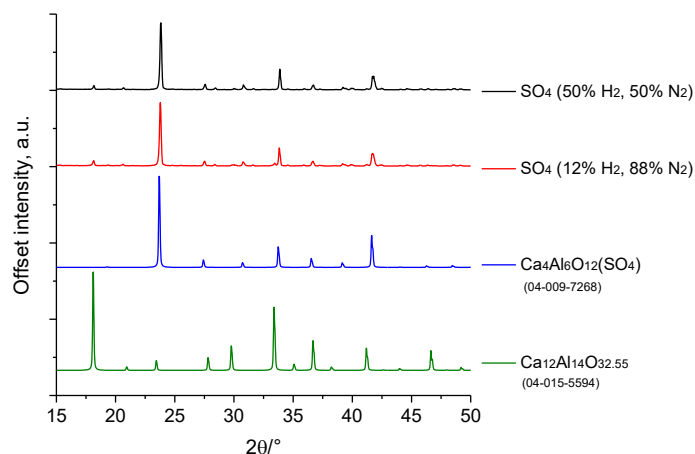**Fig. 1.** *XRD patterns of $Ca_8Al_{12}O_{24}(SO_4)_2$ intermediates before reduction and the reference patterns of phases found in database (ICDD reference code can be seen below each compound).*

XRD patterns for the $Ca_8Al_{12}O_{24}S_2$ samples reduced in 1) 50% H_2 and 50% N_2 atmosphere; 2) 12% H_2 and 88% N_2 atmosphere can be seen in Fig. 2. The diffractograms show that the mixtures consist of $Ca_8Al_{12}O_{24}S_2$ (approximately 80% in both samples according to the quantitative phase analysis), unreacted $Ca_8Al_{12}O_{24}(SO_4)_2$ and trace amounts of $Ca_{12}Al_{14}O_{32.55}$. It is likely that

$Ca_{12}Al_{14}O_{32.55}$ is the same one observed in the samples after the first synthesis step, and it has not reacted during reduction.

Due to both reduction methods yielding similar results, the rest of the samples were reduced in a 12% H_2 and 88% N_2 atmosphere.
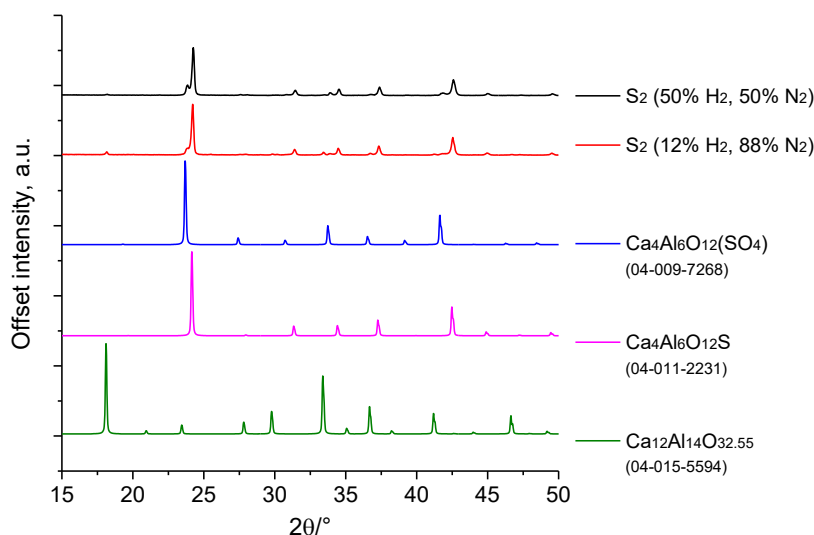

Fig. 2. *XRD patterns of $Ca_8Al_{12}O_{24}S_2$ samples reduced in 1) 12% H_2 and 88% N_2 atmosphere, 2) 50% H_2 and 50% N_2 atmosphere and the reference patterns of phases found in database (ICDD reference code can be seen below each compound).*

There was an attempt to also synthesize a calcium sodalite containing only chloride anions, which thus far has not been described in the literature to the knowledge of the author. Stoichiometric mixture was treated to the same two-step synthesis as all the other samples, however, the result was a mixture of non-sodalite aluminates as seen in Fig. 3.
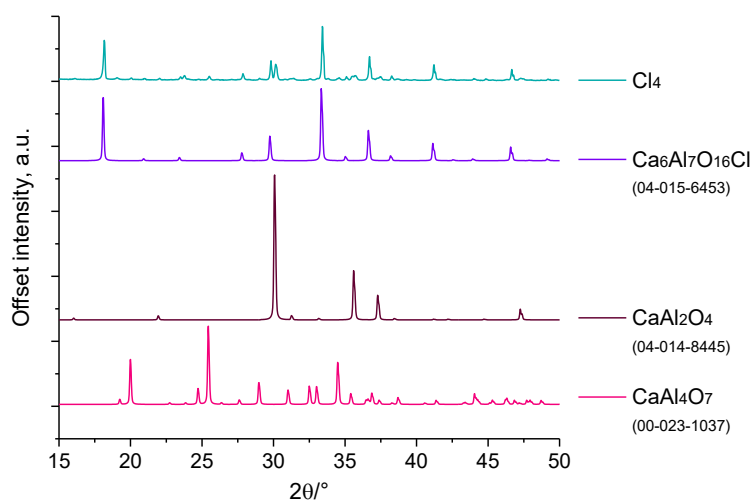
Fig. 3. *XRD patterns of the chloride containing aluminate mixture and the reference patterns of phases found in database (ICDD reference code can be seen below each compound).*

$Ca_6Al_7O_{16}Cl$, $CaAl_2O_4$ and $CaAl_4O_7$ where the three phases found in the sample. According to quantitative phase analysis $Ca_6Al_7O_{16}Cl$ was the phase with the highest concentration at 68.7%, $CaAl_2O_4$ had the second highest concentration at 22.0% while $CaAl_4O_7$ made up only 9.3% of the sample. The presence of both $CaAl_2O_4$ and $CaAl_4O_7$ was observed and explained in the S containing samples, while $Ca_6Al_7O_{16}Cl$ is a variation of $Ca_{12}Al_{14}O_{33}$, the stoichiometric version of $Ca_{12}Al_{14}O_{32.55}$. $Ca_{12}Al_{14}O_{33}$, also known as mayenite, which similarly to sodalites forms a cage-like structure capable of containing an anion, in this case – chloride ion to form chlormayenite. [33]

The lack of sodalite-like patterns seen in the diffractogram of this sample could mean that synthesis of a calcium aluminate sodalite containing only Cl ions is not possible at least at these conditions. This could be due to the large amount of extra-framework anions necessary to achieve charge neutrality.

The XRD patterns of samples containing both S and Cl ions in different ratios can be seen in Fig. 4.
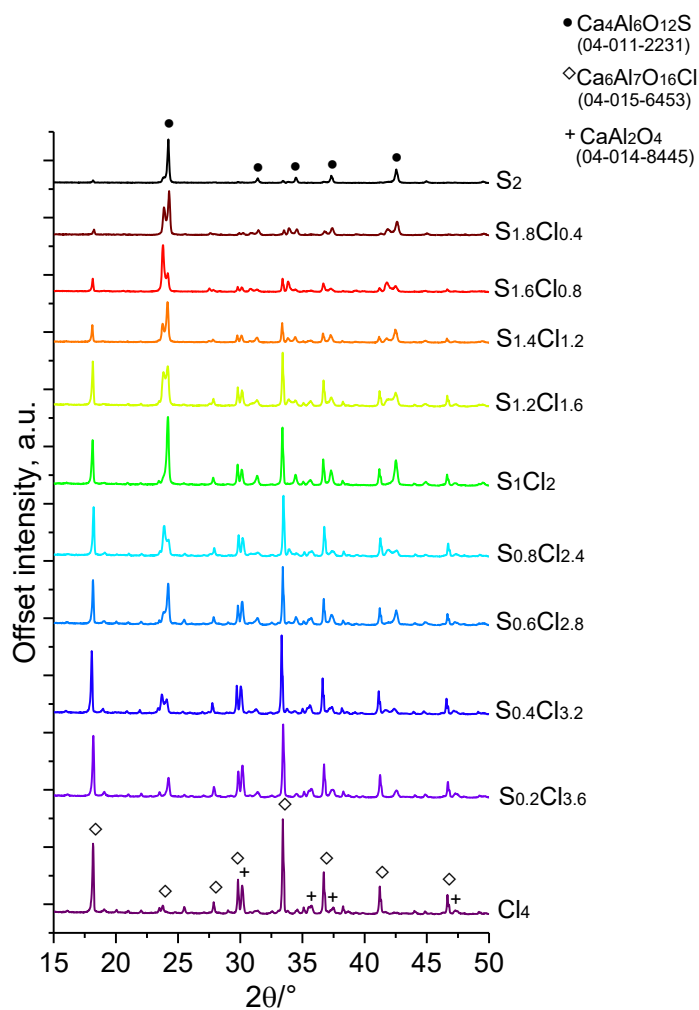

Fig. 4. *XRD patterns of $Ca_8Al_{12}O_{24}(S,Cl)_2$ samples with different S/Cl ratios, three main phases $Ca_8Al_{12}O_{24}S_2$, $Ca_6Al_7O_{16}Cl$ and $CaAlO_4$ have been marked.*

$Ca_8Al_{12}O_{24}S_2$, $Ca_8Al_{12}O_{24}(SO_4)_2$, $Ca_6Al_7O_{16}Cl$ and $CaAl_2O_4$ and small amounts of other aluminates were the main phases found in $Ca_8Al_{12}O_{24}(S,Cl)_2$ samples. Sample composition calculated from the diffraction patterns using quantitative phase analysis can be seen in Table 3.1. In almost all samples the total percentage of sulfur containing phases increases by roughly 10% except for $S_{0.8}Cl_{2.4}$ sample, which has almost the same percentage as $S_{0.6}Cl_{2.8}$ and S_2 sample, which has a similar percentage to $S_{1.8}Cl_{0.4}$.

Table 3.1. Composition of synthesized samples calculated using quantitative phase analysis.

	Phase composition			
	$Ca_8Al_{12}O_{24}S_2$, %	$Ca_8Al_{12}O_{24}(SO_4)_2$, %	$Ca_6Al_7O_{16}Cl$, %	$CaAl_2O_4$ or other aluminates, %
Cl_4	-	-	68.7	31.3
$S_{0.2}Cl_{3.6}$	10.3	-	54.4	35.3
$S_{0.4}Cl_{3.2}$	9.3	10.2	49.2	31.3
$S_{0.6}Cl_{2.8}$	28.1	-	42.7	29.2
$S_{0.8}Cl_{2.4}$	12.3	18.8	46.4	22.4
S_1Cl_2	41.0	11.1	41.0	16.9
$S_{1.2}Cl_{1.6}$	27.7	31.7	40.6	-
$S_{1.4}Cl_{1.2}$	45.1	18.6	25.8	10.5
$S_{1.6}Cl_{0.8}$	22.5	61.1	16.5	-
$S_{1.8}Cl_{0.4}$	55.8	34.8	9.4	-
S_2	80.7	11.9	-	7.4

In most samples during the reduction step a significant amount of $Ca_8Al_{12}O_{24}(SO_4)_2$ had not been reduced despite being heated at 900°C in a reducing atmosphere for 8 hours. Similarly to the chloride-only sample, the main non-sodalite phase that formed during the synthesis of the $Ca_8Al_{12}O_{24}(S,Cl)_2$ samples was $Ca_6Al_7O_{16}Cl$.

Elemental composition of the samples was analysed using XRF and the most abundant elements can be seen in Table 3.2. The weight percentage of Ca and Al was almost the same in all samples, which was expected. In most samples the Cl concentration decreased gradually with increasing S concentration, however, there was a sudden increase in Cl content in the Cl_1S_2 and $S_{1.2}Cl_{1.6}$ samples. However, based on the total percentage of sulfur containing phases discussed previously, it is unlikely that this would have had a significant impact on the formation of the sodalite phases. Si and Mg are elements that were not expected to be present in these samples especially in such high percentages.

The concentration of both elements combined is about the same as the concentration of the anions S and Cl, thus it is unlikely that they would be present as impurities in any of the precursors. Si has been known to show up in high-Al samples such as hackmanites and could be misidentified Al atoms. Mg, however, is more difficult to explain, although one of the possibilities is that they could be misidentified Ca atoms.

Table 3.2. Most abundant elements in samples with different S:Cl ratios.

	Ca, wt%	Al, wt%	Cl, wt%	S, wt%	Si, wt%	Mg, wt%
Cl_4	59	31	4.1	0.3	1.1	3.7
$S_{0.2}Cl_{3.6}$	58	33	3.5	0.5	1.1	3.4
$S_{0.4}Cl_{3.2}$	58	33	3.3	1.0	1.1	3.3
$S_{0.6}Cl_{2.8}$	57	33	3.0	1.4	1.1	3.8
$S_{0.8}Cl_{2.4}$	57	33	2.7	1.9	1.1	3.7
S_1Cl_2	58	31	3.5	2.1	1.1	3.4
$S_{1.2}Cl_{1.6}$	58	32	2.8	2.8	1.1	3.5
$S_{1.4}Cl_{1.2}$	56	33	1.8	3.9	1.1	4.3
$S_{1.6}Cl_{0.8}$	55	33	1.3	4.9	1.0	4.1
$S_{1.8}Cl_{0.4}$	56	33	0.5	5.6	1.0	3.6
S_2	53	36	0.4	6.0	1.0	4.1

3.1.2. Reflectance and luminescence measurements

Photoluminescence emission and excitation spectra of the samples were obtained using Varian Cary Eclipse spectrometer, however, the presence of excitation harmonics in some emission spectra was analysed using Edinburgh Instruments spectrometer with a long pass filter. Thermoluminescence glow curves and PeL fading curves after irradiation with UV and solar lamp for 5 minutes were also obtained. Finally, reflectance of the samples before and after irradiation with 254 nm UV was compared.

First the luminescence emission spectra of the three main phases- $Ca_8Al_{12}O_{24}S_2$, $Ca_8Al_{12}O_{24}(SO_4)_2$ and the non-sodalite aluminates- was measured using Varian Cary Eclipse spectrometer. Photoluminescence of these samples during irradiation with 254, 302 and 365 nm UV radiation can be seen in Fig. 5.
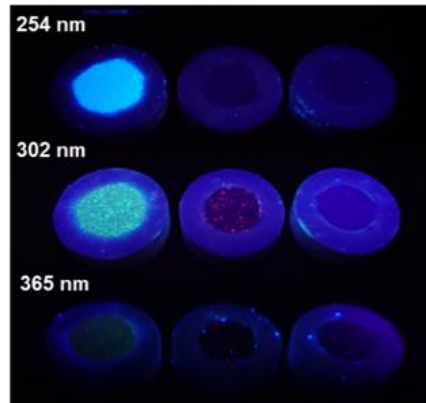
Fig. 5. *From left, photoluminescence of $Ca_8Al_{12}O_{24}S_2$, $Ca_8Al_{12}O_{24}(SO_4)_2$ and $Ca_8Al_{12}O_{24}Cl_4$ (aluminate mixture) under 254, 302 and 365 nm UV radiation.*

As can be seen in the figure above, only the reduced sodalite phase $Ca_8Al_{12}O_{24}S_2$ shows high intensity luminescence in the blue light region when irradiated with 254 and 302 nm radiation, while the non-reduced sodalite phase $Ca_8Al_{12}O_{24}(SO_4)_2$ shows weak luminescence in the red region when irradiated with 302 nm radiation. Under 365 nm radiation no luminescence is observed in any of the samples and the chloride-only aluminate mixture shows no observable luminescence under any type of radiation. The emission spectra of these samples can be seen in Fig. 6.
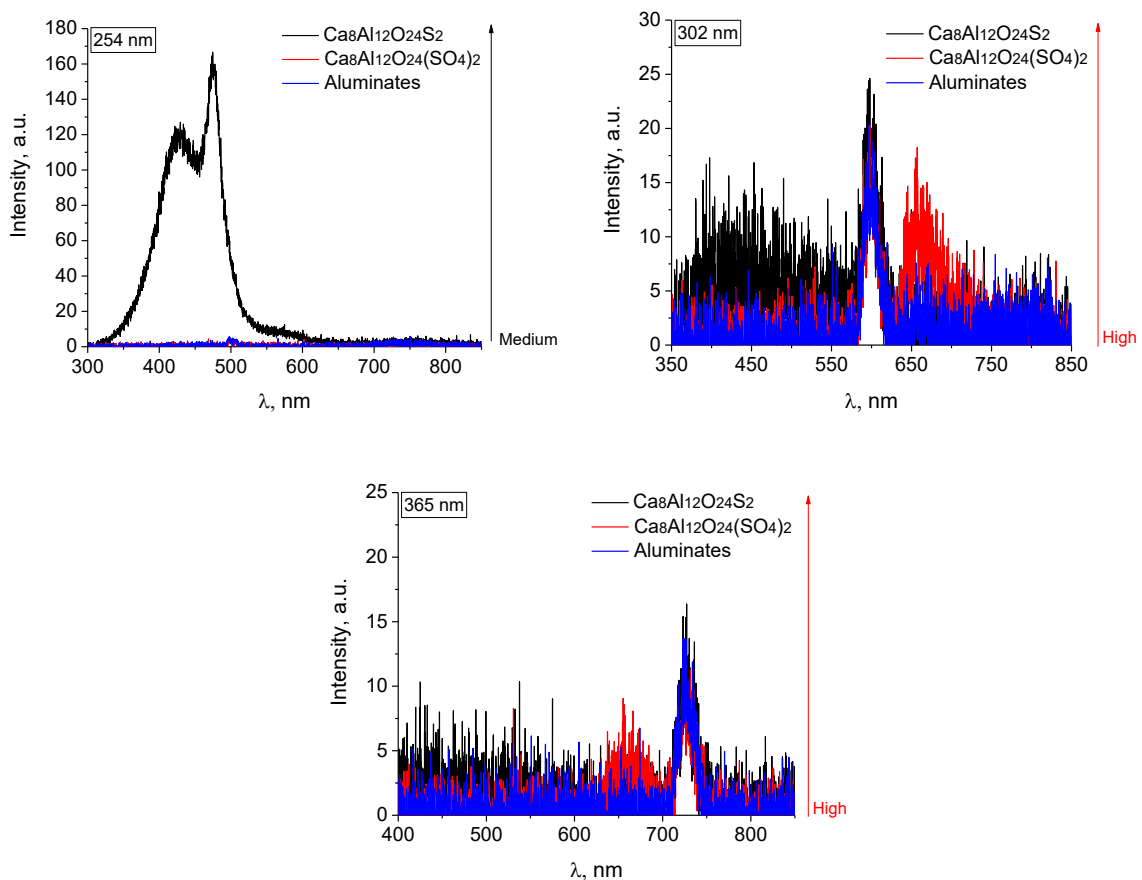
Fig. 6. *Emission spectra of $Ca_8Al_{12}O_{24}S_2$, $Ca_8Al_{12}O_{24}(SO_4)_2$ and $Ca_8Al_{12}O_{24}Cl_4$ (aluminate mixture) under 254, 302 and 365 nm UV radiation.*

22

$Ca_8Al_{12}O_{24}S_2$ emission spectrum under 254 nm radiation shows two peaks around 420 and 480 nm, under 302 nm radiation the same two peaks can be seen as well as a peak around 600 nm. When irradiated with 302 nm UV the peak at 600 nm is present in all samples. This could be due to excitation harmonics, higher orders of excitation wavelength caused by the monochromator, as the emission wavelength is twice as long as the excitation wavelength. The only peak seen in the emission spectra of the samples under 365 nm radiation is around 730 nm, which could also be due to excitation harmonics. $Ca_8Al_{12}O_{24}(SO_4)_2$ shows a single peak around 660 nm under 302 nm UV.

Luminescence emission spectra of the $Ca_8Al_{12}O_{24}(S,Cl)_2$ samples when irradiated with 254, 302 and 365 nm UV radiation measured using Varian Cary Eclipse spectrometer can be seen in Fig. 7.
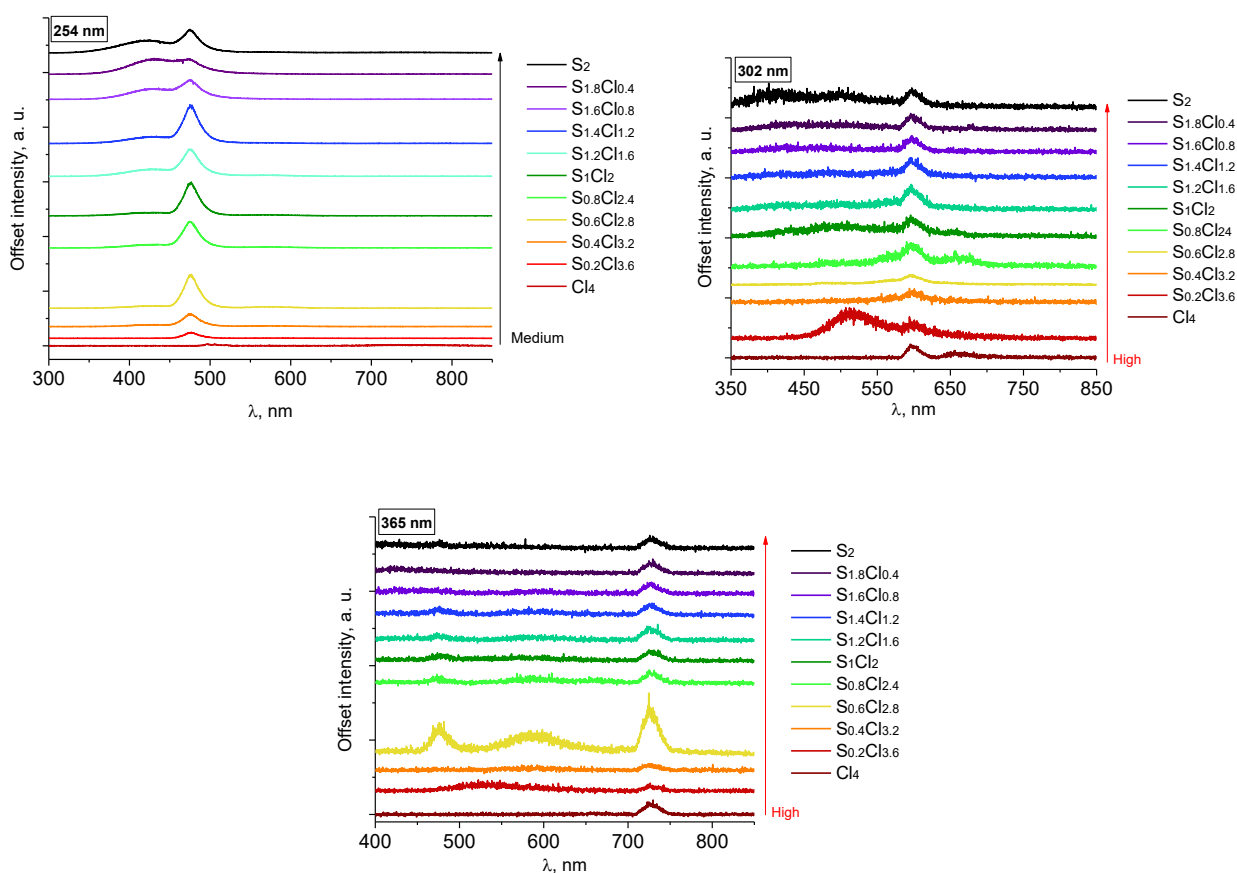
Fig. 7. *Emission spectra of $Ca_8Al_{12}O_{24}S_2$, $Ca_8Al_{12}O_{24}Cl_4$ (aluminate mixture) and $Ca_8Al_{12}O_{24}(S,Cl)_2$ samples during irradiation with 254, 302 and 365 nm UV radiation (arrows on the right side of the graph show detector sensitivity that was used to measure emissions of different samples).*

When irradiated with 254 nm UV emission peaks at 430 and 480 nm were observed. These are the same peaks that could be seen in the $Ca_8Al_{12}O_{24}S_2$ sample. When irradiated with 302 nm UV a peak at 600 nm is present in all samples, potentially due to excitation harmonics. Other peaks around 510 and 660 nm could also be observed in some samples. The peak around 660 nm is likely from the

$Ca_8Al_{12}O_{24}(SO_4)_2$ phase. When irradiated with 365 nm UV a peak around 730 nm was present in all samples, similarly to the 600 nm emission mentioned previously, this could also be due to excitation harmonics. Other peaks were observed only in $S_{0.6}Cl_{2.8}$ sample.

During irradiation with 302 nm UV orange luminescence could be observed in some of the low-sulfur high-chloride samples, which seemed to suggest that the emission at 600 nm could be more than just excitation harmonics. Photos of the $S_{0.6}Cl_{2.8}$ sample under 254 and 302 nm radiation can be seen in Fig. 8. Based on these observations another spectrometer equipped with long pass filters was used to take the emission spectra at 254 and 302 nm without the interference of excitation harmonics.
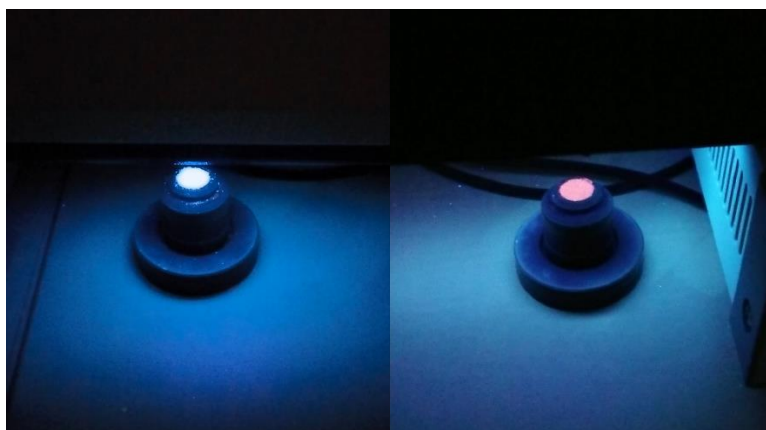
Fig. 8. *Photoluminescence of sample $S_{0.6}Cl_{2.8}$ during irradiation with 254 nm (left) and 302 nm (right) UV radiation.*

Emission spectra taken using Edinburgh Instruments spectrometer with a long pass filter can be seen in Fig. 9. While there was no difference in the emission spectra under 254 nm UV radiation, under 302 nm UV radiation a wide peak around 620 nm could be seen in the low-sulfur samples. This corresponds to the previously mentioned orange luminescence that could be observed while irradiating the samples. It is also slightly different from the luminescence of the $Ca_8Al_{12}O_{24}(SO_4)_2$ phase under 302 nm UV, which showed a peak around 660 nm. The emission peak is only present in samples with S/Cl ratio lower than S_1Cl_2 meaning that in other samples emission peak around 600 nm was likely due to excitation harmonics. It also means that it is unlikely that the luminescence around 620 nm is caused by the $Ca_8Al_{12}O_{24}(SO_4)_2$ phase, since samples with higher S/Cl ratio had a higher $Ca_8Al_{12}O_{24}(SO_4)_2$ content than that of samples with a lower S/Cl ratio. It must be noted that other peaks seen in the 302 nm emission spectra taken with the Varian Cary Eclipse spectrometer also do not show up in the emission spectra measured using the long pass filter.
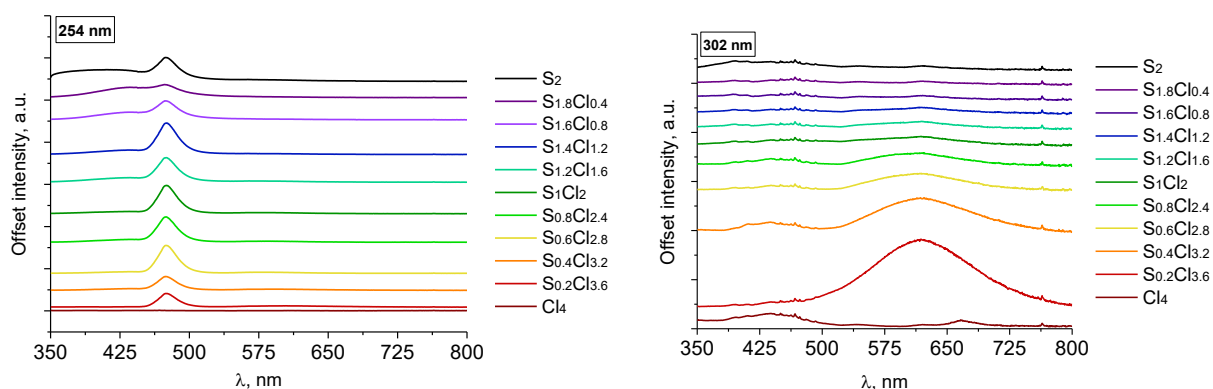
Fig. 9. *Emission spectra of $Ca_8Al_{12}O_{24}S_2$, $Ca_8Al_{12}O_{24}Cl_4$ (aluminate mixture) and $Ca_8Al_{12}O_{24}(S,Cl)_2$ samples during irradiation with 254 and 302 nm UV radiation measured using Edinburgh Instruments luminescence spectrometer.*

Excitation spectra of the most prominent emission peaks measured using the Varian Cary Eclipse spectrometer can be seen in Fig. 10. Emission peaks around 430 and 480 nm could be observed in most sulfur containing samples under 254 nm radiation, peaks around 580 and 600 nm were observed under 302 nm UV in low-sulfur samples. The excitation spectra of 580, 600, 730 nm emissions showed the highest emission intensity when irradiated with UV around 250 nm. Excitation spectra of the 480 nm emission shows two distinct peaks when irradiated with 230 and 250 nm radiation and spectra of the 430 nm emission shows highest intensity when irradiated with 230 nm radiation. Since the excitation spectra of the 730 nm emission peak shows hardly any emission intensity when irradiated with 365 nm radiation, it is safe to assume that it is likely to be caused by excitation harmonics in the emission spectra.
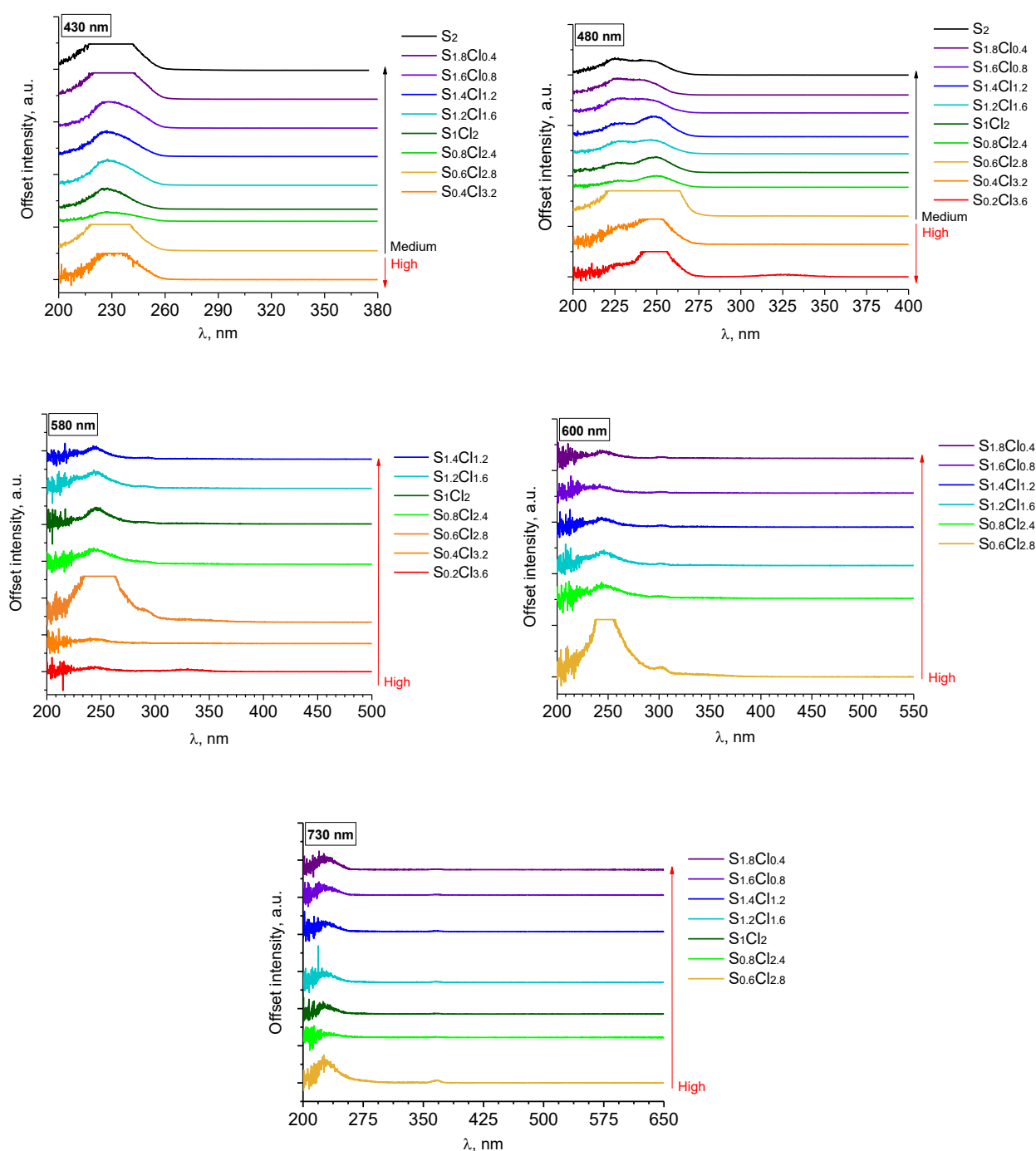
Fig. 10. *Excitation spectra of emissions around 430, 480, 580, 600 and 730 nm in $Ca_8Al_{12}O_{24}S_2$, $Ca_8Al_{12}O_{24}Cl_4$ (aluminate mixture) and $Ca_8Al_{12}O_{24}(S,Cl)_2$ samples (arrows on the right side of the graph show detector sensitivity).*

PeL is one of the most important properties in potential persistent luminescence phosphors, which is why PeL emission spectra of all samples measured one minute after irradiation with 254 nm UV was measured using the Varian Cary Eclipse spectrometer. Emission spectra can be seen in Fig. 11.
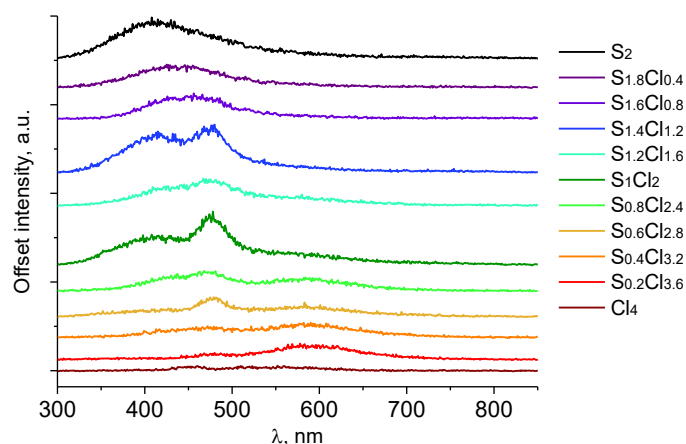
Fig. 11. *PeL emission spectra of the Ca$_8$Al$_{12}$O$_{24}$S$_2$, Ca$_8$Al$_{12}$O$_{24}$Cl$_4$ (aluminate mixture) and Ca$_8$Al$_{12}$O$_{24}$(S,Cl)$_2$ samples after irradiation with 254 nm UV radiation for 5 minutes.*

All sulfur containing samples exhibit PeL one minute after irradiation with UV. A peak with the maximum around 410-430 nm can be seen in samples S$_{1.8}$Cl$_{0.4}$ – S$_{0.8}$Cl$_{2.4}$ and the peak around 480 nm can be seen in almost all samples. In samples S$_2$ – S$_{1.6}$Cl$_{0.8}$ the shape of the emission suggests that there could be two overlapping peaks that could correspond to the previously mentioned 410-430 and 480 nm peaks in other samples. Emission around 430 and 480 nm was previously observed in the emission spectra during irradiation with 254 nm. A peak at 600 nm could only be observed in samples with lower sulfur content (S$_{0.8}$Cl$_{2.4}$ to S$_{0.2}$Cl$_{3.6}$). Excitation spectra showed the emission peak around 600 nm being most intense when irradiated with 250 nm radiation, which would explain the presence of this peak in the PeL spectra. PeL with emission peaks around 470 and 570 nm have also been observed in hackmanites after irradiation with 254 nm UV radiation. [17]

PeL fading was also measured to assess how long PeL lasts in each sample depending on irradiation wavelength. Each sample was irradiated with 254, 302, 365 nm UV or the solar lamp for 5 minutes and the fading curves were measured immediately after irradiation. 0.32 mcd/m^2 was assigned as the baseline luminance value, which is set as the standard limit by DIN 67510−1:2009−11. PeL fading curves can be seen in Fig. 12.

The longest time that luminescence could be detected above the assigned baseline was just below 300 seconds for 254 nm, around 800 seconds for 302 nm, around 4 seconds for 365 nm and around 35 for the solar lamp. Although there did not seem to be a direct correlation between the elemental composition of the samples and the duration of PeL, the samples S$_{1.4}$Cl$_{1.2}$ – S$_{0.2}$Cl$_{3.6}$, with some exceptions, showed the best results for both the duration and intensity of PeL. The initial light intensity also did not correlate with the duration of luminescence.
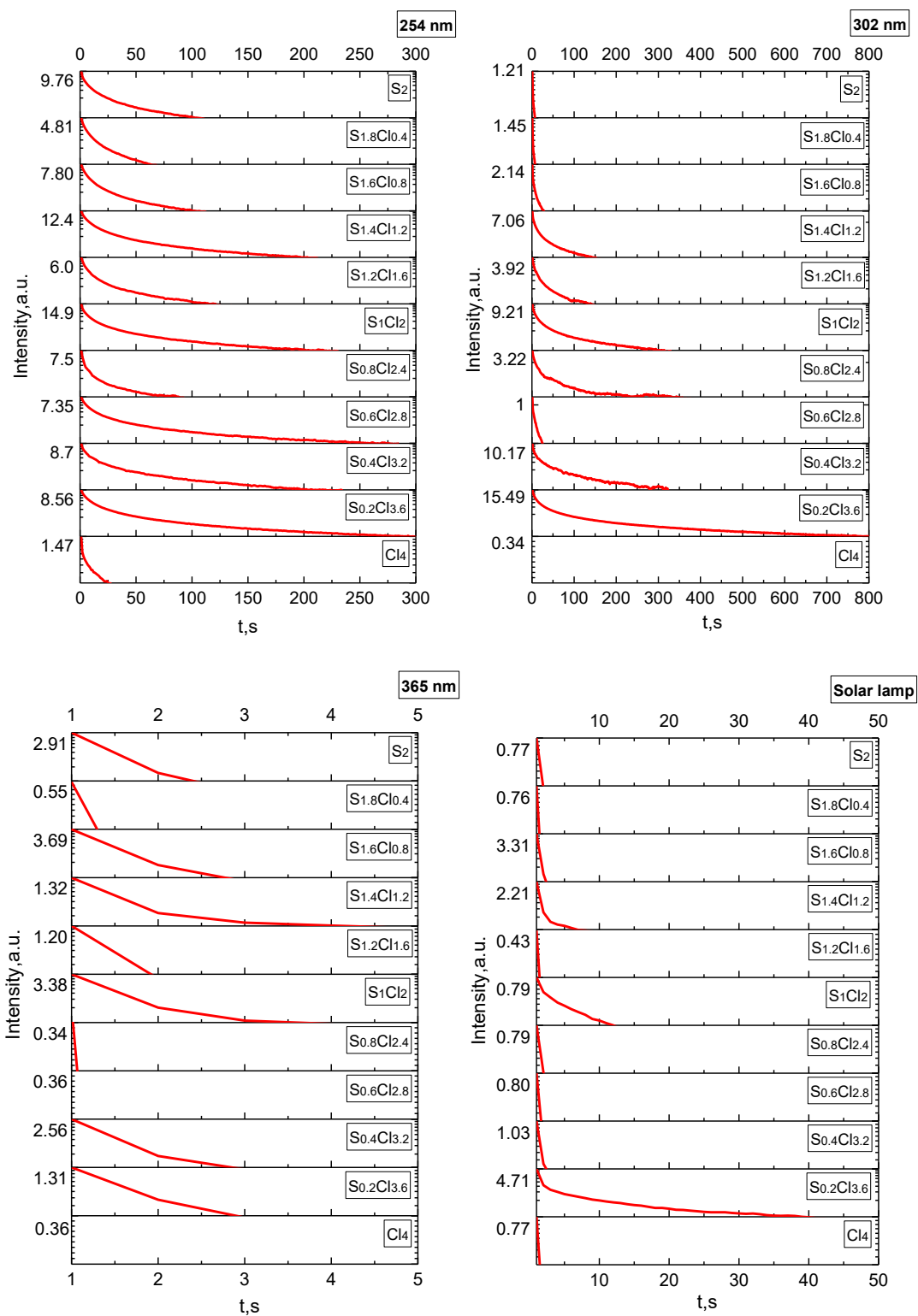
Fig. 12. *PeL fading in samples irradiated with 254, 302, 365 nm UV radiation and radiation from a solar lamp (only the highest intensity value is shown in each curve, lowest intensity value in all curves is 0.32 mcd/m²).*

TL measurements were performed to assess the charge storage capacity of these samples. They were heated up 400°C temperature before irradiation to remove any defects that might have already formed during the synthesis or from exposure to other light sources. Samples were then irradiated

with 254, 302, 365 nm UV and solar lamp for five minutes and TL was measured one minute after switching off the radiation source. TL glow curves can be seen in Fig. 13.
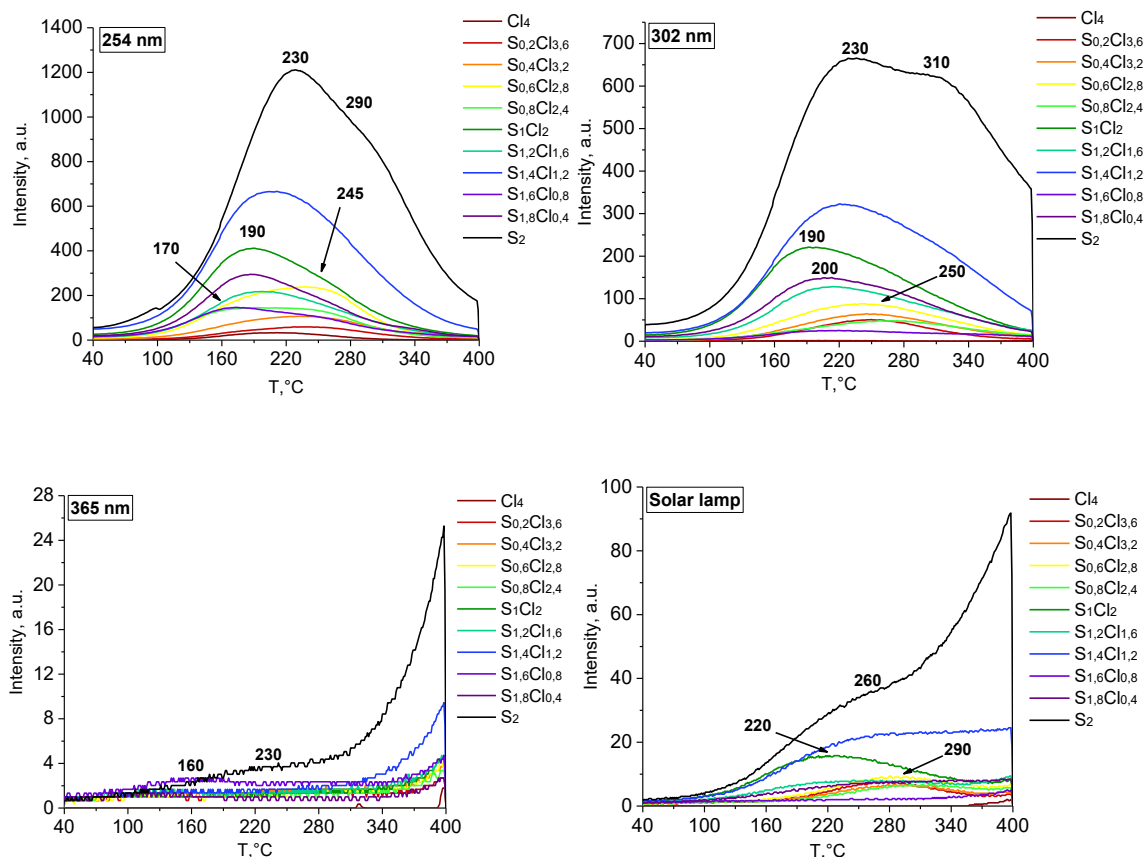
Fig. 13. *TL glow curves of $Ca_8Al_{12}O_{24}S_2$, $Ca_8Al_{12}O_{24}Cl_4$ (mixed aluminate) and $Ca_8Al_{12}O_{24}(S,Cl)_2$ samples after irradiation with 254, 302 and 365 nm UV and radiation from a solar lamp for 5 minutes.*

After irradiation with 254 and 302 nm UV the TL glow curves of all samples seem to consist of two overlapping peaks: one with maximum around 170-230°C and one around 250-310°C. TL after irradiation with 365 nm UV is hardly detectable likely due to the relatively low energy of the photons. TL after irradiation with the solar lamp is slightly more intense than after 365 nm UV due to the samples being exposed to photons with a wide range of energies. In both of the lower intensity glow curves a peak around 400°C can be observed, which could be the result of black body radiation.

An intense peak with maximum between 150 and 180°C, as well as a peak with low intensity at 250°C temperature can also be observed in both natural and synthetic hackmanites, however, specific defects that could cause luminescence at these temperatures have not been assigned. [19] A peak with maximum at 220°C has also been observed in natural α-cristobalite, a silica polymorph that often contains Al impurities, and could be linked to $[AlO_4]^0$ centres [34] that are created when the cations are removed from Al sites and electron holes from adjacent oxygen ions are compensating

the charge instead. TL peaks at temperatures 200-300°C have also been observed in natural quartz and could be attributed to the electron-hole recombination in $[AlO_4]^0$ centres. [35]

Since all of the peaks are in the 170-310°C range, these materials could potentially be used in dosimetry, however, the presence of two overlapping peaks could make quantification and dose calculation more difficult.

To compare the total charge storage capacity of the samples, integrated intensity values (total area of the glow curves) were calculated. The results can be seen in Fig. 14.
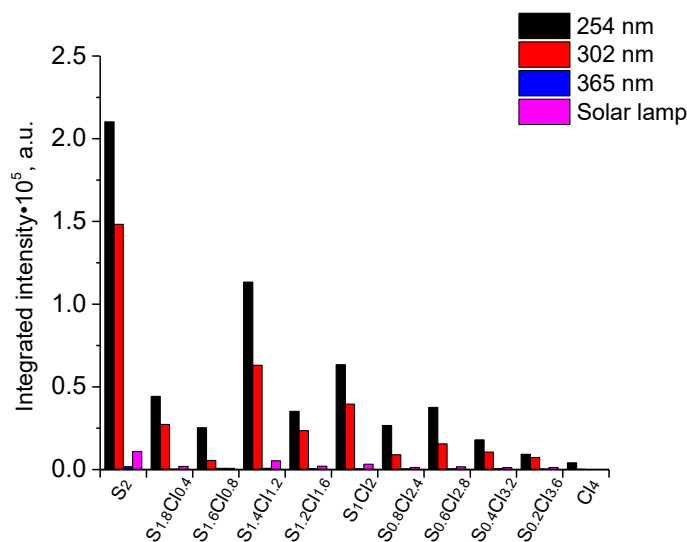
Fig. 14. *Integrated TL intensity of $Ca_8Al_{12}O_{24}S_2$, $Ca_8Al_{12}O_{24}Cl_4$ (aluminate mixture) and $Ca_8Al_{12}O_{24}(S,Cl)_2$ samples after irradiation with UV radiation with 254, 302 and 365 nm wavelength and radiation from a solar lamp for 5 minutes.*

Highest integrated intensity value was observed in samples irradiated with 254 nm UV radiation, to which followed samples irradiated with 302 nm UV radiation, then samples irradiated using a solar lamp and finally samples irradiated with 365 nm UV radiation.

In all samples except $S_{1.8}Cl_{0.4}$, $S_{1.6}Cl_{0.8}$, $S_{1.2}Cl_{1.6}$ and $S_{0.8}Cl_{2.4}$ integrated intensity values seem to follow the same trend of decreasing as sulfur content in the samples decreases. Three of the four mentioned samples with lower integrated intensity than expected ($S_{1.6}Cl_{0.8}$, $S_{1.2}Cl_{1.6}$ and $S_{0.8}Cl_{2.4}$) are also the ones with lowest $Ca_8Al_{12}O_{24}S_2$ and highest $Ca_8Al_{12}O_{24}(SO_4)_2$ content. Due to this fact it can be hypothesized that up to 400°C temperature recombination mainly occurs in the $Ca_8Al_{12}O_{24}S_2$ phase.

Reflectance measurements of samples irradiated with 254 nm UV radiation were obtained in order to assess their tenebrescence. Difference in reflectance before and after irradiation can be seen in Fig. 15.
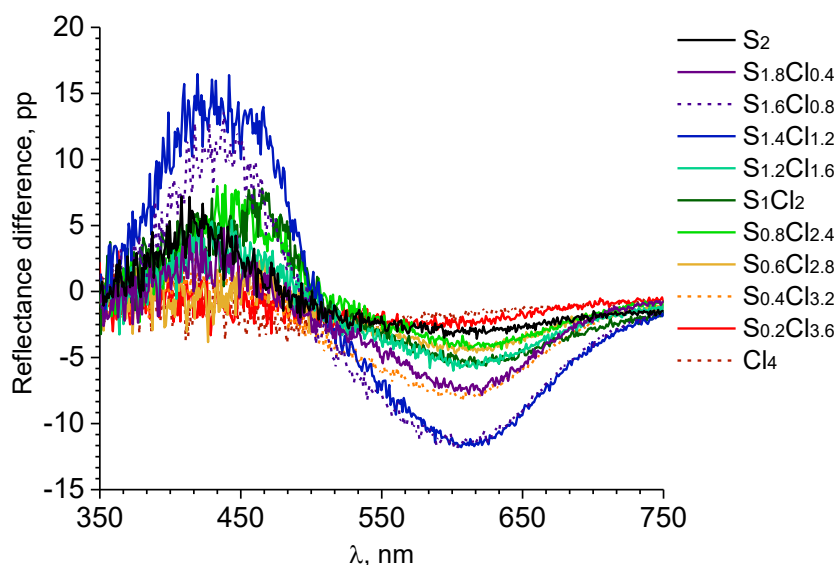
Fig. 15. *Difference in reflectance in $Ca_8Al_{12}O_{24}S_2$, $Ca_8Al_{12}O_{24}Cl_4$ (aluminate mixture) and $Ca_8Al_{12}O_{24}(S,Cl)_2$ samples before and after irradiation with 254 nm UV radiation.*

Decrease in reflectance at 610 nm and two emission peaks at 420 and 460 nm indicating PeL were observed. While absorption of radiation at 610 nm means that the observed colour of the compounds should be in the blue-violet part of the spectra, no visible change in coloration could be seen. A maximum of approximately 12 percentage point (pp) difference in reflectance was observed in samples $S_{1.6}Cl_{0.8}$ and $S_{1.4}Cl_{1.2}$ and almost no change was observed in samples S_2, $S_{0.2}Cl_{3.6}$ and Cl_4. Since sulfur ions are necessary for the tenebrescence mechanism in sodalites, it is not surprising to see that $S_{0.2}Cl_{3.6}$ and Cl_4 which have little to no sulfur content have almost no change in reflectance. $S_{0.4}Cl_{3.2}$, however, shows an unexpected change in reflectance after irradiation as it exceeds that of most samples with a higher sulfur content.

3.2. Composition, luminescence, and reflectance of optimally reduced samples with different S/Cl ratios

Calcium containing samples with various S/Cl content ratios were synthesized twice. First the two-step process was followed as written in the experimental section. In most samples the result of this synthesis was a mixture of both the reduced $Ca_8Al_{12}O_{24}S_2$ phase and the non-reduced $Ca_8Al_{12}O_{24}(SO_4)_2$ phase. To compare the effects of the sulfate ions on the optical properties of these materials, another batch was prepared using the same precursor amounts and reduced in a 12% H_2/88% N_2 atmosphere until there were no longer any major changes in the concentration of the $Ca_8Al_{12}O_{24}(SO_4)_2$ phase. The composition, luminescence and reflectance results of these optimally reduced samples will be discussed in this chapter.

3.2.1. X-ray powder diffraction and X-ray fluorescence spectroscopy

The phase composition of the optimally reduced samples can be seen in Table 3.3. Only four of the samples have a detectable amount of the non-reduced sodalite phase $Ca_8Al_{12}O_{24}(SO_4)_2$. The concentration of $Ca_6Al_7O_{16}Cl$ has also increased in most samples at the expense of the other non-sodalite aluminate phases. The total S/Cl however, was more or less the same as in the previous samples.

Table 3.3. Composition of the optimally reduced samples calculated using quantitative phase analysis.

	Phase composition			
	$Ca_8Al_{12}O_{24}S_2$, %	$Ca_8Al_{12}O_{24}(SO_4)_2$, %	$Ca_6Al_7O_{16}Cl$, %	$CaAl_2O_4$ or other aluminates, %
$S_{0.2}Cl_{3.6}$	13.7	-	67.8	18.5
$S_{0.4}Cl_{3.2}$	22.8	-	63.7	13.5
$S_{0.6}Cl_{2.8}$	31.1	-	52.2	16.6
$S_{0.8}Cl_{2.4}$	40.7	-	46.9	12.4
S_1Cl_2	49.7	-	50.3	-
$S_{1.2}Cl_{1.6}$	52.7	-	47.3	-
$S_{1.4}Cl_{1.2}$	49.0	15.9	35.1	-
$S_{1.6}Cl_{0.8}$	75.0	0.5	24.5	-
$S_{1.8}Cl_{0.4}$	73.2	15.9	10.8	-
S_2	75.3	19.5	-	5.2

The elemental composition of the optimally reduced samples can be seen in Table 3.4. There are some noticeable differences between the optimally reduced samples and the previous ones. Firstly, the average Ca concentration has increased by 5-10 wt% in the optimally reduced samples, while the concentration of Al has decreased by approximately 8 wt%. The Si and Mg content has also slightly decreased, while some samples now contain trace amounts of Sr. These changes in element composition could have occurred during sample preparation, however, they have not had much of an effect on the phase composition and S/Cl ratio as can be seen in Table 3.3.

Table 3.4. Most abundant elements in the optimally reduced samples with different S:Cl ratios.

	Ca, wt%	Al, wt%	Cl, wt%	S, wt%	Si, wt%	Mg, wt%	Sr, wt%
$S_{0.2}Cl_{3.6}$	65.77	24.85	5.16	0.40	0.89	2.65	-
$S_{0.4}Cl_{3.2}$	65.68	24.93	5.19	0.61	0.86	2.45	0.12
$S_{0.6}Cl_{2.8}$	65.38	25.36	4.41	1.20	0.88	2.41	-
$S_{0.8}Cl_{2.4}$	66.36	24.49	4.14	1.49	0.89	2.30	0.14
S_1Cl_2	66.46	24.50	3.66	2.09	0.84	2.11	-
$S_{1.2}Cl_{1.6}$	66.09	24.39	3.58	2.21	0.92	2.41	0.12
$S_{1.4}Cl_{1.2}$	65.34	25.11	2.62	3.53	0.86	2.29	-
$S_{1.6}Cl_{0.8}$	64.15	26.15	1.72	4.59	0.84	2.27	0.11
$S_{1.8}Cl_{0.4}$	62.29	27.70	0.70	5.48	0.97	2.60	0.11
S_2	63.12	27.05	0.14	5.72	0.95	2.74	0.13

3.2.2. Reflectance and luminescence measurements

The luminescence properties of the optimally reduced samples were analysed and compared to the previously synthesized samples. During preliminary testing, no visible differences were observed in samples with similar S/Cl ratios when under 254 nm UV, however, a clear difference in the emission colour of some samples could be seen under 302 nm UV radiation. More specifically, the orange luminescence previously seen in samples with low S/Cl ratio was no longer present in the optimally reduced samples. Luminescence of samples with $S_{1.2}Cl_{1.6}$ S/Cl ratio depending on the phase composition can be seen in Fig. 16.
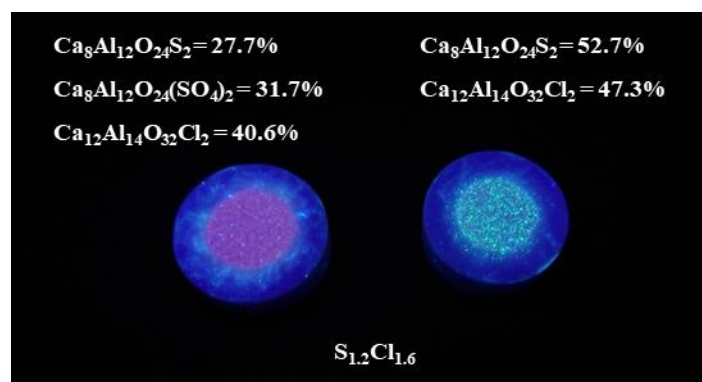

Fig. 16. *Photoluminescence of two $S_{1.2}Cl_{1.6}$ samples with different phase compositions under 302 nm UV radiation.*

The emission spectra of the optimally reduced samples were also taken using Varian Cary Eclipse spectrometer, the spectra can be seen in Fig. 17.
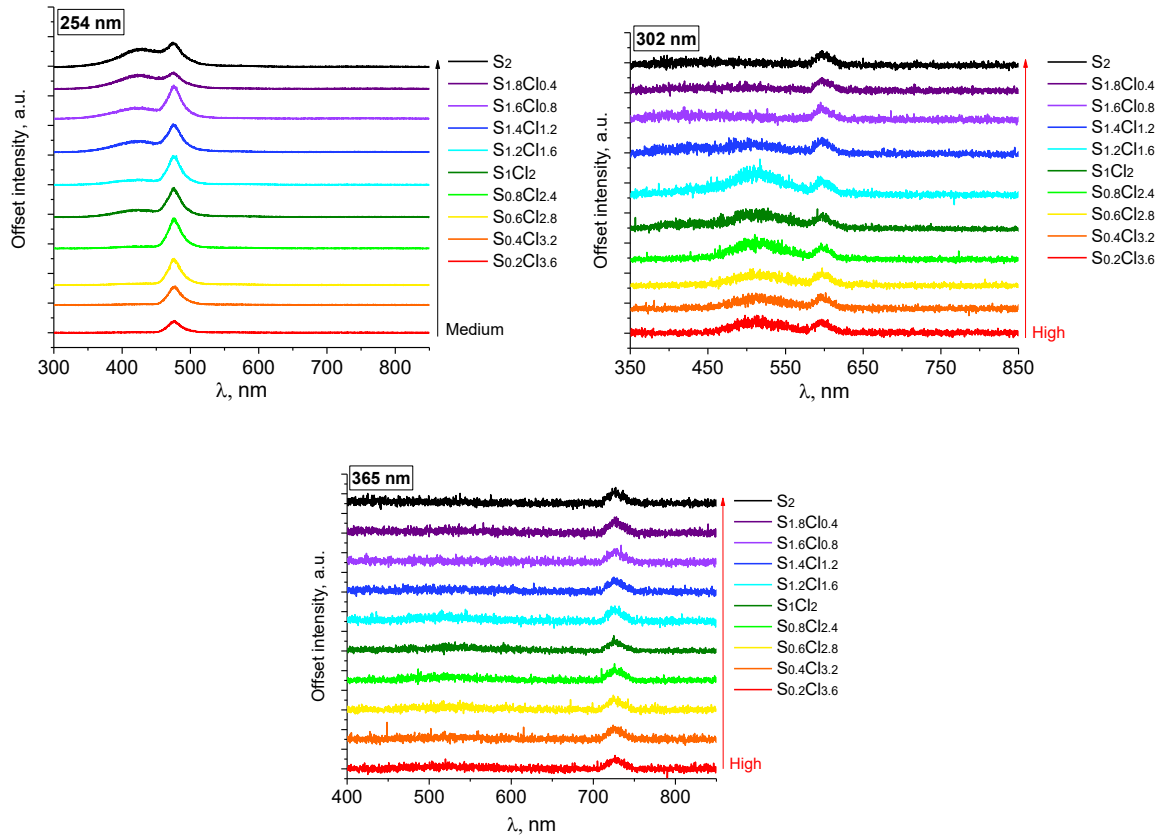
Fig. 17. *Emission spectra of the optimally reduced $Ca_8Al_{12}O_{24}S_2$ and $Ca_8Al_{12}O_{24}(S,Cl)_2$ samples during irradiation with 254, 302 and 365 nm UV radiation.*

The main difference in the emission spectra of samples irradiated with 254 nm UV is that the peak intensity has increased in samples $S_2 - S_{1.2}Cl_{1.6}$. This can be easily explained by the significant increase in $Ca_8Al_{12}O_{24}S_2$ content in these samples. In samples irradiated with 302 nm UV, there is a peak around 500 nm that can be seen in the emission spectra. This peak was present in only one of the previously synthesized samples – $S_{0.2}Cl_{3.8}$, and while it was not detected in the emission spectrum taken using the long pass filter, it could have overlapped with the more intense peak around 620 nm. The peak around 600 nm could be caused by excitation harmonics. There is almost no change in the emission spectra during irradiation with 365 nm, there is only one peak around 730 nm, likely due to excitation harmonics, however, this time no other peaks can be seen in the emission spectra of $S_{0.6}Cl_{2.8}$.

Excitation spectra of the emissions with 420, 480 and 730 nm wavelength were the same for the optimally reduced samples as they were for the previously synthesized samples, thus they will not be shown here. These excitation spectra can be seen in appendix 1. The excitation spectra of the emissions around 500 nm, which were not observed previously, and emissions around 600 nm can be seen in Fig. 18.
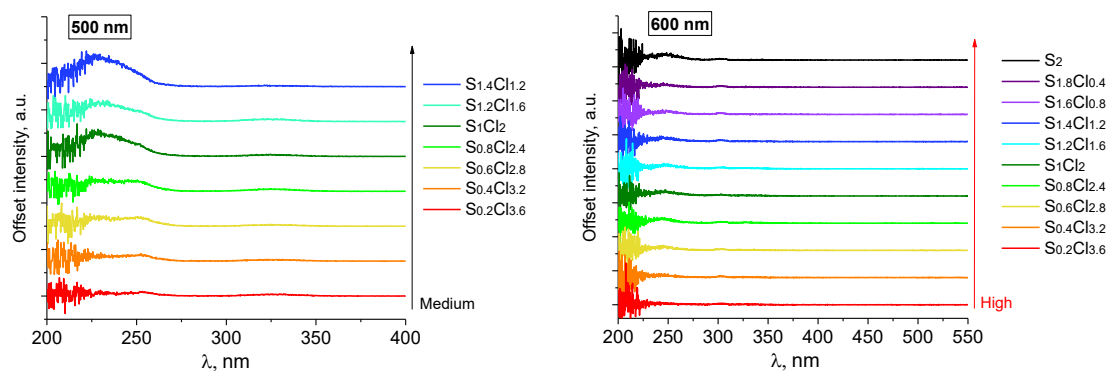
Fig. 18. *Excitation spectra of emissions around 500 and 600 nm in optimally reduced $Ca_8Al_{12}O_{24}S_2$ and $Ca_8Al_{12}O_{24}(S,Cl)_2$ samples.*

As previously stated, the emission peak at around 500 nm could only be observed in one of the previously synthesized, not fully reduced samples, which is why it was not analysed further. The excitation spectra of this emission peak are similar to the rest of the emissions, having the highest intensity, when irradiated with UV radiation in the 200-250 nm range. The intensity of the emission also increases as the S/Cl ratio of the sample increases. The intensity of the emission around 600 nm has decreased especially in the $S_{0.6}Cl_{2.8}$ sample.

The PeL emission spectra of the optimally reduced samples can be seen in Fig. 19. There are still two main peaks that can be seen in the PeL emission spectra: one at about 420 and one at 480 nm. The only difference is that in the optimally reduced samples the peak at 420 nm has higher intensity in samples $S_{1.8}Cl_{0.4} - S_1Cl_2$, while in the previously synthesized samples the peak at 480 nm was more intense. There is also no longer a peak around 600 nm which was present in the samples $S_{0.8}Cl_{2.4} - S_{0.2}Cl_{3.6}$, which is supported by the lower emission intensity observed in the excitation spectra.
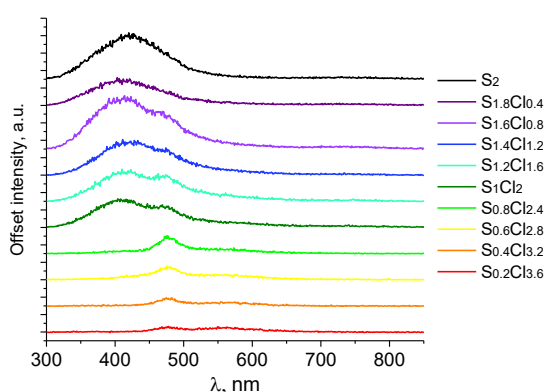

Fig. 19. *PeL emission spectra of the optimally reduced $Ca_8Al_{12}O_{24}S_2$ and $Ca_8Al_{12}O_{24}(S,Cl)_2$ samples after irradiation with 254 nm UV radiation for 5 minutes.*

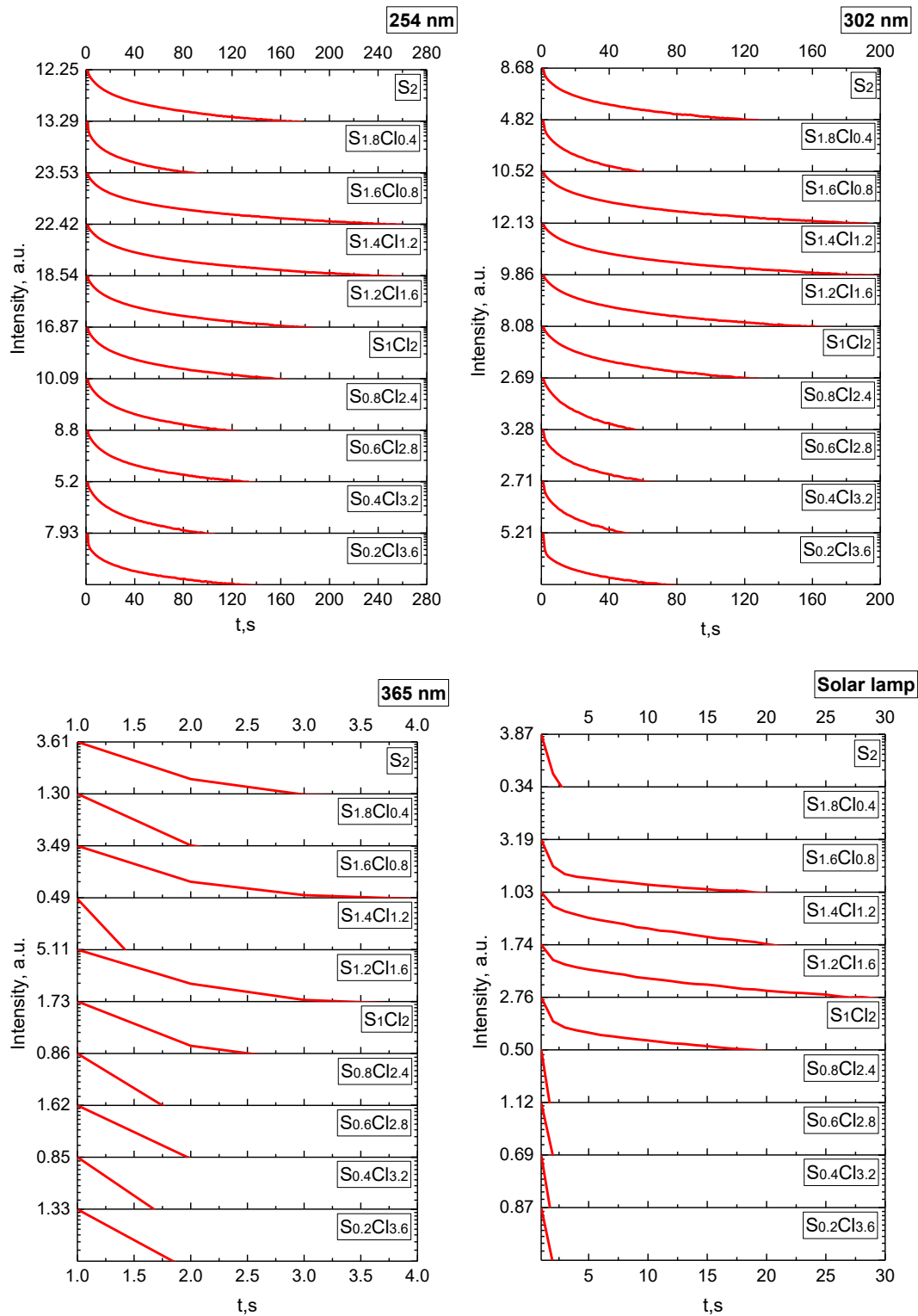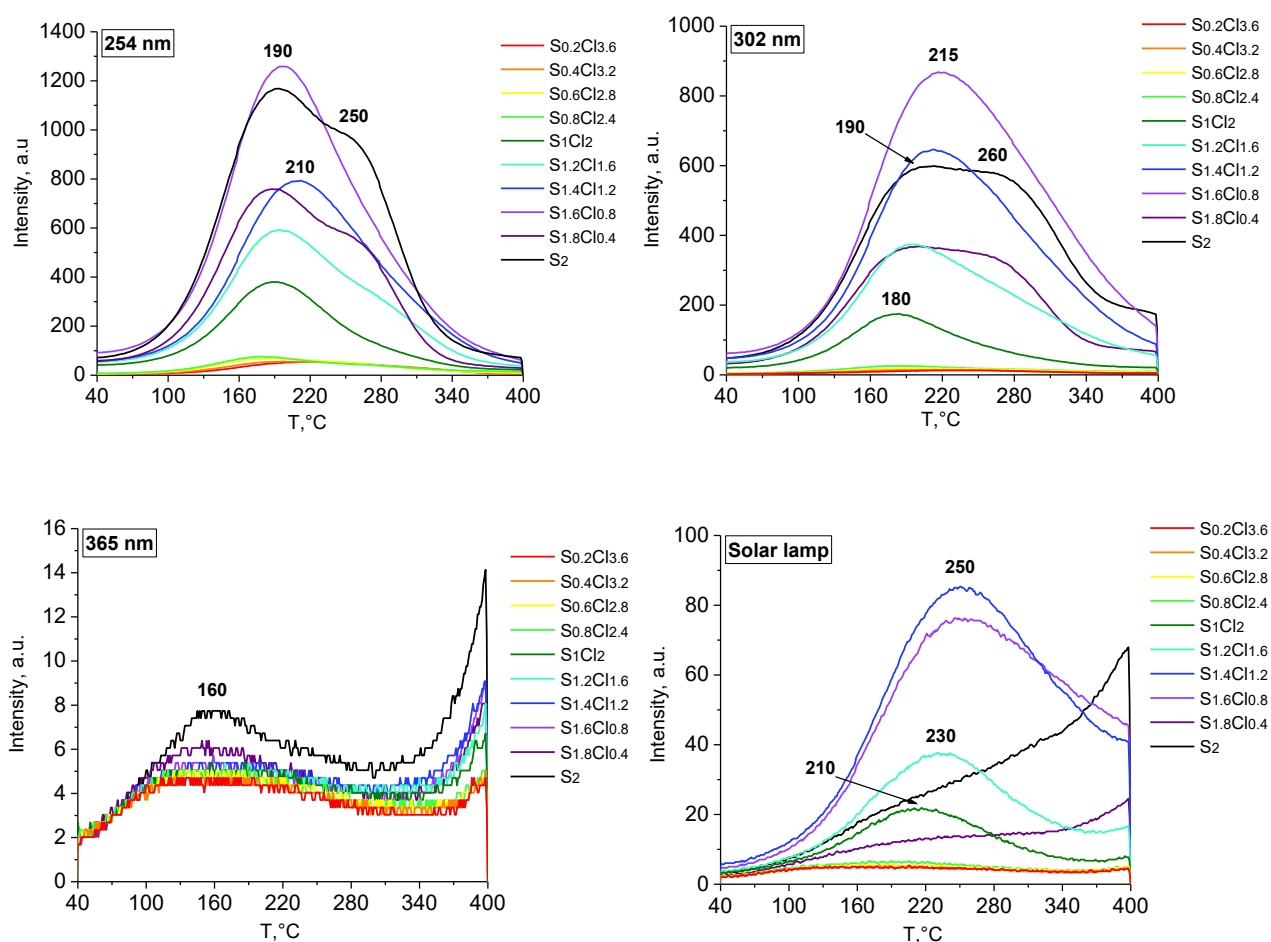PeL fading curves of the optimally reduced samples can be seen in Fig. 20.

35

Fig. 20. *PeL fading in the optimally reduced samples irradiated with 254, 302, 365 nm UV radiation and radiation from a solar lamp (only the highest intensity value is shown in each curve, lowest intensity value in all curves is 0.32 mcd/m²).*

Unlike in the previously synthesized samples, which showed longer PeL in samples with a lower S/Cl ratio ($S_1Cl_2 - S_{0.2}Cl_{3.6}$, but especially $S_{0.2}Cl_{3.6}$), in the optimally reduced samples longer PeL can be observed in samples with a higher S/Cl ratio. Samples $S_{1.6}Cl_{0.8}$ and $S_{1.4}Cl_{1.2}$ on average

seem to have the best results when it comes to long lasting PeL. The previously mentioned PeL emission spectra could help explain the sudden change in PeL fading results. The spectra showed that in previously synthesized samples the emission around 600 nm was present in samples $S_{0.8}Cl_{2.4}$ – $S_{0.2}Cl_{3.6}$, which could have increased the duration of PeL.

TL glow curves seen in Fig. 21. In the glow curves after irradiation with 254 and 302 nm UV, there are still one or two peaks, same as in the previously synthesized samples, although the peak maxima have shifted slightly. In the S_2 sample in particular the peak which used to be around 230°C is now around 190°C, while the peak that was around 290°C is now at 250°C. In other samples the difference is not as noticeable, and the peaks are in the same range as noted before around 170-230°C and 250-310°C respectively.
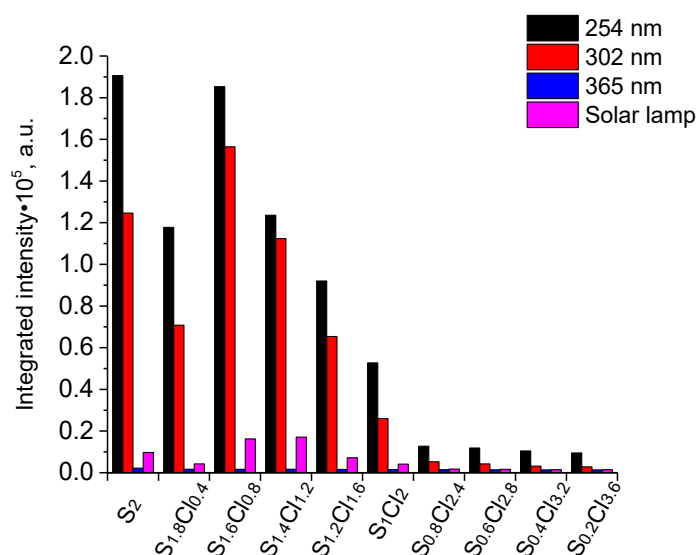

Fig. 21. *TL glow curves of optimally reduced $Ca_8Al_{12}O_{24}S_2$ and $Ca_8Al_{12}O_{24}(S,Cl)_2$ samples after irradiation with 254, 302 and 365 nm UV and radiation from a solar lamp for 5 minutes.*

Glow curves of the optimally reduced samples under 365 nm UV radiation and solar lamp show significantly different results than those of the previously synthesized samples. The peak around 160°C, which was seen in a few of the previously synthesized samples, has a higher intensity and is

present in all the optimally reduced samples. Samples $S_{1.6}Cl_{0.8} - S_{1.2}Cl_{1.6}$ show more intense TL after irradiation with the solar spectrum.

Integrated area of TL glow curves can be seen in Fig. 22. Integrated intensity still follows the same sequence as before with samples after irradiation with 254 nm UV showing the highest total TL intensity, followed by 302 nm, solar lamp and finally the 365 nm UV. The integrated intensity values also increase with increasing sulfur content, which was also the case with the previously synthesized samples. It was hypothesized that the defects that are unstable in temperatures up to 400°C form mainly in the $Ca_8Al_{12}O_{24}S_2$ phase or are somehow affected by the formation of $Ca_8Al_{12}O_{24}S_2$ as the integrated intensity values seemed to follow $Ca_8Al_{12}O_{24}S_2$ content in the previously synthesized samples. This would also be the case with the optimally reduced samples with $S_{1.8}Cl_{3.6}$ being the only exception.

Fig. 22. *Integrated TL intensity of optimally reduced $Ca_8Al_{12}O_{24}S_2$ and $Ca_8Al_{12}O_{24}(S,Cl)_2$ samples after irradiation with 254, 302 and 365 nm UV and radiation from a solar lamp for 5 minutes.*

Reflectance of the optimally reduced S_2 sample before, immediately after and 7 minutes after irradiation with 254 nm UV radiation can be seen in Fig. 23. No significant change in reflectance could be seen in any of the samples, which is why the rest of the reflectance spectra will not be discussed and can be seen in appendix 2. The slight changes in the baseline could be due to change in the sample position between irradiation and reflectance measurements and the was no visible colour change before and after irradiation.
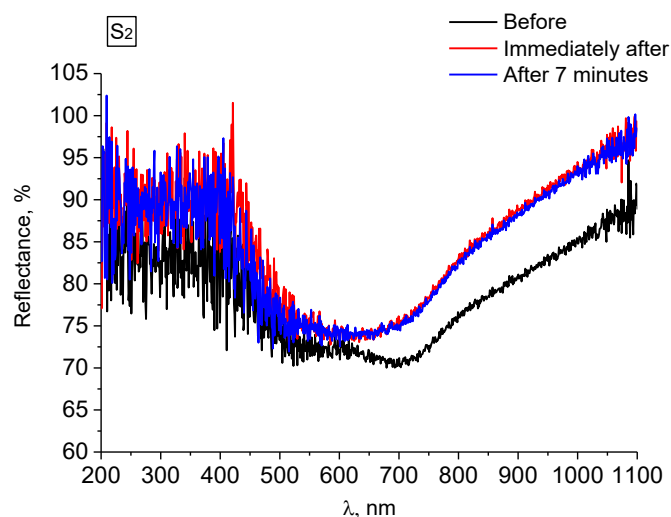
Fig. 23. *Reflectance of the optimally reduced $Ca_8Al_{12}O_{24}S_2$ sample before, immediately after and seven minutes after irradiation with 254 nm UV radiation.*

3.3. Composition, luminescence, and reflectance of sodalite containing samples with different Ca/alkali metal ratios

From previous results $S_{1.4}Cl_{1.2}$ sample was concluded to be one of the more promising materials due to high photoluminescence intensity and duration and good TL intensity at around 200°C indicating possible use as a dosimeter. Therefore, $S_{1.4}Cl_{1.2}$ was chosen as the S/Cl ratio for the Ca exchanged samples. To analyse the effect of alkali metal dopants on the luminescence and tenebrescence properties of calcium aluminate sodalites, Ca ions were exchanged with Li, Na, K and Rb to the samples in ratios: $M_{1.2}Ca_{7.4}$, M_4Ca_6, M_8Ca_4, $M_{12}Ca_2$ and fully exchanged M_{16}, where M is the alkali metal.

3.3.1. X-ray powder diffraction and X-ray fluorescence spectroscopy

XRD diffractograms were taken to evaluate the sodalite phase content in each sample using the qualitative phase analysis. Diffractograms of the samples and reference materials with their respective ICDD codes can be seen in Fig. 24.
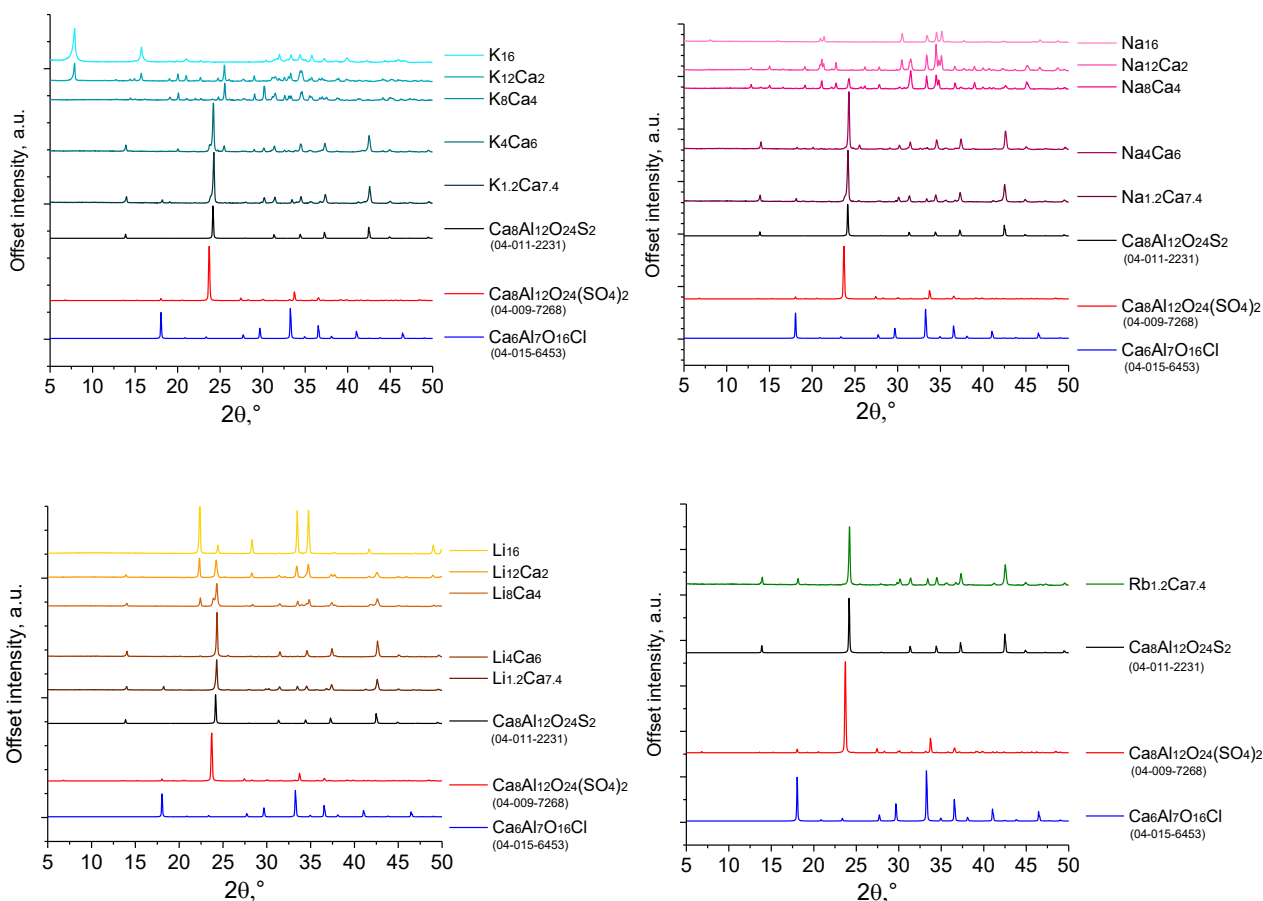
Fig. 24. *XRD patterns of the $(M,Ca)_8Al_{12}O_{24}S_{1.4}Cl_{1.2}$ samples and the reference patterns of phases found in database (ICDD reference code can be seen below each compound).*

As can be seen in Fig. 24. the XRD patterns of the samples showed multiple non-sodalite aluminate phases forming as the alkali metal concentration in the samples increased. This is likely due to a double the amount of alkali metal ions being necessary to compensate for the lack of Ca ions resulting in the collapse of the sodalite structure. Phase composition and the concentration of $Ca_8Al_{12}O_{24}S_2$ and $Ca_8Al_{12}O_{24}(SO_4)_2$ in the alkali metal doped samples can be seen in Table 3.5. The samples with a high alkali metal concentration, such as $M_{12}Ca_2$ and M_{16} had XRD patterns that could not be fully identified. Due to the pattern becoming more and more complex, multiple overlapping peaks or peaks in close proximity to each other could be seen and some did not correspond to any of the compounds in the database. For this reason, only the phases that could be correctly identified and were present in multiple samples will be mentioned.

Table 3.5. Composition of the alkali metal doped samples calculated using quantitative phase analysis.

	Phase composition			
	$Ca_8Al_{12}O_{24}S_2$, %	$Ca_8Al_{12}O_{24}(SO_4)_2$, %	$CaAl_2O_4$, other Ca aluminates or salts, %	Alkali metal aluminates or salts, %
$Li_{1.2}Ca_{7.4}$	76.5	-	23.6	-
Li_4Ca_6	96.1	-	3.9	-
Li_8Ca_4	57.6	8.7	-	33.7
$Li_{12}Ca_2$	29.9	-	10.5	59.6
Li_{16}	-	-	-	100
$Na_{1.2}Ca_{7.4}$	56.4	24.8	18.8	-
Na_4Ca_6	75.6	-	24.4	-
Na_8Ca_4	34.4	-	18.5	47.1
$Na_{12}Ca_2$	-	0.2	10.0	89.7
Na_{16}	-	-	-	100
$K_{1.2}Ca_{7.4}$	26.9	52.5	20.6	-
K_4Ca_6	76.6	-	23.4	-
K_8Ca_4	0.5	-	99.5	-
$K_{12}Ca_2$	-	-	66.4	33.6
K_{16}	-	-	-	100
$Rb_{1.2}Ca_{7.4}$	45.6	39.2	15.1	-

Out of Li, Na and K, the Li doped samples contained the highest concentration of sodalites at the M/Ca ratio M_8Ca_4. In the rest of the samples with the same M/Ca ratio sodalite concentration decreased as the radius of the doped ions increased. Since these samples contain a similar proportion of mostly sodalite containing and mostly non-sodalite containing samples, this section will be about the mostly sodalite (up to 50%) containing samples, while those samples containing mostly alkali metal aluminates will be discussed in the next section. Samples discussed in this section are $Li_{1.2}Ca_{7.4}$, Li_4Ca_6, Li_8Ca_4, $Na_{1.2}Ca_{7.4}$, Na_4Ca_6, $K_{1.2}Ca_{7.4}$, K_4Ca_6, and $Rb_{1.2}Ca_{7.4}$.

Elemental composition of the samples can be seen in Table 3.6.

Table 3.6. Most abundant elements in the sodalite containing alkali metal doped samples with different M/Ca ratios.

	Ca, wt%	Al, wt%	S, wt%	Cl, wt%	Mg, wt%	Si, wt%	K, wt%	Zn, wt%	Rb, ppm
$Li_{1.2}Ca_{7.4}$	55.27	34.23	4.96	1.33	2.89	0.87	-	0.29	-
Li_4Ca_6	48.03	41.55	6.06	0.12	3.14	0.93	-	-	17.8
Li_8Ca_4	40.59	48.43	5.78	0.14	3.40	1.04	0.35	0.15	37.4
	Ca, wt%	Al, wt%	S, wt%	Cl, wt%	Mg, wt%	Si, wt%	Na, wt%	K, Wt%	Rb, ppm
$Na_{1.2}Ca_{7.4}$	54.68	35.60	5.41	0.49	2.73	0.90	-	-	-
Na_4Ca_6	48.33	41.43	5.39	0.15	3.27	0.87	-	0.38	22.7
	Ca, wt%	Al, wt%	S, wt%	Cl, wt%	Mg, wt%	Si, wt%	K, wt%	Zn, wt%	Rb, Ppm
$K_{1.2}Ca_{7.4}$	54.49	35.57	5.47	0.52	2.87	0.91	-	50.2 (ppm)	-
K_4Ca_6	48.91	41.15	5.32	0.10	3.35	0.99	-	751.7 (ppm)	22.0
	Ca, wt%	Al, wt%	S, wt%	Cl, wt%	Mg, wt%	Si, wt%	-	-	Rb, ppm
$Rb_{1.2}Ca_{7.4}$	54.27	35.74	4.99	1.12	2.82	0.88	-	-	35.4

As mentioned in the experimental section the XRF spectrometer used in this paper can detect elements heavier than Na and lighter than U. This means that a Li and to some extent Na content cannot be accurately analysed. Interestingly, K in the $K_{1.2}Ca_{7.4}$ and K_4Ca_6 samples could not be detected either, however, it was detected in the Na_4Ca_6 sample. As before Mg and Si were also detected and another element that was not in any of the precursors is Zn, which was detected in $Li_{1.2}Ca_{7.4}$, Li_8Ca_4 and Na_4Ca_6 in significant amounts. There could be Zn impurities in one of the shared precursors, however, like with Si and Mg, their presence in the samples cannot be explained.

3.3.2. Reflectance and luminescence measurements

The emission spectra of the alkali metal doped samples can be seen in Fig. 25 and Fig. 26. Emission spectra of the alkali metal doped sodalite containing samples during irradiation with 365 nm UV radiation can be seen in appendix 3. In these spectra only the peak around 730 nm, which is likely due to excitation harmonics could be seen, thus it will not be discussed here.
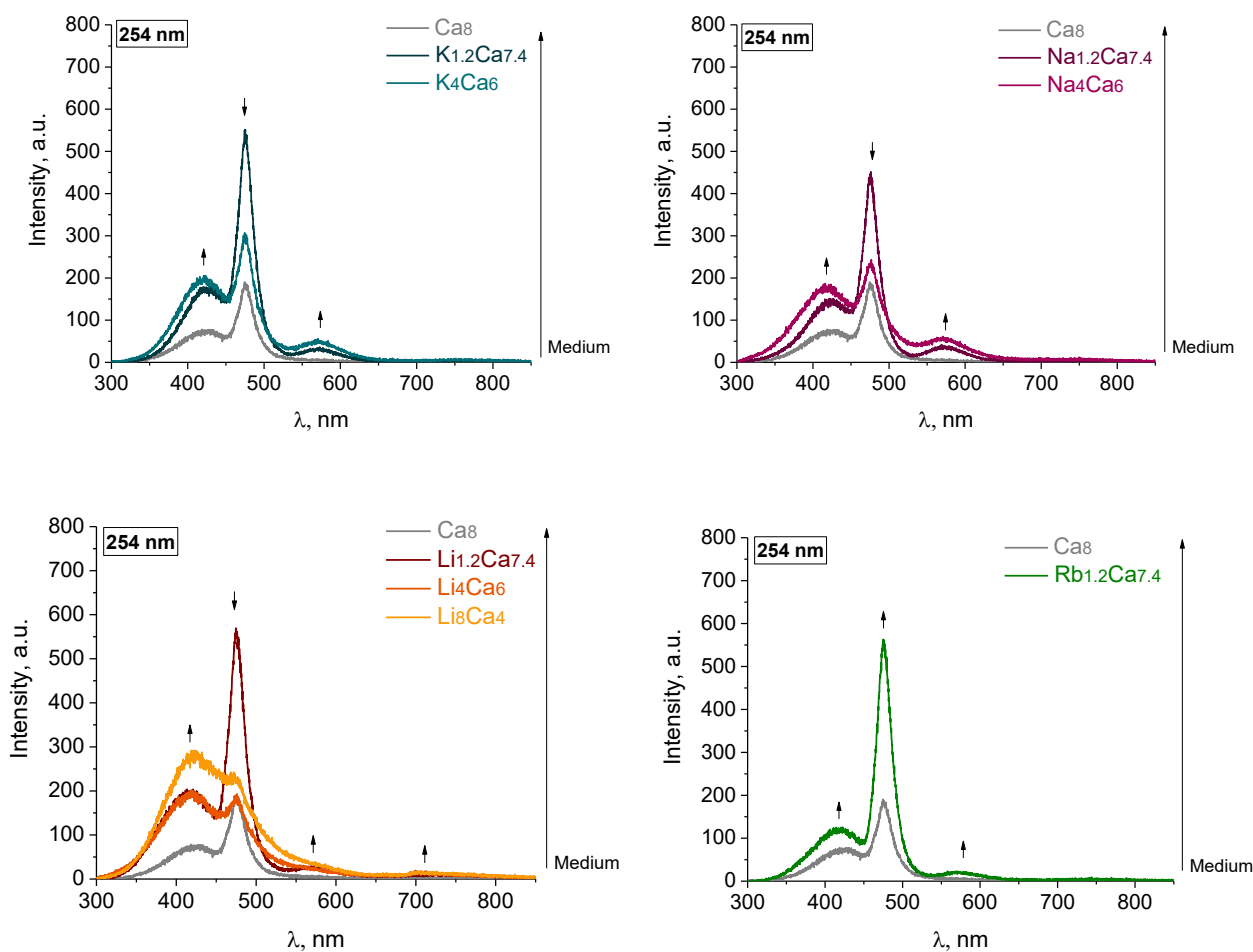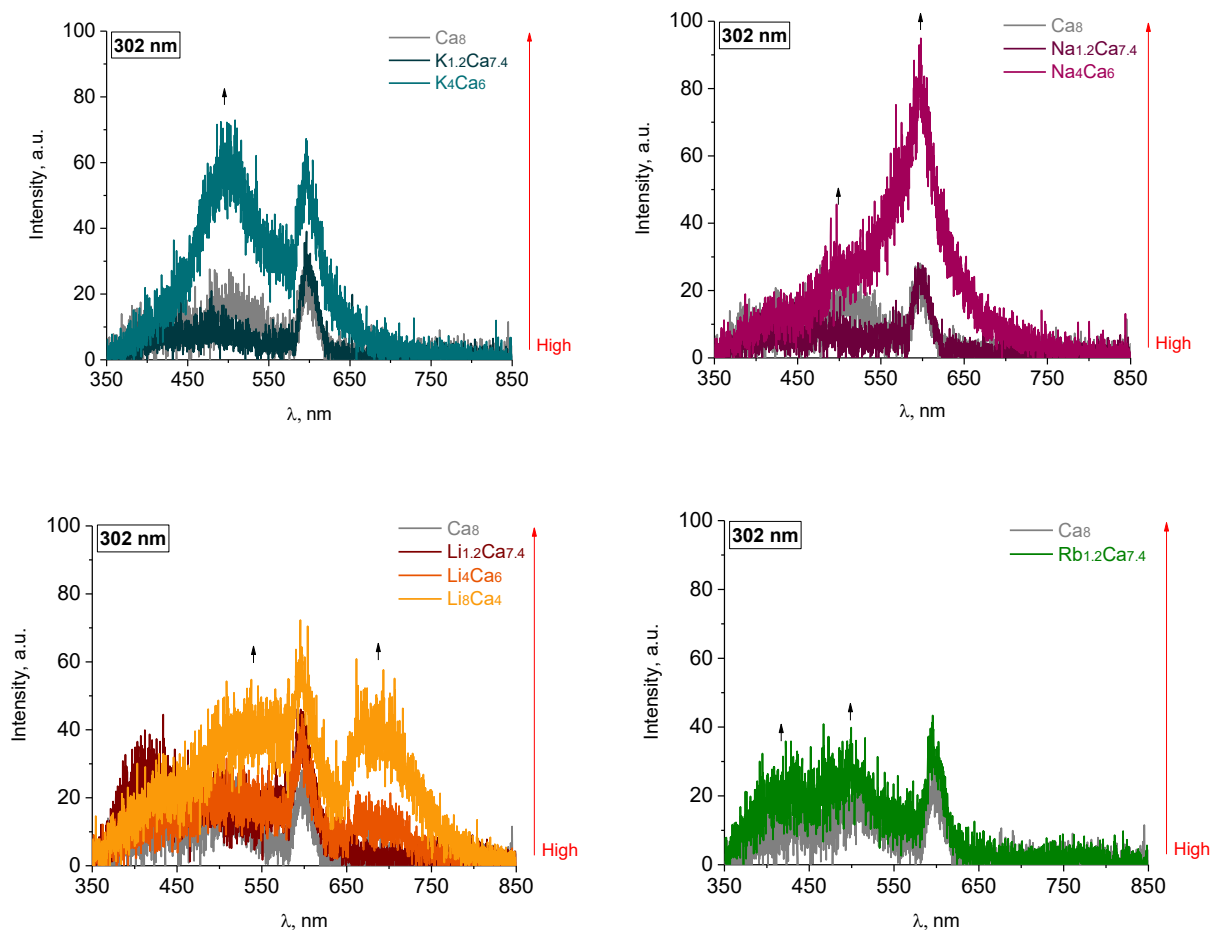
Fig. 25. *Emission spectra of $Ca_8Al_{12}O_{24}S_{1.4}Cl_{1.2}$ and the alkali metal doped $(M,Ca)_8Al_{12}O_{24}S_{1.4}Cl_{1.2}$ samples during irradiation with 254 nm UV radiation.*

During irradiation with 254 nm UV radiation three peaks could be seen in the emission spectra, Fig. 25. Peaks around 420 and 480 nm were also observed in the sulfur containing Ca only samples and is thought to originate from $Ca_8Al_{12}O_{24}S_2$. The peak around 580 nm was also present in the $Ca_8Al_{12}O_{24}S_2$ sample seen in Fig. 6. A peak around 710 nm also seems to be forming in the Li_8Ca_4 sample, although it could originate from one of the non-sodalite phases as this sample had the lowest sodalite content out of all samples and the same peak cannot be found in other spectra. In all samples adding a dopant increases luminescence intensity and samples with $M_{1.2}Ca_{7.4}$ M/Ca ratio show the highest intensity. There are some key differences between the samples with this ratio, in the Na sample the peak around 480 nm is not as intense as it is in the Li, K and Rb samples, while the peak at 580 nm is at higher intensity than in the rest of the samples. 420 nm emissions have the highest intensity in the K and Li doped samples.

When irradiated with 302 nm UV radiation, peaks around 500 and 600 nm can be observed as seen in Fig. 26. The intensity of the peaks increases in all samples as the concentration of the dopant

increases. The peak around 500 nm can also be seen in the Ca samples with lower sulfur content and could originate from the same defects. As said before the peak around 600 nm in the lower intensity emission spectra could be due to excitation harmonics.

Fig. 26. *Emission spectra of $Ca_8Al_{12}O_{24}S_{1.4}Cl_{1.2}$ and the alkali metal doped $(M,Ca)_8Al_{12}O_{24}S_{1.4}Cl_{1.2}$ samples during irradiation with 302 nm UV radiation.*

Excitation spectra of the emissions seen in the alkali metal doped samples can be seen in Fig. 27. For the most part the excitation spectra of emissions also observed in Ca only samples, for example around 420, 480, 580 and 600 nm are the same as before, with the most intense emissions being in the 200-270 nm region. Li_4Ca_6 and Li_8Ca_4, however, show a entirely different excitation spectra around 690, 710 and 730 nm. Since this only occurs in these two samples, it is possible that the emissions with these wavelengths could possibly be caused by other impurities.
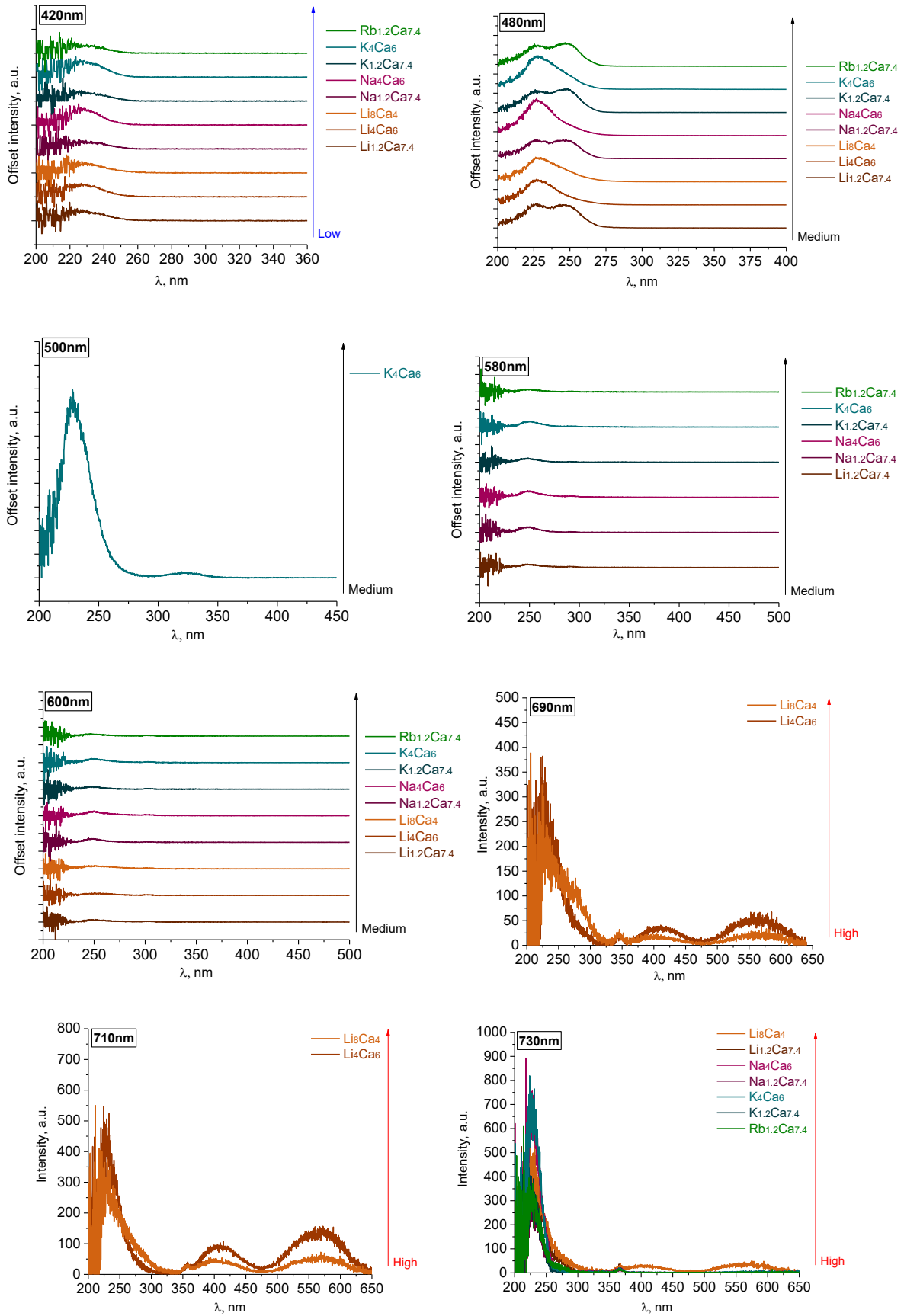
Fig. 27. *Excitation spectra of emissions around 420, 480, 500, 580, 600, 690, 710 and 730 nm in alkali metal doped $(M,Ca)_8Al_{12}O_{24}S_{1.4}Cl_{1.2}$ samples.*

PeL emission spectra of the alkali metal doped sodalite containing samples can be seen in Fig. 28.
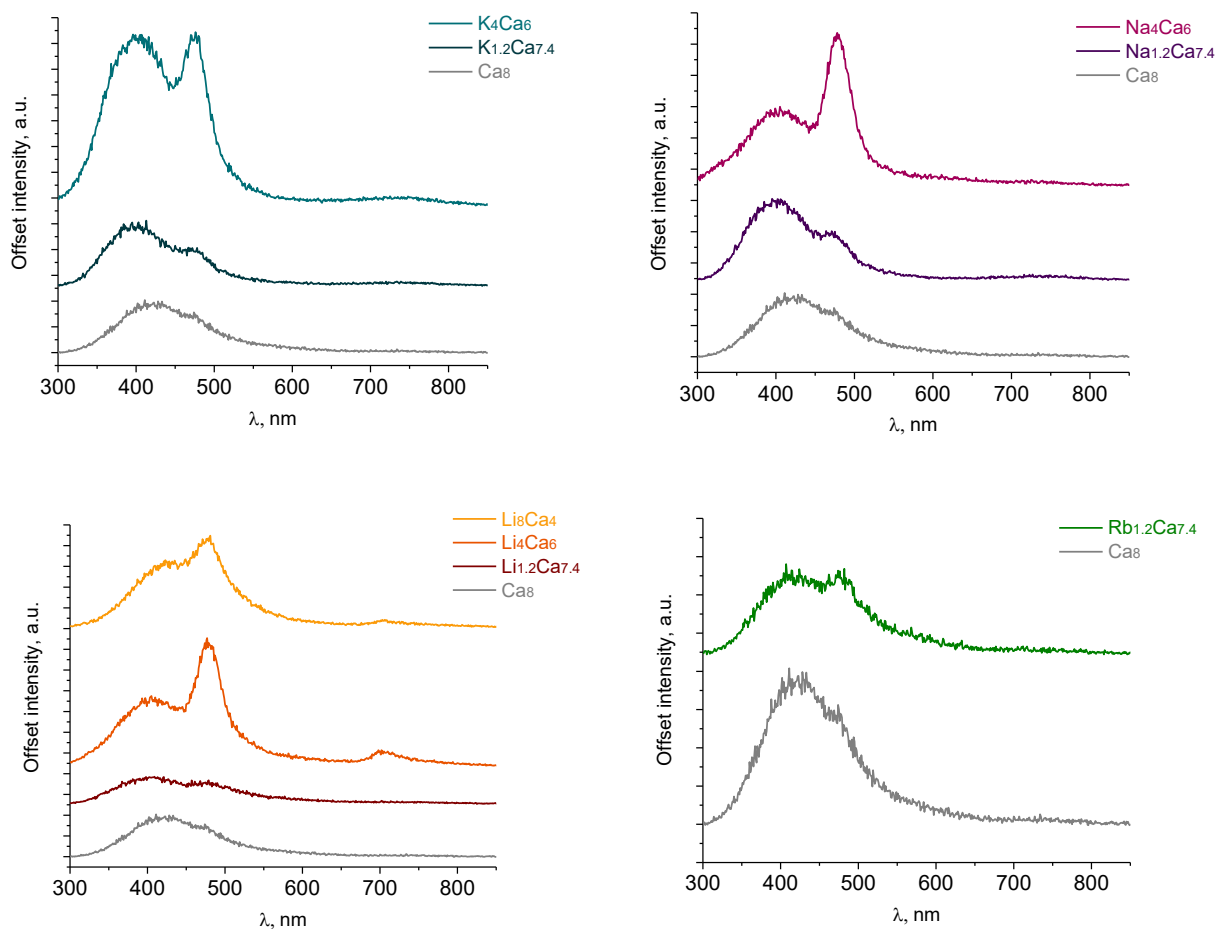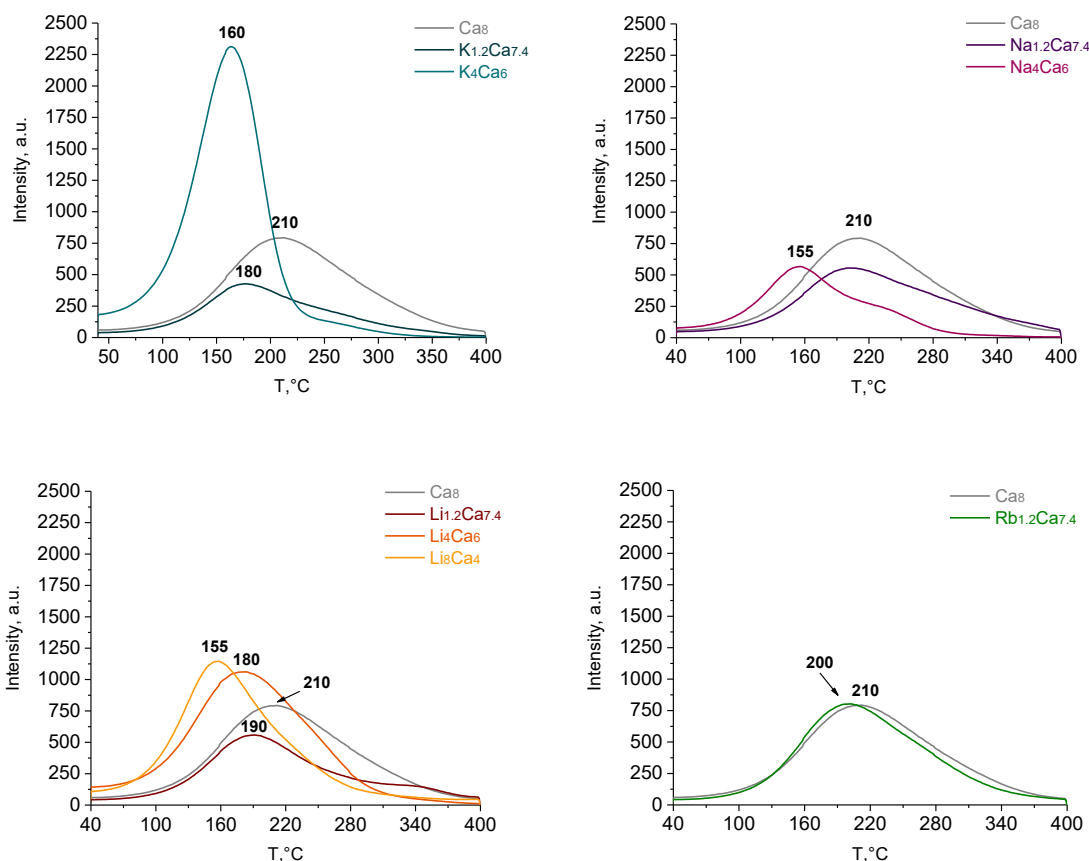

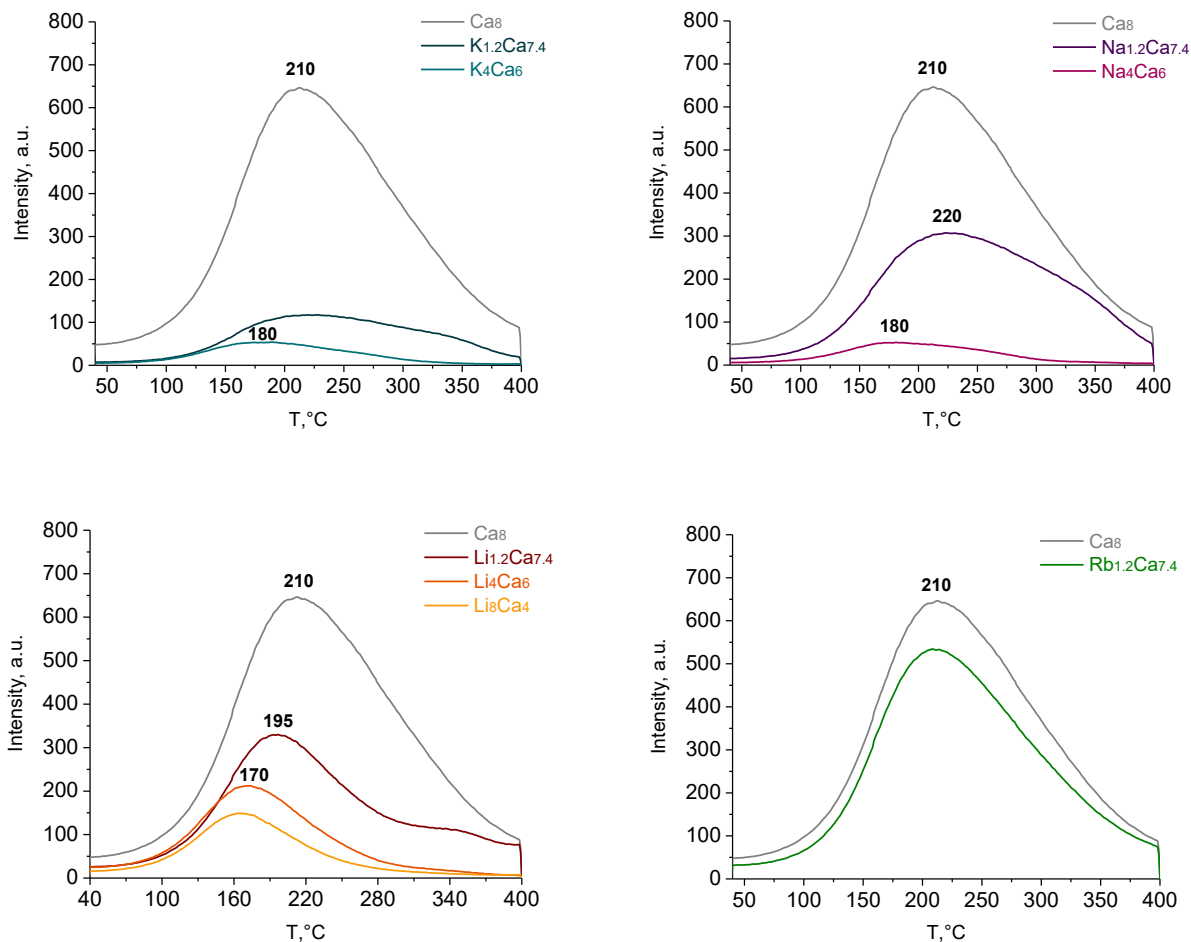**Fig. 28.** *PeL emission spectra of the alkali metal doped $(M,Ca)_8Al_{12}O_{24}S_{1.4}Cl_{1.2}$ samples after irradiation with 254 nm UV radiation for 5 minutes.*

In all spectra the two peaks around 420 and 480 nm seen in the Ca only samples can be seen, however the peak around 420 nm shifts closer to 400 nm in the doped samples. In all samples the intensity of PeL increases with increasing dopant content with the $M_{1.2}Ca_{7.4}$ samples being the only exception despite showing the highest emission intensity during irradiation as seen in Fig. 25. In Li_4Ca_6 and Li_8Ca_4 samples a peak around 710 nm can be seen that is not observed in any other sample. The excitation spectra of this peak can be seen in Fig. 27 and as said before, the presence of this emission could be due to some kind of impurities.

PeL fading curves of these samples can be seen in Fig. 29. Li_4Ca_6, Li_8Ca_4, Na_4Ca_6 and K_4Ca_6 show the highest luminescence intensity right after irradiation. The same thing can be seen in the PeL emission spectra one minute after irradiation. These samples also have the longest luminescence duration with a few exceptions.
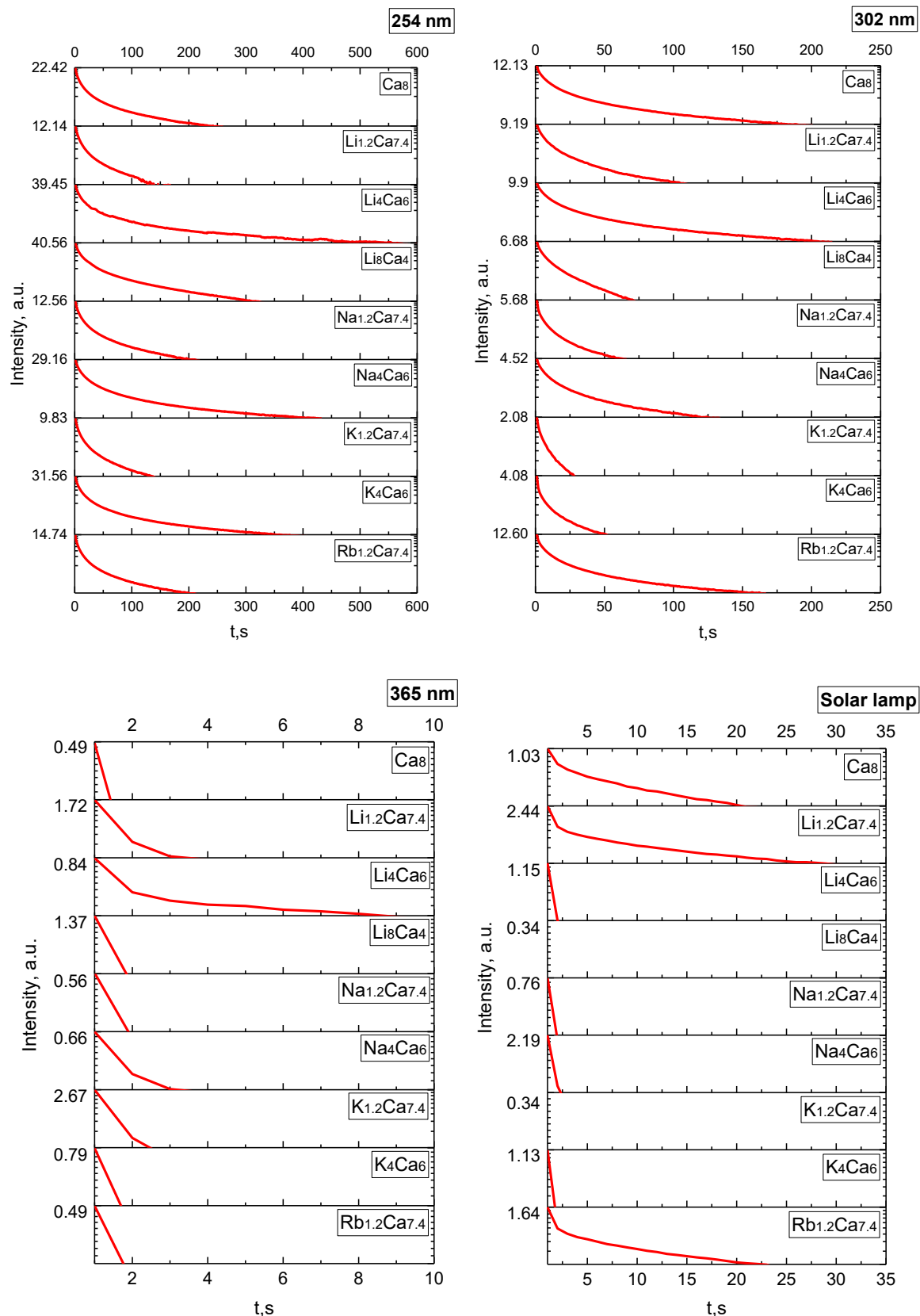
Fig. 29. *PeL fading in the alkali metal doped $(M,Ca)_8Al_{12}O_{24}S_{1.4}Cl_{1.2}$ samples irradiated with 254, 302, 365 nm UV radiation and radiation from a solar lamp (only the highest intensity value is shown in each curve, lowest intensity value in all curves is 0.32 mcd/m²).*

TL glow curves of the samples irradiated with 254 and 302 nm UV radiation can be seen in Fig. 30 and Fig. 31. TL glow curves of the samples irradiated with 365 nm UV radiation and radiation from the solar lamp showed a decrease in intensity from the Ca only sample and contained only a few peaks could be distinguished, therefore they will not be discussed here and can be seen in appendices 4 and 5.

Fig. 30. *TL glow curves of alkali metal doped $(M,Ca)_8Al_{12}O_{24}S_{1.4}Cl_{1.2}$ samples after irradiation with 254 nm UV radiation for 5 minutes.*

In almost all samples after irradiation with 254 nm UV radiation, seen in Fig. 30, the TL peak had shifted to lower temperatures, meaning that the doped samples would likely no longer be usable in dosimetry. Li_4Ca_6, Li_8Ca_4 and K_4Ca_6 in particular show high intensity TL (higher than the Ca only sample) at significantly lower temperatures, which is typically associated with longer and more intense PeL. This is also confirmed by the PeL spectra in Fig. 28.

A shift to lower temperatures in TL glow curves can also be observed after irradiation with 302 nm UV seen in Fig. 31. Unlike after irradiation with 254 nm UV, the TL intensity of the doped samples decreases significantly in comparison to the Ca only sample.

Fig. 31. *TL glow curves of alkali metal doped $(M,Ca)_8Al_{12}O_{24}S_{1.4}Cl_{1.2}$ samples after irradiation with 302 nm UV radiation for 5 minutes.*

Reflectance measurements were once again measured before, immediately after and 10 minutes after (to remove PeL) irradiation with 254 nm UV radiation, however, the results once again showed very little difference in sample reflectance before and 10 minutes after irradiation. A slight decrease in reflectance at 600 nm could be seen in some of the samples immediately after irradiation along with two emission peaks in the range of 300-500 nm like in Fig. 15. Due to the high energy of the PeL, it is possible that auto-bleaching might have occured. The reflectance spectra can be seen in appendinx 6.

3.4. Composition, luminescence, and reflectance of non-sodalite alkali metal aluminates.

Samples $Li_{12}Ca_2$, Li_{16}, Na_8Ca_4, $Na_{12}Ca_2$, Na_{16}, K_8Ca_4, $K_{12}Ca_2$ and K_{16} had little to no sodalite content, however still exhibited luminescence and in case of Li_{16} tenebrescence properties. Photos of all doped samples, both sodalite containing and non-containing, under 254, 302 and 365 nm UV

radiation can be seen in appendix 7. Li_8Ca_4 will also be discussed in this section as it consists of a significant portion of non-sodalite aluminates.

3.4.1. X-ray powder diffraction and X-ray fluorescence spectroscopy

Table 3.7 shows a more detailed phase composition of the non-sodalite alkali metal doped samples.

Table 3.7. Composition of the alkali metal doped samples calculated using quantitative phase analysis.

	Phase composition			
	$Ca_8Al_{12}O_{24}S_2$, %	$Ca_8Al_{12}O_{24}(SO_4)_2$, %	$CaAl_2O_4$, other Ca aluminates or salts, %	Alkali metal aluminates or salts, %
Li_8Ca_4	57.6	8.7	-	33.7 ($LiAlO_2$, 04-014-1660)
$Li_{12}Ca_2$	29.9	-	10.5 ($Al_{2.67}O_4$)	59.6 ($LiAlO_2$, 04-014-1660)
Li_{16}	-	-	-	100 ($LiAlO_2$, 04-014-1660)
Na_8Ca_4	34.4	-	18.5 ($CaAl_2O_4$, 00-062-0217)	47.1 ($NaAlO_2$, 04-066-9358)
$Na_{12}Ca_2$	-	0.2	10.0 (CaS, 04-004-1202)	89.7 ($NaAlO_2$, 04-066-9358)
Na_{16}	-	-	-	97.6 ($NaAlO_2$, 04-066-9358) 2.4 ($NaAl_{11}O_{17}$ 04-010-0578)

	Phase composition			
	$Ca_8Al_{12}O_{24}S_2$, %	$Ca_8Al_{12}O_{24}(SO_4)_2$, %	$CaAl_2O_4$, other Ca aluminates or salts, %	Alkali metal aluminates or salts, %
K_8Ca_4	0.5	-	61.4 ($CaAl_4O_7$, 04-007-7465) 38.1 ($CaAl_2O_4$, 01-080-3836)	-
$K_{12}Ca_2$	-	-	66.4 ($CaAl_4O_7$, 00-023-1037)	33.6 ($KAl_{11}O_{17}$, 00-023-1037)
K_{16}	-	-	-	93.2 ($KAl_{11}O_{17}$, 00-023-1037) 6.8 (K_2S, 01-074-1030)

The only samples that contain a significant amount of sodalite are Li_8Ca_4, $Li_{12}Ca_2$ and Na_8Ca_4. The rest of the samples mainly contain either $CaAl_2O_4$ and $CaAl_4O_7$ or the analogue alkali metal aluminates. K containing samples are the only ones that contain aluminates with $(Al_{11}O_{17})^-$ species.

Table 3.8 shows all the abundant elements in these samples. The elements present are the same as in the sodalite-containing alkali metal doped samples.

Table 3.8. Most abundant elements in the alkali metal aluminate samples with different M/Ca ratios.

	Ca, wt%	Al, wt%	S, wt%	Cl, wt%	Mg, wt%	Si, wt%	K, wt%	Zn, wt%	Rb, ppm
Li_8Ca_4	40.59	48.43	5.78	0.14	3.40	1.04	0.35	0.15	37.4
$Li_{12}Ca_2$	34.88	54.86	3.02	0.38	4.11	1.94	0.42	-	140.0
Li_{16}	0.41	86.00	1.74	0.81	6.13	3.51	0.35	0.69	86.3
	Ca, wt%	Al, wt%	S, wt%	Cl, wt%	Mg, wt%	Si, wt%	Na, wt%	K, Wt%	Rb, ppm
Na_8Ca_4	40.89	45.09	6.37	0.10	3.33	1.17	2.11	0.75	51.0
$Na_{12}Ca_2$	21.33	49.60	2.71	0.32	3.89	2.10	19.25	0.52	64.0

	Ca, wt%	Al, wt%	S, wt%	Cl, wt%	Mg, wt%	Si, wt%	Na, wt%	K, Wt%	Rb, ppm
Na16	0.60	59.25	0.31	0.34	5.41	2.05	31.46	0.39	9.7
	Ca, wt%	Al, wt%	S, wt%	Cl, wt%	Mg, wt%	Si, wt%	K, wt%	Zn, wt%	Rb, Ppm
K8Ca4	41.29	50.48	1.86	0.15	3.65	1.51	0.76	0.18	98.2
K12Ca2	25.40	58.34	0.86	0.18	3.82	1.44	9.61	0.20	172.7
K16	3.55	65.47	0.31	0.18	4.65	1.53	23.94	0.24	191.6

3.4.2. Reflectance and luminescence measurements

Emission spectra of the alkali metal doped samples can be seen in Fig. 32, Fig. 33 and Fig. 34.
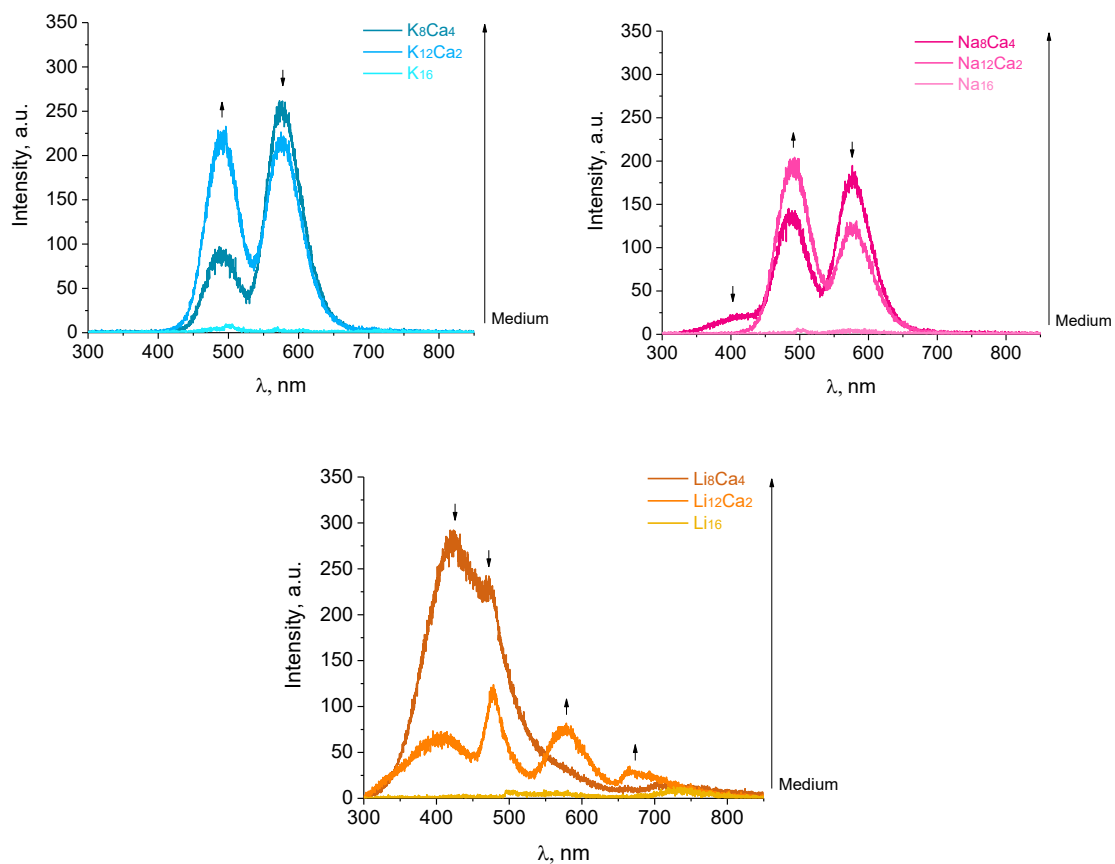
Fig. 32. *Emission spectra of the alkali metal doped samples during irradiation with 254 nm UV radiation.*

When irradiated with 254 nm UV radiation (Fig. 32) peaks at 500 and 580 nm could be seen in the K containing samples, peaks at 420, 500 and 580 nm were observed in the Na containing samples and peaks at 420, 480, 580, 660 and 730 nm could be observed in Li containing samples.

Peaks at 420 and 480 nm are probably due to the small amount of $Ca_8Al_{12}O_{24}S_2$ in these samples, since these peaks can only be seen in the emission spectra of Li_8Ca_4, $Li_{12}Ca_2$ and Na_8Ca_4 and these are the only samples with significant amounts of the sodalite phase.

During irradiation with 302 nm UV radiation, emission spectra can be seen in Fig. 33, peaks at 490 and 580 nm could be seen in both K and Na containing samples. These are the same peaks that were observed when irradiating the samples with 254 nm UV. It seems that K and Na containing samples have luminescence centres with similar energies and only the intensity of the emission causes the difference in luminescence colour.

In Li containing samples peaks at 520, 560, 590 and 670 nm could be observed. Many of the peaks are overlapping and it is possible that other emission peaks simply are not distinguishable.
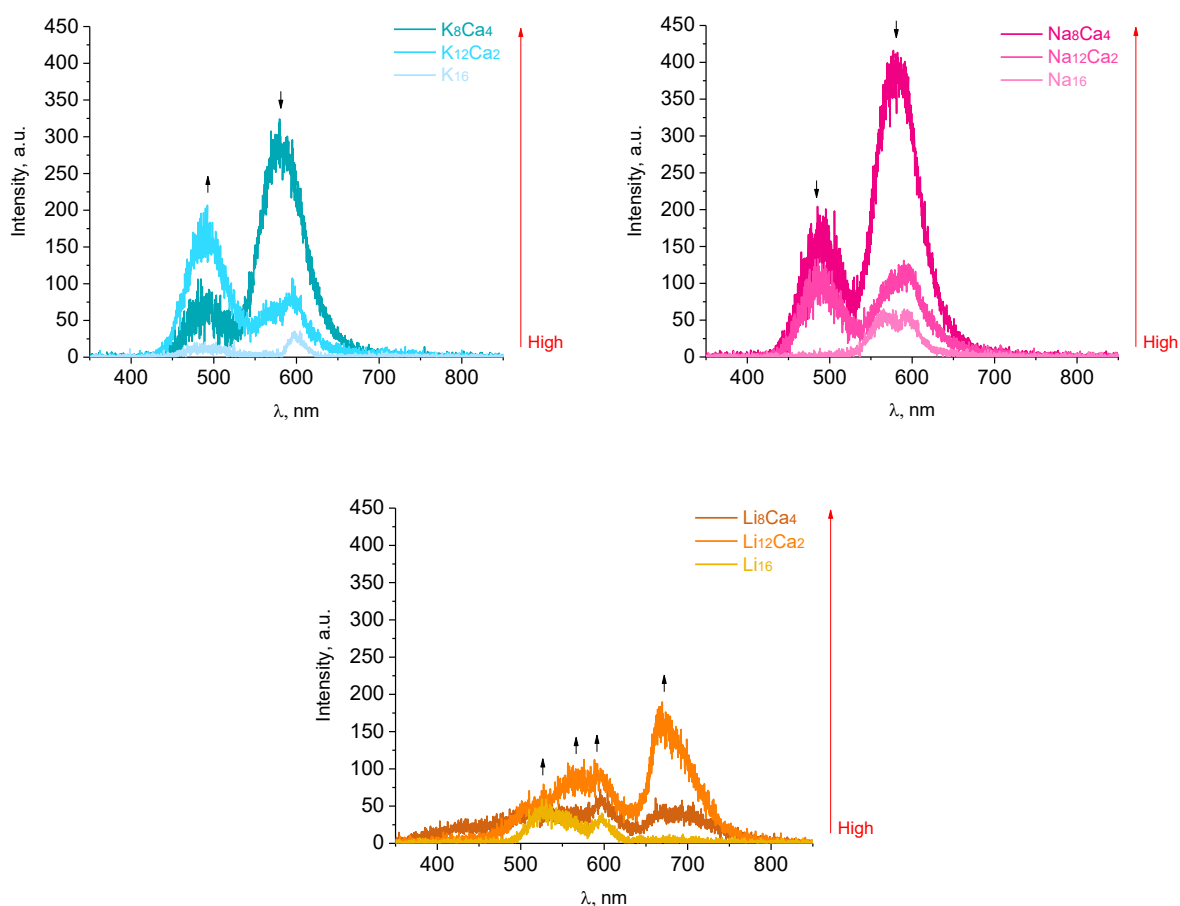
Fig. 33. *Emission spectra of the alkali metal doped samples during irradiation with 302 nm UV radiation.*

During irradiation with 365 nm UV radiation (Fig. 34) various peaks could be seen in the emission spectra of the K containing samples – peaks around 580 and 730 nm are the only ones that could be easily distinguished. A wide peak that could potentially be a group of overlapping peaks were also observed in 550-700 nm range. In Na containing samples peaks around 500 nm, 580 nm,

an extremely narrow peak around 690 nm and the peak at 730 nm, which could be due to excitation harmonics, were observed. In Li containing samples only peaks an extremely narrow peak at 710 nm and the peak at 730 nm could be observed.
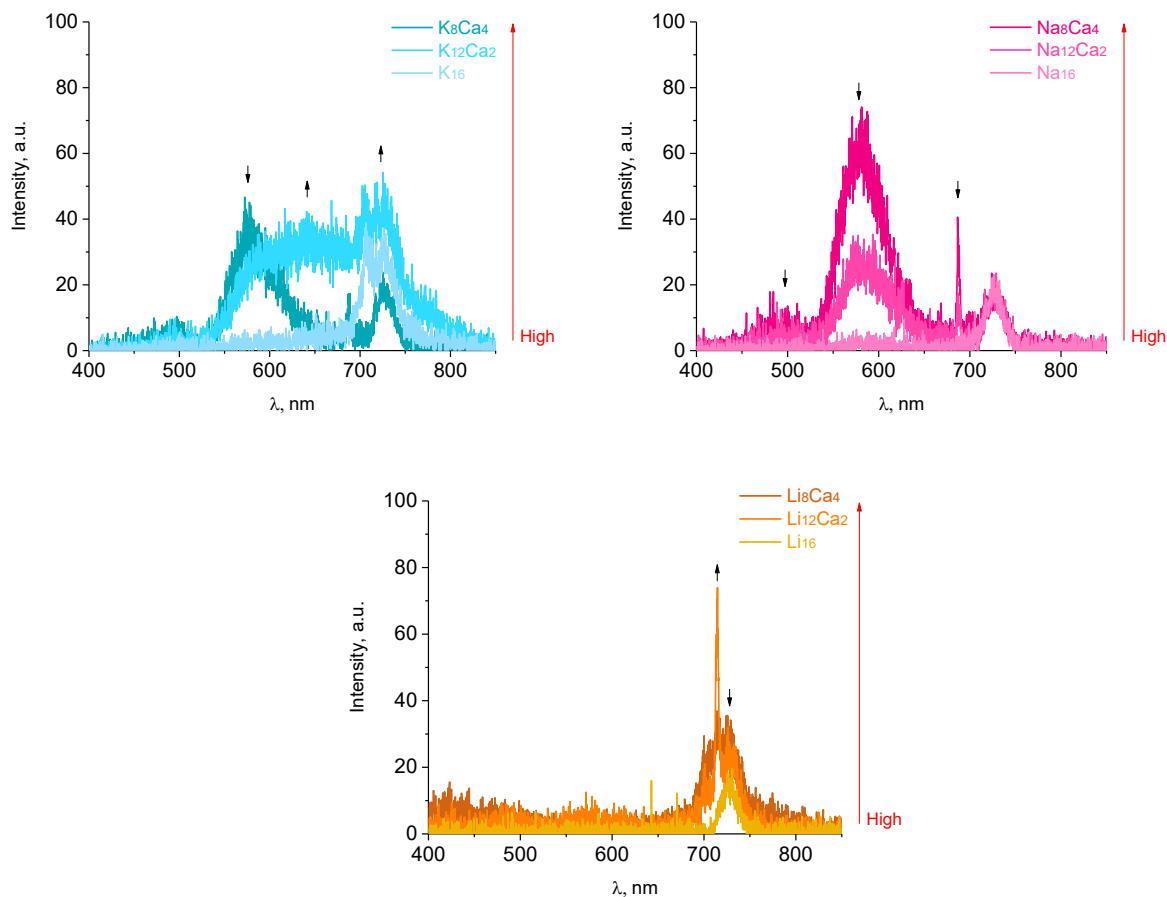
Fig. 34. *Emission spectra of the alkali metal doped samples during irradiation with 365 nm UV radiation.*

The excitation spectra of the sodalite non-containing alkali metal doped samples were the same as those that were seen in the sodalite containing alkali metal doped samples, therefore they will not be discussed in detail. The excitation spectra can be seen in appendix 8. It has to be noted that the multi-peak excitation spectra that could be seen in Fig. 27, where it was hypothesized to be due to impurities in Li_4Ca_6 and Li_8Ca_4, also shows up in all Na and K samples when measuring the excitation of emissions with 690, 710 and 730 nm wavelength.

PeL emission spectra seen in Fig. 35 show that in all samples the same peaks as were seen during irradiation with 254 nm UV slightly shift as the alkali metal concentration increases. Intensity of PeL decreases in K and Na containing samples with increasing alkali metal ion concentration, however in the Li containing samples it briefly increases and in the Li_{16} sample almost no PeL is detected.
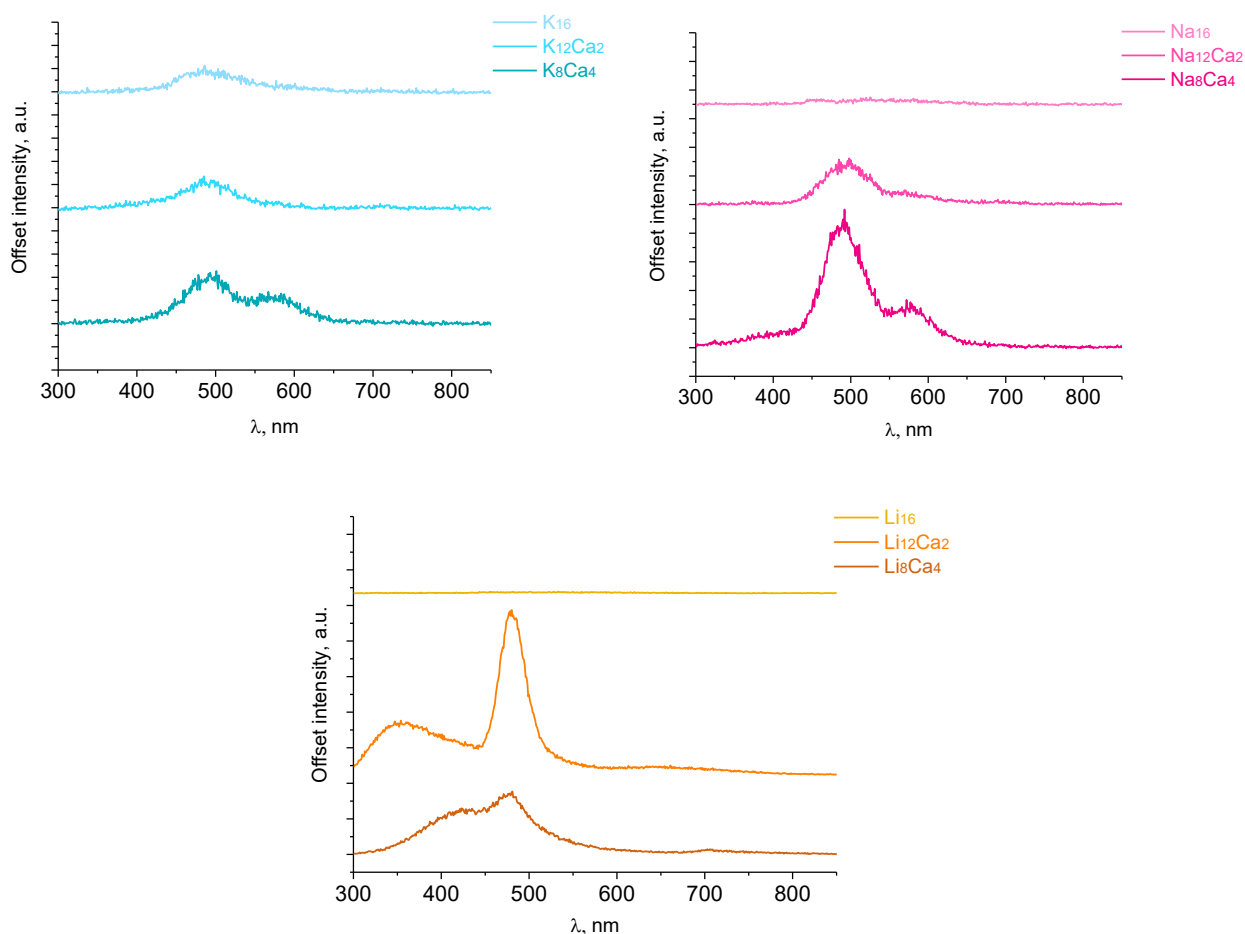
Fig. 35. *PeL emission spectra of the non-sodalite alkali metal doped samples after irradiation with 254 nm UV radiation for 5 minutes.*

PeL fading of the samples can be seen in appendix 9. The results follow the same trend as in the case of the sodalite containing alkali metal doped samples. All Li samples except for Li_{16} as well as Na_8Ca_4 and K_8Ca_4 show high initial luminescence intensity and long luminescence duration.

TL glow curves showed similar results in after irradiation with 254, 302 and 365 UV and radiation from the solar lamp. TL curves after irradiation with 254 nm UV can be seen in Fig. 36. The rest of the glow curves can be seen in appendix 10.

As previously mentioned, the peak placement did not change depending on the irradiation source and the only thing that varied was TL intensity. Li samples showed the highest TL intensity after being exposed all types of radiation. These were also the only samples that had only one peak, although 160-170°C rendering Li materials unfit for use in dosimetry. K and Na samples had two peaks- in K samples a peak around 160°C and 270°C could be observed, while in Na samples around 160°C and 220°C. The peak around 220°C was only present in Na samples after irradiation with 254 nm UV radiation.
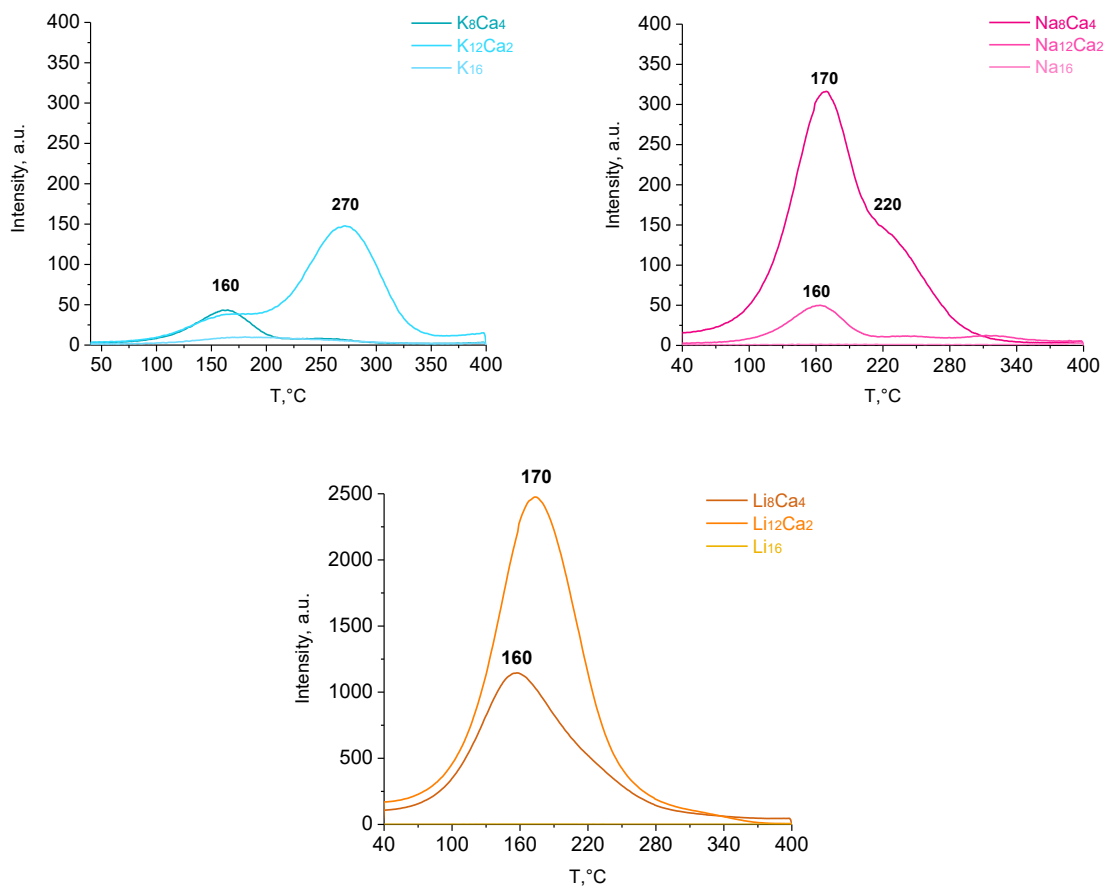
Fig. 36. *TL glow curves of non-sodalite containing alkali metal doped samples after irradiation with 254 nm UV radiation for 5 minutes.*

The results of reflectance measurements before, immediately after and 10 minutes after irradiation with 254 nm UV radiation for 5 minutes were the same as in the case of sodalite containing alkali metal doped samples. No visible colour change was observed before and 10 minutes after irradiation, however, in some samples during measurements immediately after irradiation in which PeL was also detected the reflectance in some parts of the samples decreased. These results can be seen in appendix 11.

Visible colour change was, however, observed in the 100% $LiAlO_2$ containing Li_{16} (a) sample after one hour of irradiation with X-rays from the XRF measurement. Another sample Li_{16} (b) with the same amounts of precursor was prepared in order to compare the results, however, this time there was no colour change after the XRF measurement. The reflectance spectra and photos of both samples can be seen in Fig. 37.
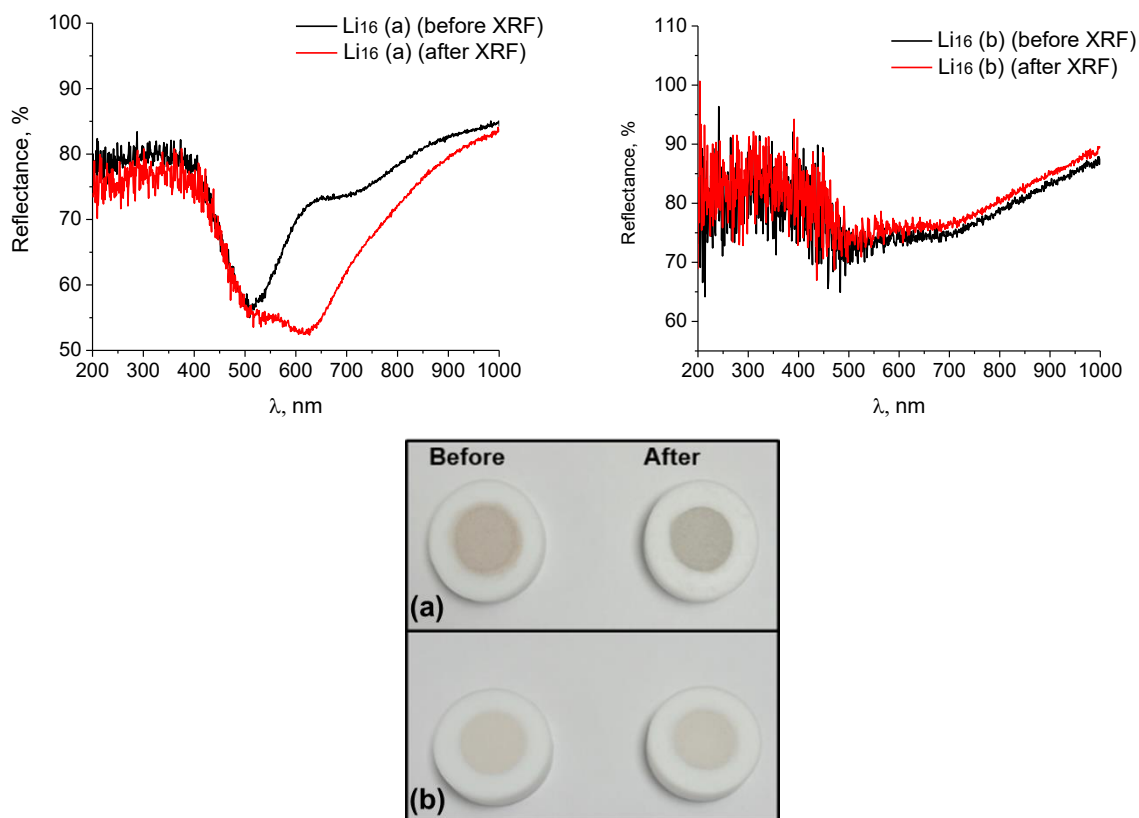
Fig. 37. *Reflectance measurements of Li₁₆ (a) and (b) before and after irradiation with X-rays from the XRF measurement for one hour (top) and photos of the same samples (bottom).*

XRF data from both samples can be seen in Table 3.9. According to these results, the only elements that change significantly are Al, S and Zn. Changes in Al have not caused tenebrescence in any other samples, therefore it could either be the presence of S or Zn causing the colour change.

Table 3.9. Most abundant elements in the LiAlO₂ containing Li₁₆ (a) and (b) samples.

	Ca, wt%	Al, wt%	S, wt%	Cl, wt%	Mg, wt%	Si, wt%	K, wt%	Zn, wt%	Rb, ppm
Li₁₆ (a)	0.41	86.00	1.74	0.81	6.13	3.51	0.35	0.69	86.3
Li₁₆ (b)	0.81	89.98	0.17	0.64	7.30	3.57	0.25	506.4 (ppm)	121.5

CONCLUSIONS

In this work calcium aluminate sodalites with varying S/Cl ratios were synthesized. The photoluminescence, thermoluminescence and tenebrescence properties of these materials were analysed for the first time. Two calcium aluminate sodalite species were present in the samples – reduced sodalite $Ca_8Al_{12}O_{24}S_2$ and non-reduced sodalite $Ca_8Al_{12}O_{24}(SO_4)_2$, samples contained also $Ca_6Al_7O_{16}Cl$ and different calcium aluminates in samples with added Cl ions. Calcium aluminate sodalites containing only Cl anions could not be synthesized likely due to the large number of ions needed to replace the bivalent S ions. $Ca_8Al_{12}O_{24}S_2$ was the only one of these phases that showed luminescence in the blue light region when isolated, while $Ca_8Al_{12}O_{24}(SO_4)_2$ and the calcium aluminates showed little to no luminescence.

Although it showed no luminescence when isolated, samples with high concentration of $Ca_8Al_{12}O_{24}(SO_4)_2$ showed some changes in luminescence, like the presence of an orange emission band when irradiated with 302 nm UV radiation, which was not observed in fully reduced samples. Integrated intensity of TL glow curves, which is proportional to the concentration of defects also showed that the TL properties of these samples could be affected by the concentration of $Ca_8Al_{12}O_{24}S_2$ versus $Ca_8Al_{12}O_{24}(SO_4)_2$ phases. Increase in the integrated intensity value in samples with higher $Ca_8Al_{12}O_{24}S_2$ content could be observed.

Sample with the S/Cl ratio of $S_{1.4}Cl_{1.2}$ had some of the best photo- and thermoluminescence results of all calcium aluminate sodalite containing samples, which is why this S/Cl ratio was selected to analyse the effect of Li, Na, K and Rb dopants on the luminescence and tenebrescence properties of these samples. Li doped samples had the highest sodalite content even up to Li/Ca ratio of Li_8Ca_4, followed by Na_4Ca_6 and K_4Ca_6. Like in the case of the Cl anions the collapse of the sodalite cage could have been due to the size and the number of exchanged cations. Only one sample containing Rb was synthesized, the Rb/Ca ratio was $Rb_{1.2}Ca_{7.4}$.

All dopants increased the photoluminescence emission intensity of the base material, with $M_{1.2}Ca_{7.4}$ (M – alkali metal) being the ratio with the highest intensity in all doped samples. Adding Li, K and Na ions in M_4Ca_6 ratio to Ca ions led to an increase in PeL emission intensity and duration as seen in the PeL emission spectra and PeL fading curves. The excitation spectra of emissions around 690, 710 and 730 nm in Li_4Ca_6 and Li_8Ca_4 samples, which were significantly different from the other samples, signified that there could be other impurities present that act as luminescence centres. While adding dopants increased the total TL intensity in some cases, it also caused the peaks to shift closer to the room temperature, making these materials unusable for dosimetry applications.

Samples containing little to none of the sodalite phase still exhibited luminescence under UV radiation. Unfortunately, the same excitation spectra that could be found in Li_4Ca_6 and Li_8Ca_4 samples that could have been due to impurities were also present in the majority of these samples.

While none of the sodalite containing samples and most of the aluminate samples showed no tenebrescence after irradiation with 254 nm UV, Li_{16} which was a sample containing only the $LiAlO_2$ phase, showed visible colour change after irradiation with X-ray from the XRF measurement. By attempting and failing to repeat this experiment with a new sample synthesized the same way, Zn and S were concluded to be the only two elements that had a significant concentration difference in both samples. Therefore, either Zn or S could be the cause of tenebrescence in $LiAlO_2$.

Based on the observations made during this work, future research on aluminate sodalites could focus on exchanging the extra-framework ions of $Ca_8Al_{12}O_{24}S_2$ with larger bivalent ions. That would solve the problem of the sodalite cage collapsing due to twice as many monovalent ions being necessary to neutralize the charge. Strontium aluminate sodalites in particular could potentially have good photoluminescence properties as some strontium aluminates are well known phosphors, like Eu and Dy doped $SrAl_2O_4$.

There is also potential for practical applications of aluminate sodalites. Due to the structural similarities with ye'elimite in the previously discussed sulfoaluminate cements, photoluminescent aluminate sodalites could be used as an additive in these cements to obtain a material with both high mechanical strength and good photoluminescence properties. This type of material could be a more durable alternative to photoluminescent paints for road marking, which have gained increasing interest due to better visibility in low light environments.

LIST OF REFERENCES

1. Al-Qahtani, S. D.; Alzahrani, S. O.; Snari, R. M.; Al-Ahmed, Z. A.; Alkhamis, K.; Alhasani, M.; El-Metwaly, N. M. Preparation of Photoluminescent and Photochromic Smart Glass Window Using Sol-Gel Technique and Lanthanides-Activated Aluminate Phosphor. *Ceramics International* **2022**, *48* (12), 17489–17498. https://doi.org/10.1016/j.ceramint.2022.03.013.

2. Yang, Z.; Hu, J.; Van der Heggen, D.; Jiao, M.; Feng, A.; Vrielinck, H.; Smet, P.; Poelman, D. A Versatile Photochromic Dosimeter Enabling Detection of X-Ray, Ultraviolet, and Visible Photons. *Laser & Photonics Review* **2023**, *17*. https://doi.org/10.1002/lpor.202200809.

3. Tang, W.; Zuo, C.; Ma, C.; Wang, Y.; Li, Y.; Yuan, X.; Wang, E.; Wen, Z.; Cao, Y. Designing Photochromic Materials with High Photochromic Contrast and Large Luminescence Modulation for Hand-Rewritable Information Displays and Dual-Mode Optical Storage. *Chemical Engineering Journal* **2022**, *435*, 134670. https://doi.org/10.1016/j.cej.2022.134670.

4. Jiang, X.; Guo, Y.; Wang, L.; Zhang, Q. Dynamic Photoluminescent and Photochromic Properties of $CaAl_{12}O_{19}$:Eu,Tb: A Novel Phosphor for Advanced Dual-Modal Multicolor Anticounterfeiting. *Ceramics International* **2023**. https://doi.org/10.1016/j.ceramint.2023.09.325.

5. Kayani, A. B. A.; Kuriakose, S.; Monshipouri, M.; Khalid, F. A.; Walia, S.; Sriram, S.; Bhaskaran, M. UV Photochromism in Transition Metal Oxides and Hybrid Materials. *Small* **2021**, *17* (32), 2100621. https://doi.org/10.1002/smll.202100621.

6. Badour, Y.; Jubera, V.; Andron, I.; Frayret, C.; Gaudon, M. Photochromism in Inorganic Crystallised Compounds. *Optical Materials: X* **2021**, *12*, 100110. https://doi.org/10.1016/j.omx.2021.100110.

7. Byron, H.; Swain, C.; Paturi, P.; Colinet, P.; Rullan, R.; Halava, V.; Le Bahers, T.; Lastusaari, M. Highly Tuneable Photochromic Sodalites for Dosimetry, Security Marking and Imaging. *Advanced Functional Materials* **2023**. https://doi.org/10.1002/adfm.202303398.

8. Valeur, B.; Berberan Santos, M. N. A Brief History of Fluorescence and Phosphorescence before the Emergence of Quantum Theory. *Journal of Chemical Education* **2011**, *88*. https://doi.org/10.1021/ed100182h.

9. Vedda, A.; Fasoli, M. Tunneling Recombinations in Scintillators, Phosphors, and Dosimeters. *Radiation Measurements* **2018**, *118*, 86–97. https://doi.org/10.1016/j.radmeas.2018.08.003.

10. Mehare, M. D.; Mehare, C. M.; Swart, H. C.; Dhoble, S. J. Recent Development in Color Tunable Phosphors: A Review. *Progress in Materials Science* **2023**, *133*, 101067. https://doi.org/10.1016/j.pmatsci.2022.101067.

11. Townsend, P. D.; Wang, Y.; McKeever, S. W. S. Spectral Evidence for Defect Clustering: Relevance to Radiation Dosimetry Materials. *Radiation Measurements* **2021**, *147*, 106634. https://doi.org/10.1016/j.radmeas.2021.106634.

12. Zhao, Y.; Wang, X.; Zhang, Y.; Li, Y.; Yao, X. Optical Temperature Sensing of Up-Conversion Luminescent Materials: Fundamentals and Progress. *Journal of Alloys and Compounds* **2020**, *817*, 152691. https://doi.org/10.1016/j.jallcom.2019.152691.

13. Sun, S.-K.; Wang, H.-F.; Yan, X.-P. Engineering Persistent Luminescence Nanoparticles for Biological Applications: From Biosensing/Bioimaging to Theranostics. *Accounts of Chemical Research* **2018**, *51* (5), 1131–1143. https://doi.org/10.1021/acs.accounts.7b00619.

14. Wu, H.; Wang, M.; Huai, L.; Wang, W.; Zhang, J.; Wang, Y. Optical Storage and Operation Based on Photostimulated Luminescence. *Nano Energy* **2021**, *90*, 106546. https://doi.org/10.1016/j.nanoen.2021.106546.

15. Nieto, J. A. Present Status and Future Trends in the Development of Thermoluminescent Materials. *Applied Radiation and Isotopes* **2016**, *117*, 135–142. https://doi.org/10.1016/j.apradiso.2015.11.111.

16.   Du, J.; Yang, Z.; Lin, H.; Poelman, D. Inorganic Photochromic Materials: Recent Advances, Mechanism, and Emerging Applications. *Responsive Materials* **2024**, *2*, e20240004. https://doi.org/10.1002/rpm.20240004.

17.   Norrbo, I.; Gluchowski, P.; Paturi, P.; Sinkkonen, J.; Lastusaari, M. Persistent Luminescence of Tenebrescent $Na_8Al_6Si_6O_{24}(Cl,S)_2$: Multifunctional Optical Markers. *Inorganic Chemistry* **2015**, *54* (16), 7717–7724. https://doi.org/10.1021/acs.inorgchem.5b00568.

18.   Friis, H. Sodalite—a Mineralogical Chameleon. *Geology Today* **2011**, *27* (5), 194–198. https://doi.org/10.1111/j.1365-2451.2011.00809.x.

19.   Agamah, C.; Vuori, S.; Colinet, P.; Norrbo, I.; de Carvalho, J. M.; Okada Nakamura, L. K.; Lindblom, J.; van Goethem, L.; Emmermann, A.; Saarinen, T.; Laihinen, T.; Laakkonen, E.; Lindén, J.; Konu, J.; Vrielinck, H.; Van der Heggen, D.; Smet, P. F.; Bahers, T. L.; Lastusaari, M. Hackmanite—The Natural Glow-in-the-Dark Material. *Chemistry of Materials* **2020**, *32* (20), 8895–8905. https://doi.org/10.1021/acs.chemmater.0c02554.

20.   Finch, A. A.; Friis, H.; Maghrabi, M. Defects in Sodalite-Group Minerals Determined from X-Ray-Induced Luminescence. *Physics and Chemistry of Minerals* **2016**, *43* (7), 481–491. https://doi.org/10.1007/s00269-016-0816-7.

21.   Colinet, P.; Byron, H.; Vuori, S.; Lehtiö, J.-P.; Laukkanen, P.; Goethem, L. V.; Lastusaari, M.; Bahers, T. L. The Structural Origin of the Efficient Photochromism in Natural Minerals. *Proceedings of the National Academy of Sciences* **2022**, *119* (23), e2202487119. https://doi.org/10.1073/pnas.2202487119.

22.   Williams, E. R.; Simmonds, A.; Armstrong, J. A.; Weller, M. T. Compositional and Structural Control of Tenebrescence. *Journal of Materials Chemistry* **2010**, *20* (48), 10883–10887. https://doi.org/10.1039/C0JM02066D.

23.   Brenchley, M. E.; Weller, M. T. Synthesis and Structure of Sulfide Aluminate Sodalites. *Journal of Materials Chemistry* **1992**, *2* (10), 1003–1005. https://doi.org/10.1039/JM9920201003.

24.   Heard, C. J.; Grajciar, L.; Nachtigall, P. The Effect of Water on the Validity of Löwenstein's Rule. *Chemical Science* **2019**, *10* (22), 5705–5711. https://doi.org/10.1039/C9SC00725C.

25.   Khessaimi, Y. E.; Hafiane, Y. E.; Smith, A.; Trauchessec, R.; Diliberto, C.; Lecomte, A. Solid-State Synthesis of Pure Ye'elimite. *Journal of the European Ceramic Society* **2018**, *38* (9), 3401–3411. https://doi.org/10.1016/j.jeurceramsoc.2018.03.018.

26.   Abir, F.-Z.; Hafiane, Y. E.; Smith, A.; Kondo, Y.; Sakai, Y.; Asaka, T.; Fukuda, K.; Mesnaoui, M.; Abouliatim, Y.; Nibou, L. Chemical Synthesis and Crystallographic Data on Iron Doped Cubic Ye'elimite. *Cement and Concrete Research* **2023**, *173*, 107257. https://doi.org/10.1016/j.cemconres.2023.107257.

27.   Khessaimi, Y. E.; Hafiane, Y. E.; Smith, A. Ye'elimite Synthesis by Chemical Routes. *Journal of the European Ceramic Society* **2019**, *39* (4), 1683–1695. https://doi.org/10.1016/j.jeurceramsoc.2018.10.025.

28.   Revankar, S. G.; Gedekar, K. A.; Moharil, S. V. Luminescent Materials Based on Aluminates: A Review. *physica status solidi (a)* **2022**, *219* (23), 2200346. https://doi.org/10.1002/pssa.202200346.

29.   Abdelhameed, M. M.; Attia, Y. A.; Abdelrahman, M. S.; Khattab, T. A. Photochromic and Fluorescent Ink Using Photoluminescent Strontium Aluminate Pigment and Screen Printing towards Anticounterfeiting Documents. *Luminescence* **2021**, *36* (4), 865–874. https://doi.org/10.1002/bio.3987.

30.   Lin, Y.; Smedskjaer, M. M.; Mauro, J. C. Structure, Properties, and Fabrication of Calcium Aluminate-Based Glasses. *International Journal of Applied Glass Science* **2019**, *10* (4), 488–501. https://doi.org/10.1111/ijag.13417.

31.   Degen, T.; Sadki, M.; Bron, E.; König, U.; Nénert, G. The HighScore Suite. *Powder Diffraction* **2014**, *29* (S2), S13–S18. https://doi.org/10.1017/S0885715614000840.

32. Gates-Rector, S.; Blanton, T. The Powder Diffraction File: A Quality Materials Characterization Database. *Powder Diffraction* **2019**, *34* (4), 352–360. https://doi.org/10.1017/S0885715619000812.

33. Zengeya, M. A.; Ge, D.; Li, X.; Zhu, N.; Zhou, P.; Xie, P.; Huang, S. Porous Carbon Endows Mayenite with High Activity to Achieve Closed-Loop Removal of Chloride Ions from Desulfurization Wastewater. *Chemical Engineering Journal* **2024**, *490*, 151834. https://doi.org/10.1016/j.cej.2024.151834.

34. Correcher, V.; Garcia-Guinea, J.; Bustillo, M.; García, R. Study of the Thermoluminescence Emission of a Natural α-Cristobalite†. *Radiation Effects & Defects in Solids* **2009**, *164*, 59–67. https://doi.org/10.1080/10420150802270995.

35. Souza, L. B. F. de; Guzzo, P. L.; Khoury, H. J. Correlating the TL Response of γ-Irradiated Natural Quartz to Aluminum and Hydroxyl Point Defects. *Journal of Luminescence* **2010**, *130* (8), 1551–1556. https://doi.org/10.1016/j.jlumin.2010.03.028.

APPENDICES

Appendix 1. Excitation spectra of emissions around 500, 510 and 600 nm in optimally reduced $Ca_8Al_{12}O_{24}S_2$ and $Ca_8Al_{12}O_{24}(S,Cl)_2$ samples.
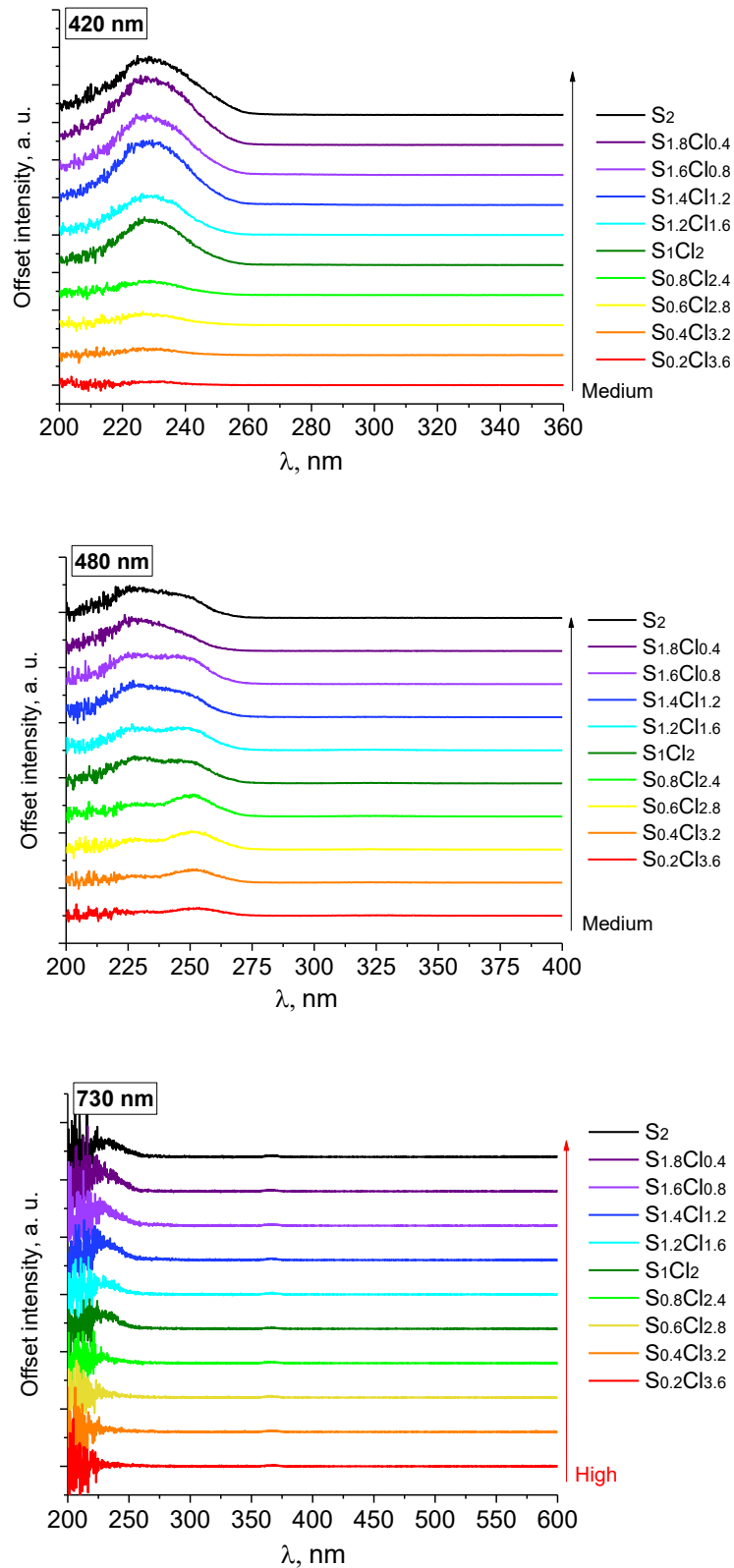
Appendix 2. Reflectance of the optimally reduced samples before, immediately after and seven minutes after irradiation with 254 nm UV radiation.
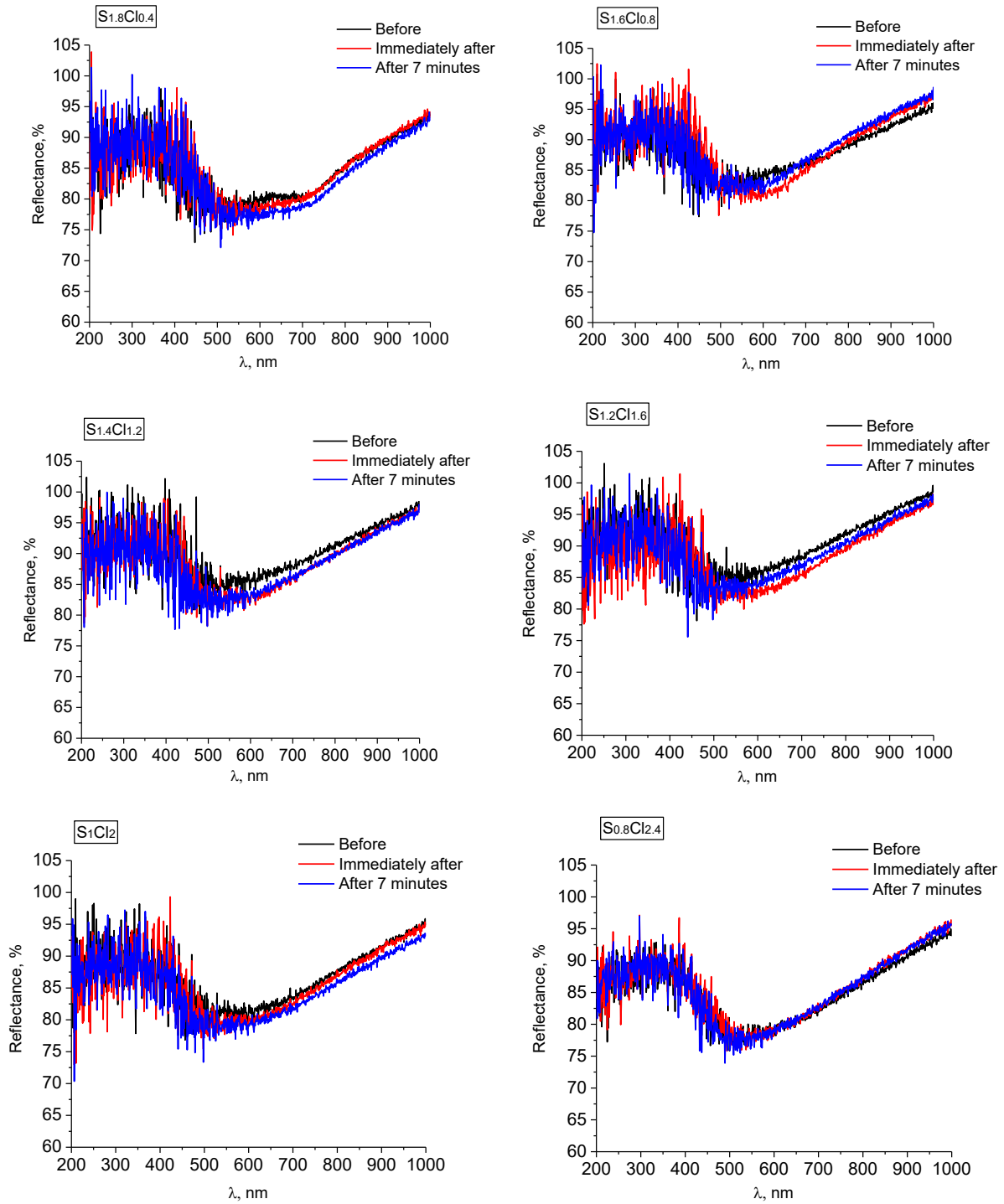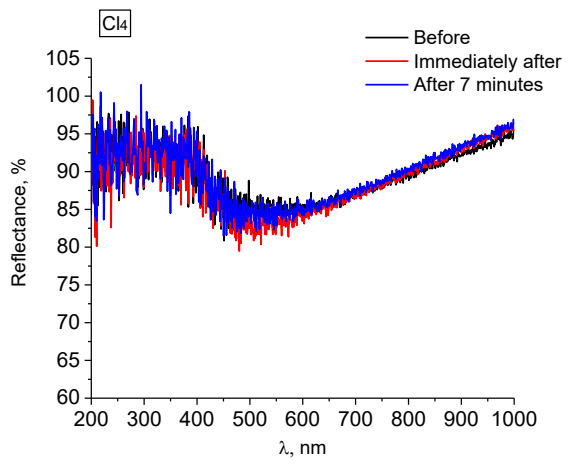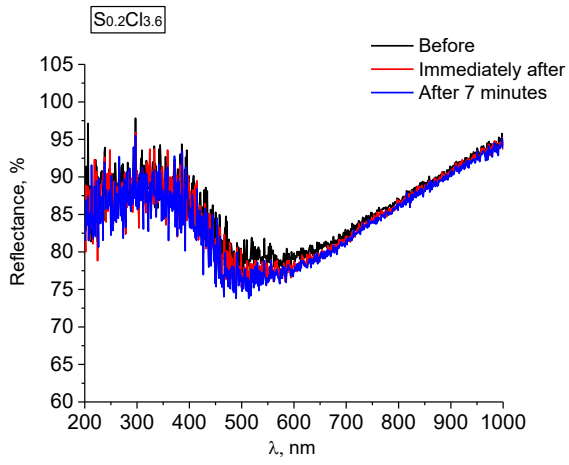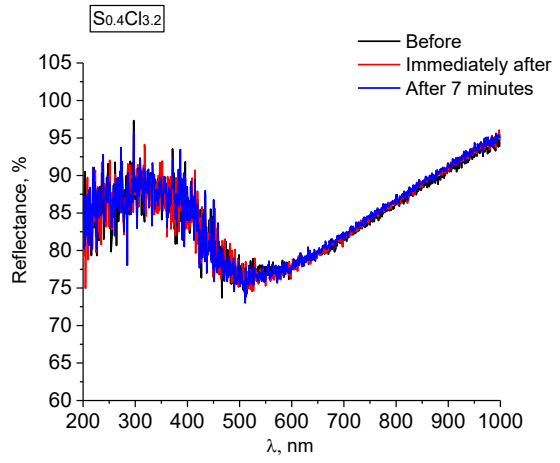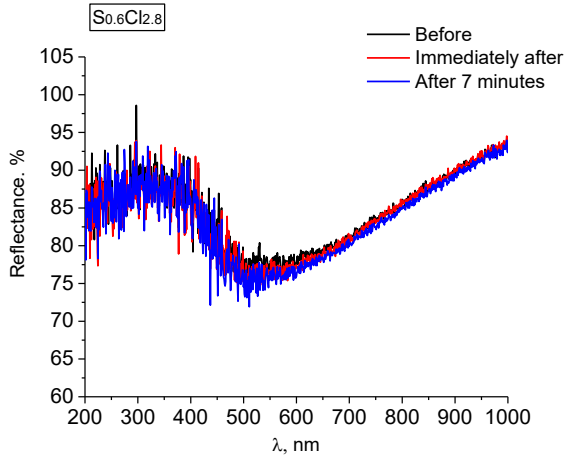
Appendix 3. Emission spectra of $Ca_8Al_{12}O_{24}S_{1.4}Cl_{1.2}$ and the alkali metal doped sodalite containing samples $(M,Ca)_8Al_{12}O_{24}S_{1.4}Cl_{1.2}$ under 365 nm UV radiation.
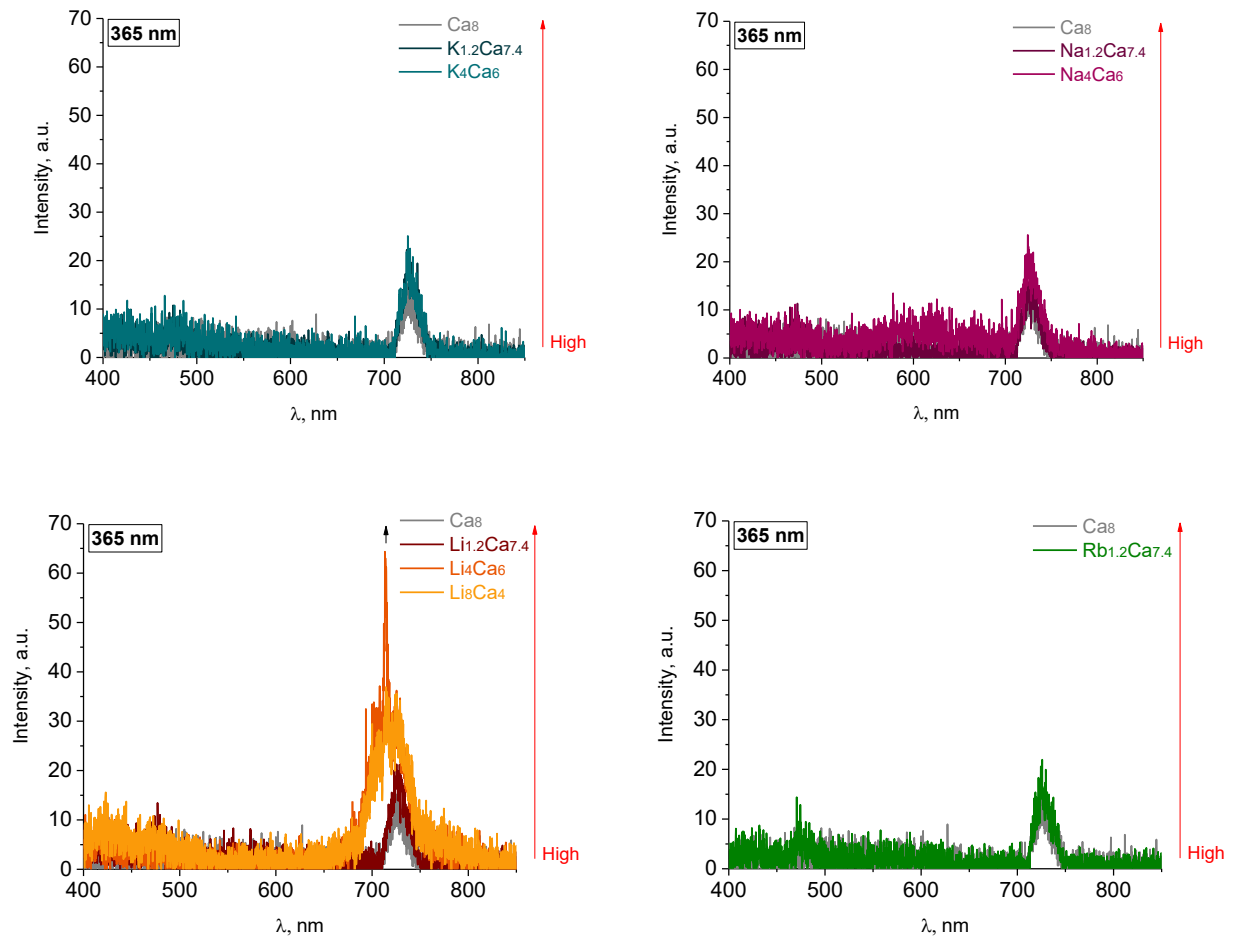
Appendix 4. TL glow curves of sodalite containing alkali metal doped $(M,Ca)_8Al_{12}O_{24}S_{1.4}Cl_{1.2}$ samples after irradiation with 365 nm UV radiation for 5 minutes.
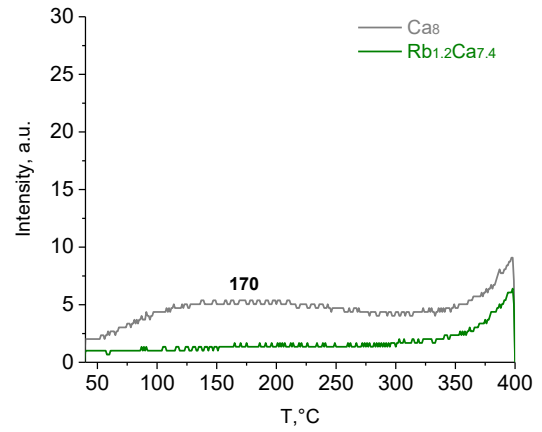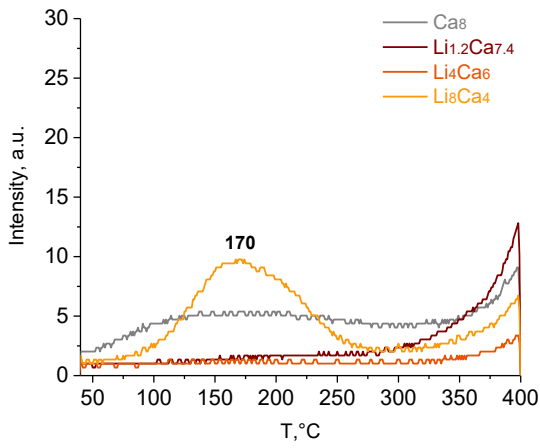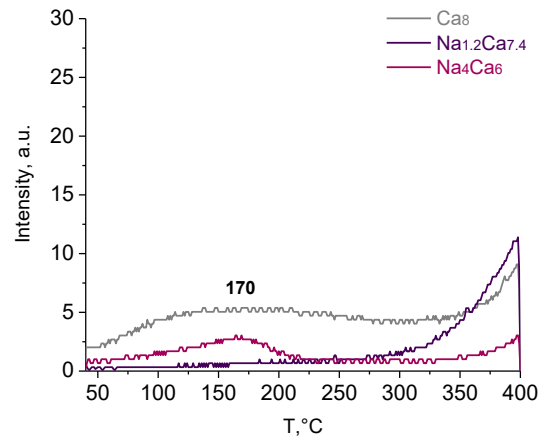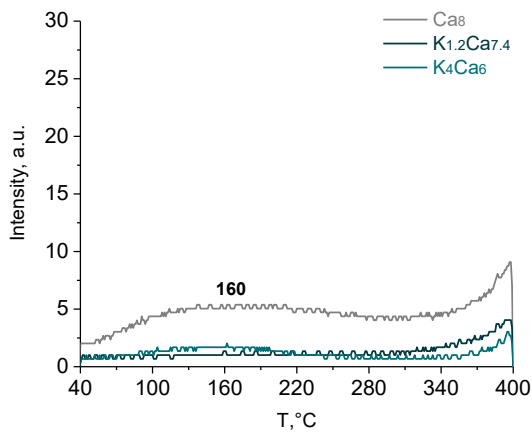
Appendix 5. TL glow curves of sodalite containing alkali metal doped $(M,Ca)_8Al_{12}O_{24}S_{1.4}Cl_{1.2}$ samples after irradiation with radiation from the solar lamp for 5 minutes.
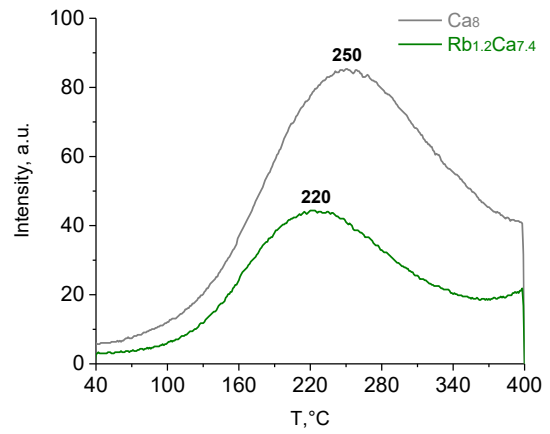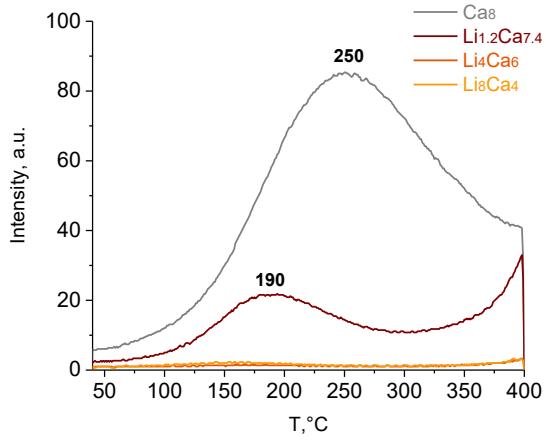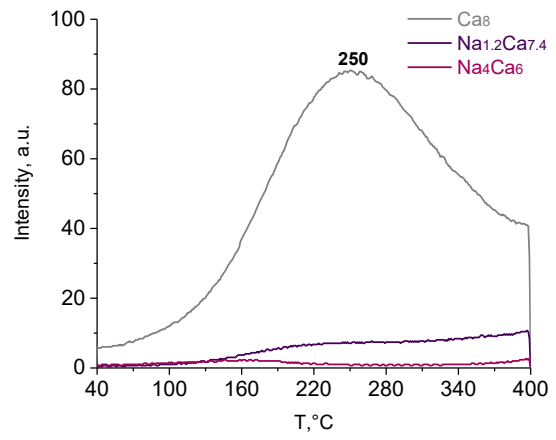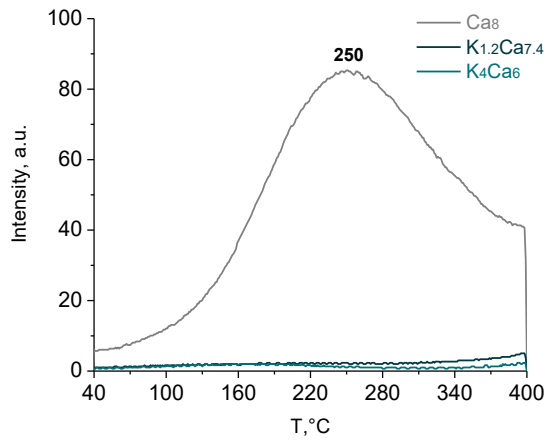
Appendix 6. Reflectance of the sodalite containing alkali metal doped $(M,Ca)_8Al_{12}O_{24}S_{1.4}Cl_{1.2}$ samples before, immediately after and 10 minutes after irradiation with 254 nm UV radiation.
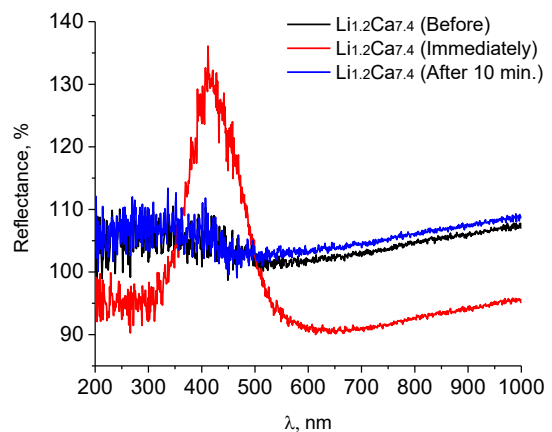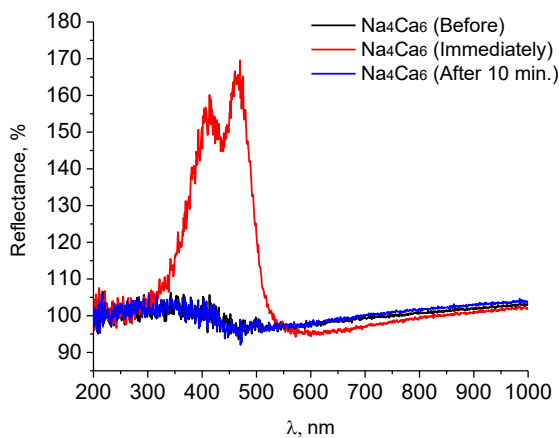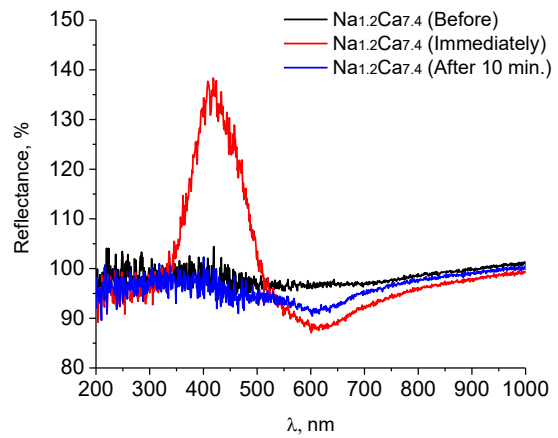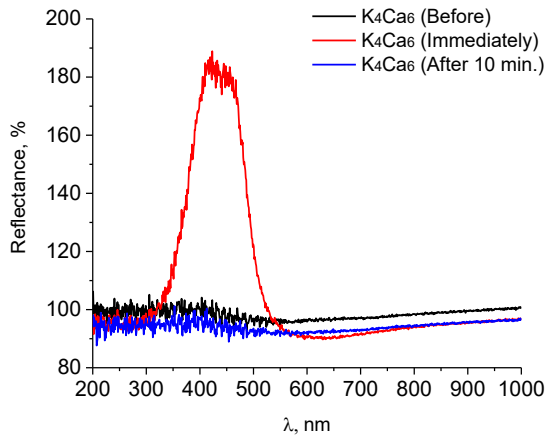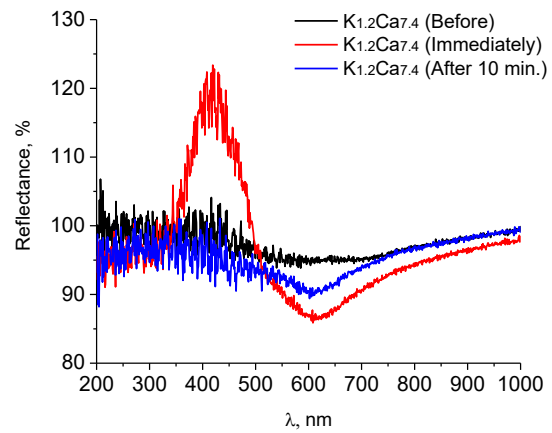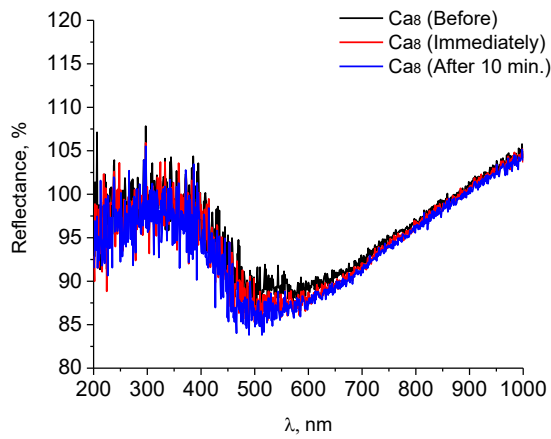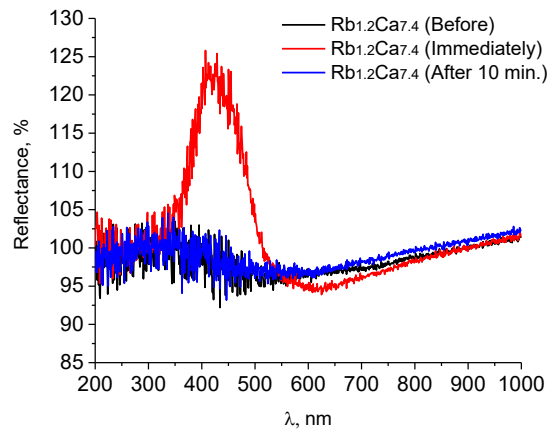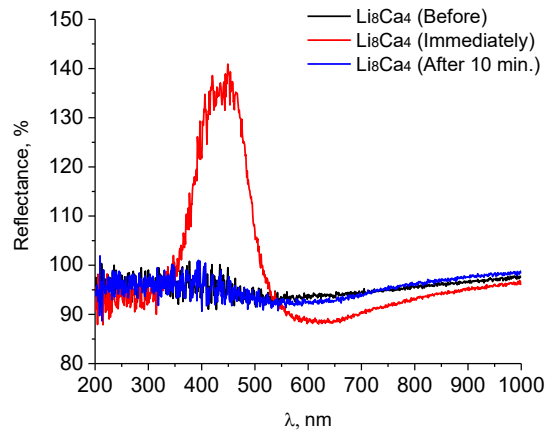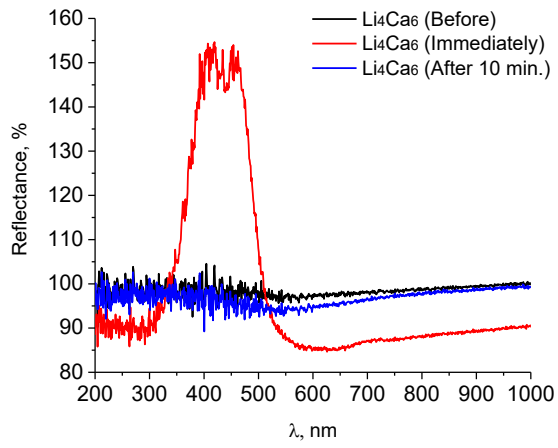
Appendix 7. Photos of all luminescent doped samples, both sodalite containing and non-containing, under 254, 302 and 365 nm UV radiation (the red line divides samples with high vs low sodalite content).

Under 254 nm - photos
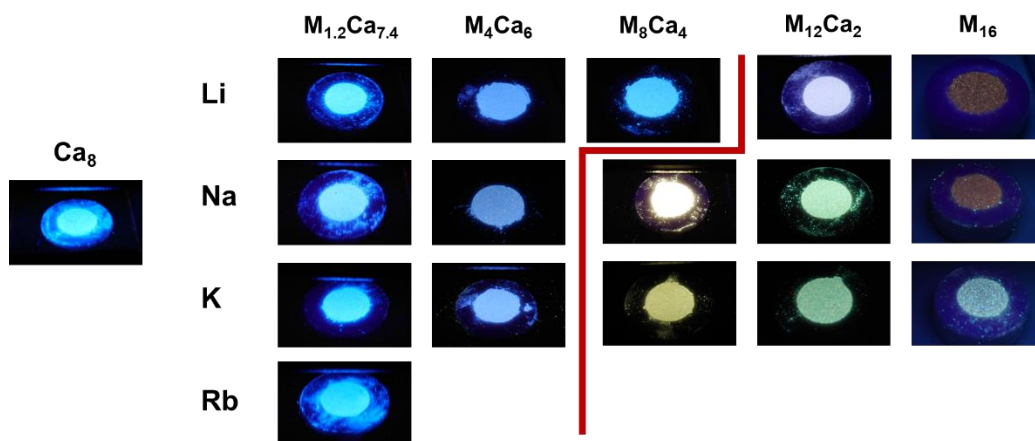
Under 302 nm - photos
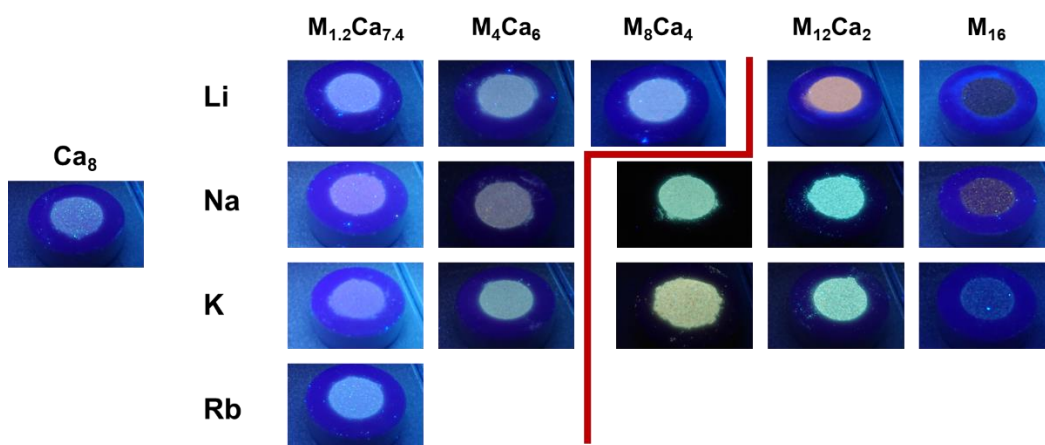
Under 365 nm - photos
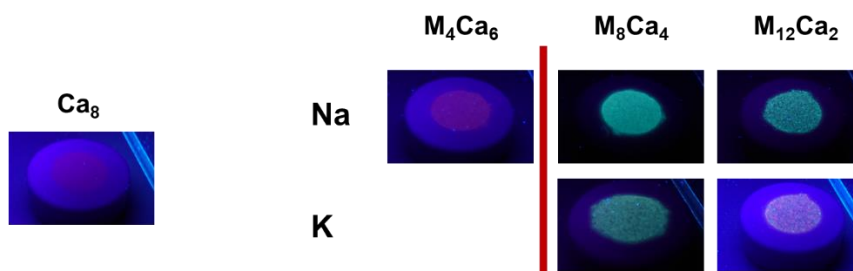
# Appendix 8. Excitation spectra of the non-sodalite alkali metal doped samples.
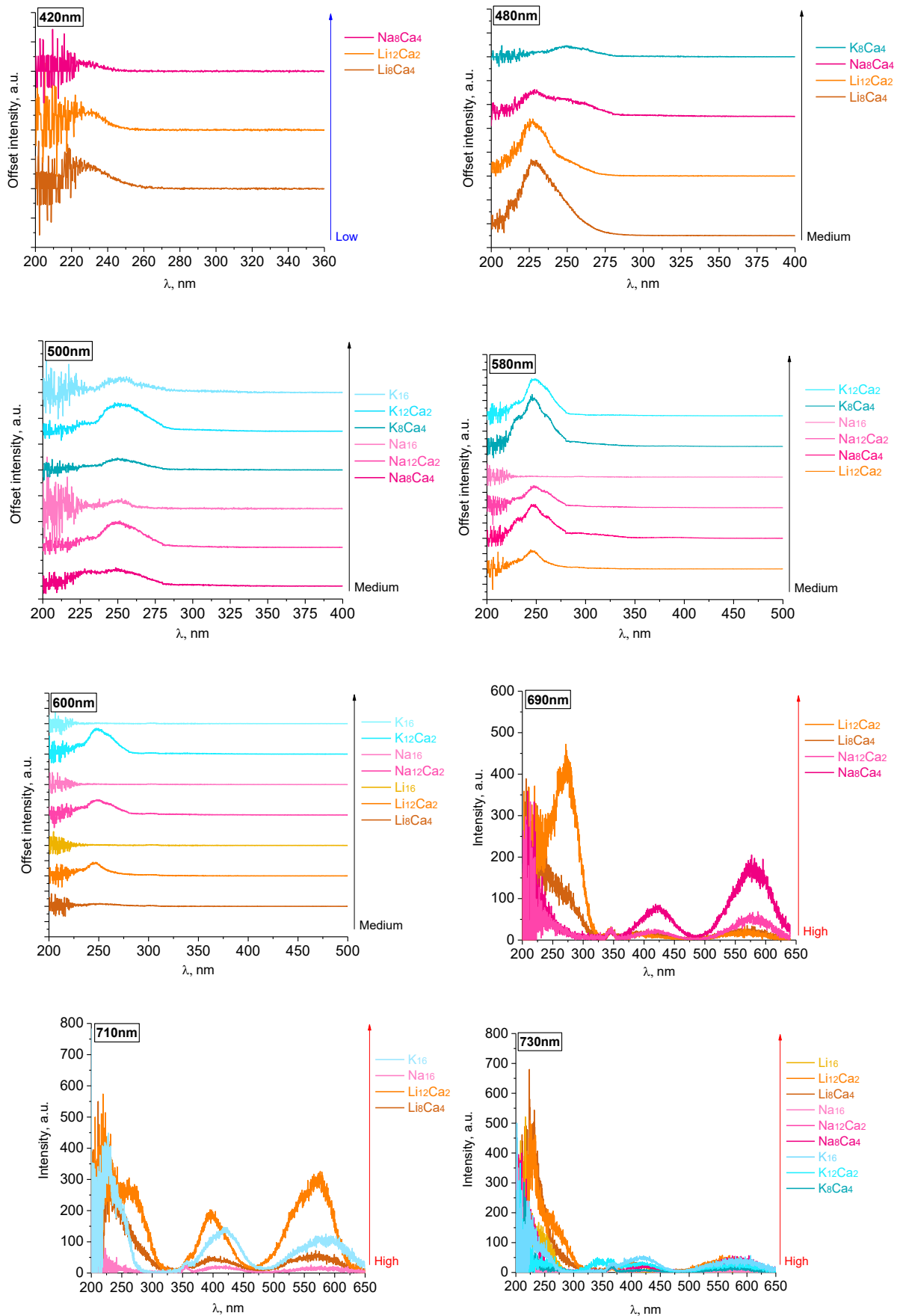
Appendix 9. PeL fading in the non-sodalite alkali metal doped samples irradiated with 254, 302, 365 nm UV radiation and radiation from a solar lamp (only the highest intensity value is shown in each curve, lowest intensity value in all curves is 0.32 mcd/m^2).
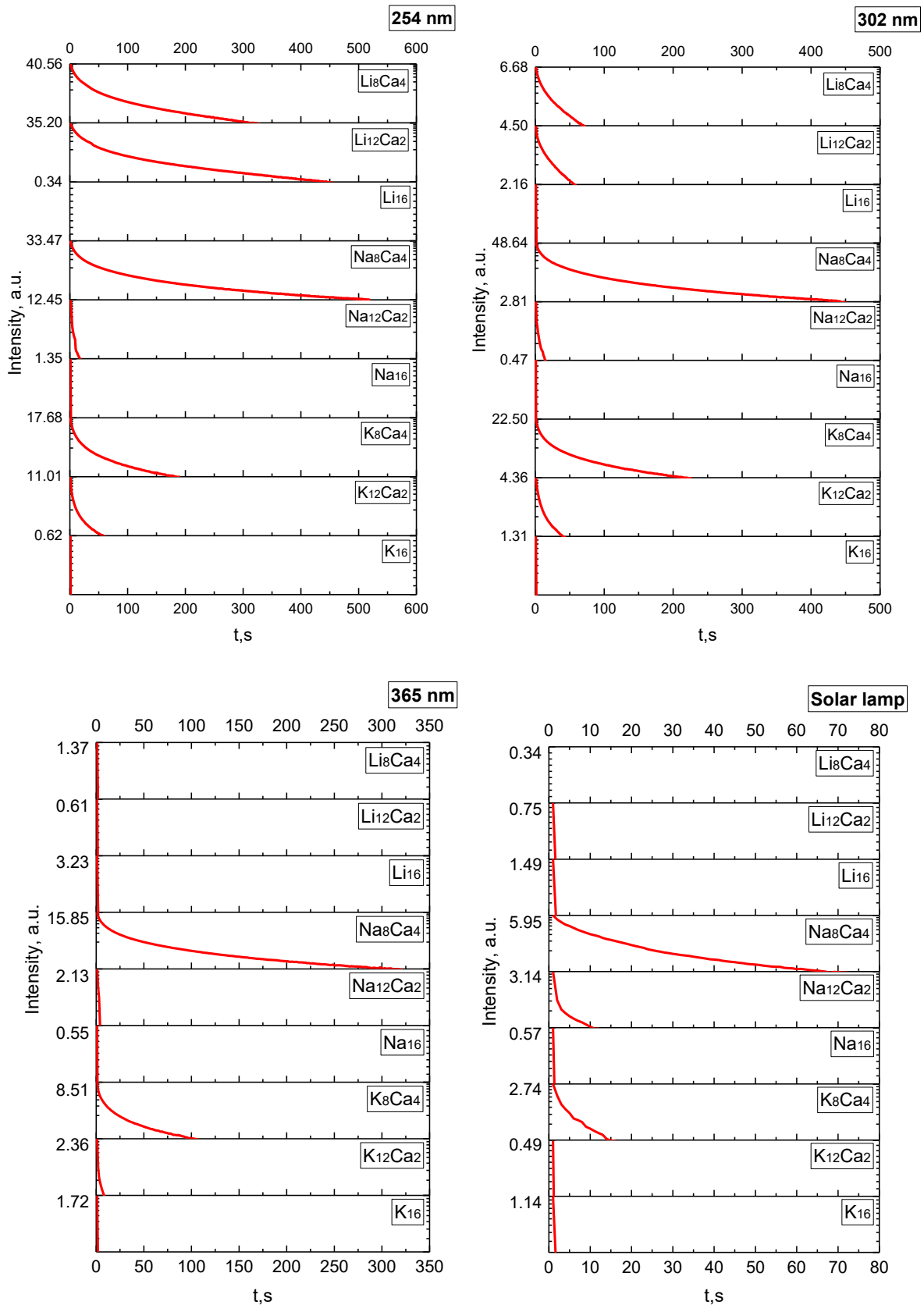
Appendix 10. TL glow curves of non-sodalite containing alkali metal doped samples after irradiation with 302 and 365 nm UV and radiation from the solar lamp for 5 minutes.
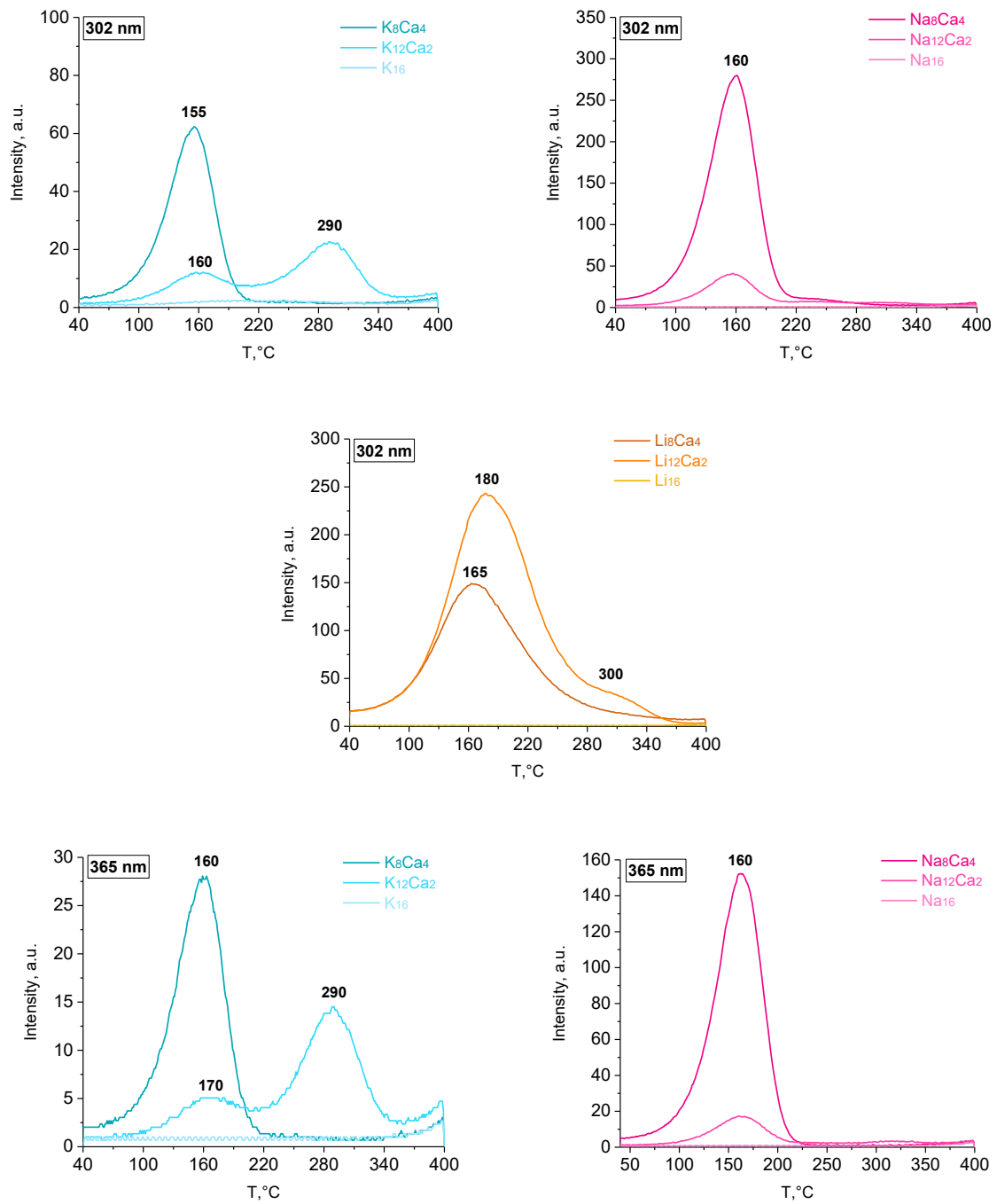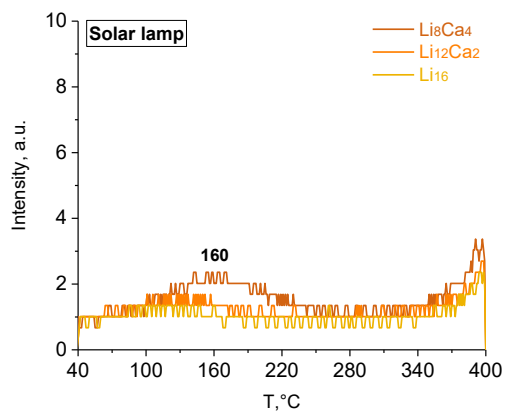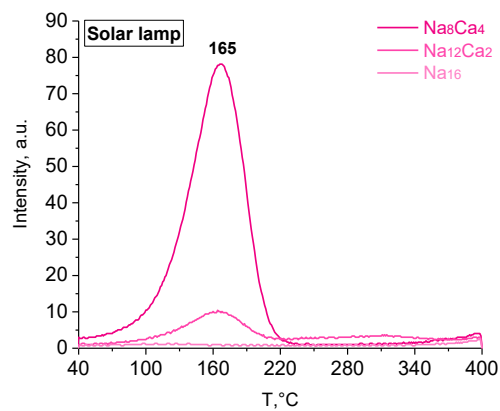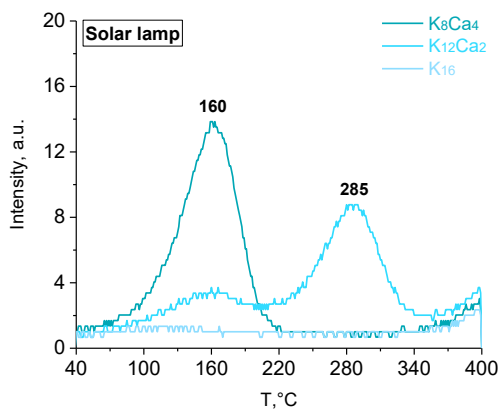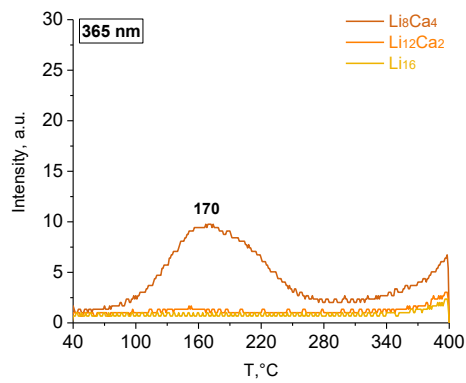
Appendix 11. Reflectance of the non-sodalite containing alkali metal doped samples before, immediately after and 10 minutes after irradiation with 254 nm UV radiation.